AFGL-TR-86-0013

Dependence of $C_n^2(C_T^2)$ in the Atmospheric Boundary Layer on Conventional Meteorological Variables

Edward Ryznar
Joseph A. Bartlo

The University of Michigan
College of Engineering
Department of Atmospheric & Oceanic Science
Ann Arbor, MI 48109-2143

January 1986

Final Report
15 September 1983 - 14 December 1985

AIR FORCE GEOPHYSICS LABORATORY
AIR FORCE SYSTEMS COMMAND
UNITED STATES AIR FORCE
HANSCOM AIR FORCE BASE, MASSACHUSETTS 01731

This technical report has been reviewed and is approved for publication.

EDMOND M. DEWAN
Contract Manager

ROBERT W. FENN
Branch Chief

FOR THE COMMANDER

JOHN S. GARING
Division Director

This report has been reviewed by the ESD Public Affairs Office (PA) and is releasable to the National Technical Information Service (NTIS).

Qualified requestors may obtain additional copies from the Defense Technical Information Center. All others should apply to the National Technical Information Service.

If your address has changed, or if you wish to be removed from the mailing list, or if the addressee is no longer employed by your organization, please notify AFGL/DAA, Hanscom AFB, MA 01731. This will assist us in maintaining a current mailing list.

Unclassified

SECURITY CLASSIFICATION OF THIS PAGE

REPORT DOCUMENTATION PAGE

1a. REPORT SECURITY CLASSIFICATION: Unclassified	1b. RESTRICTIVE MARKINGS
2a. SECURITY CLASSIFICATION AUTHORITY	3. DISTRIBUTION/AVAILABILITY OF REPORT: APPROVED FOR PUBLIC RELEASE; DISTRIBUTION UNLIMITED.
2b. DECLASSIFICATION/DOWNGRADING SCHEDULE	
4. PERFORMING ORGANIZATION REPORT NUMBER(S): 021082-F	5. MONITORING ORGANIZATION REPORT NUMBER(S): AFGL-TR-86-0013
6a. NAME OF PERFORMING ORGANIZATION: University of Michigan College of Engineering; 6b. OFFICE SYMBOL (If applicable)	7a. NAME OF MONITORING ORGANIZATION: Air Force Geophysics Laboratory
6c. ADDRESS (City, State and ZIP Code): Department of Atmospheric & Oceanic Science Ann Arbor, Michigan 48109-2143	7b. ADDRESS (City, State and ZIP Code): Hanscom AFB Massachusetts 01731
8a. NAME OF FUNDING/SPONSORING ORGANIZATION; 8b. OFFICE SYMBOL (If applicable)	9. PROCUREMENT INSTRUMENT IDENTIFICATION NUMBER: F19628-83-K-0040
8c. ADDRESS (City, State and ZIP Code)	10. SOURCE OF FUNDING NOS

PROGRAM ELEMENT NO.	PROJECT NO.	TASK NO.	WORK UNIT NO.
62101F	6687	05	BI

11. TITLE (Include Security Classification): Dependence of $C_n^2(C_T^2)$ in the Atmospheric Boundary Layer on Conventional Meteorological Variables

12. PERSONAL AUTHOR(S): Edward Ryznar, Joseph A. Bartlo

13a. TYPE OF REPORT	13b. TIME COVERED	14. DATE OF REPORT (Yr., Mo., Day)	15. PAGE COUNT
FINAL REPORT	FROM 15 Sep 83 TO 14 Dec 85	1986 January	152

16. SUPPLEMENTARY NOTATION

17 COSATI CODES			18 SUBJECT TERMS (Continue on reverse if necessary and identify by block number)
FIELD	GROUP	SUB GR	Optical turbulence, structure parameter profiles, atmospheric boundary layer, $C_n^2(C_T^2)$ measurements

19. ABSTRACT (Continue on reverse if necessary and identify by block number)

The dependence of optical turbulence, parameterized by the structure function coefficients for the index of refraction, C_n^2, or for temperature, C_T^2, on the vertical distributions of temperature and wind speed in the atmospheric boundary layer led to a study to determine the dependence in terms of conventional, more readily available, meteorological variables. The study was conducted with data sets consisting of measurements of structure parameters and meteorological variables that were obtained from the Air Force Geophysics Laboratory, from the Rome Air Development Center and from the Boulder Atmospheric Observatory.

Daytime and nighttime periods with half or less of the sky cloud-covered were selected, processed and analyzed to determine relationships of C_n^2 to solar irradiance and wind speed at one height. These were the basis for determining C_n^2 profiles through the atmosphere's first 3000 meters. For a 10-meter reference height, it is shown that for daytime conditions, (1) C_n increases linearly from about $0.1 \times 10^{-6} m^{-1/3}$ to (Continued on reverse.)

20. DISTRIBUTION/AVAILABILITY OF ABSTRACT	21. ABSTRACT SECURITY CLASSIFICATION
UNCLASSIFIED/UNLIMITED ☐ SAME AS RPT ☒ DTIC USERS ☐	Unclassified

22a. NAME OF RESPONSIBLE INDIVIDUAL	22b. TELEPHONE NUMBER (Include Area Code)	22c. OFFICE SYMBOL
Edmond M. Dewan		AFGL/OPA

DD FORM 1473, 83 APR EDITION OF 1 JAN 73 IS OBSOLETE.

Unclassified

SECURITY CLASSIFICATION OF THIS PAGE

$0.6 \times 10^{-6} m^{-1/3}$ as solar irradiance increases from about 0.1 ly min^{-1} to 1.2 ly min^{-1}, but then C_n decreases at higher irradiances and that (2) for irradiances greater than 0.5 ly min^{-1}, C_n increases with wind speed, reaches a maximum near 2-3 ms^{-1} and decreases at higher speeds. Their relationship is a third-order polynomial equation. A method for calculating solar irradiance with cloud and other information is described, applied and tested that, combined with wind speed measurements, enables C_n^2 at a reference height to be calculated. The profile of C_n^2 through a convective boundary layer is then calculated with the reference value of C_n^2 and estimates of the depth of the convective boundary layer as input variables to a modified version of the C_n^2 profile model of Kukharets and Tsvang.

For nighttime conditions, it is shown that C_n^2 at a reference height of 10 meters increases with wind speed until a speed of 4 ms^{-1} is reached and then decreases sharply to a minimum at higher speeds. The relationship is fitted with a normal curve that is used with a -4/3 height variation of C_n^2 to obtain its profile through a stable boundary layer.

The models for unstable and stable stratification are evaluated by comparing claculated values of C_n^2 with measurements obtained with thermosondes by Air Force Geophysics Laboratory personnel at White Sands, NM. Details of the software for the models are described, compatibility of various methods of measuring C_n^2 is discussed, and a listing of the Fortran IV computer programs for the models is given in two Appendices.

PREFACE

This is the final report of research conducted for the Atmospheric Optics Branch of the Optical Physics Division, Air Force Geophysics Laboratory. The research was conducted under Contract F 19628 83 K 0040 from 15 September 1983 through 14 December 1985 and was coordinated with Dr. Edmond M. Dewan, Scientific Program Officer.

This report elaborates on aspects of the work described in Quarterly Status Reports (021082-1-S through 021082-10-S) and in the first Annual Report (021082-I) submitted in October 1984. In addition, an indexed compilation of 193 abstracts of articles and reports on optical turbulence for the period 1970-1982 was submitted in January, 1984. Supplementing these reports of progress was a preliminary version of a stepwise procedure for computing optical turbulence from temperature and wind measurements at 4 and 14 meters that was submitted in September, 1984.

The objective of the research was to develop methods for estimating optical turbulence in the atmospheric boundary layer with conventional meteorological variables. There are many such variables, considered here to be those observed and reported hourly from weather stations throughout the world. An additional requirement imposed by the research, however, is that the variables chosen, compared to the others, also have the most pronounced effects on optical turbulence in the atmospheric boundary layer.

The two variables that meet the requirements of conventionality and effectiveness are cloudiness and wind speed. Both are measured or estimated at least once each hour, they are reported in standard weather

observations and together, they determine the intensity of optical turbulence in the atmospheric boundary layer. The amounts, types and heights of clouds, for example, through their effects both on (1) the amount of solar radiation available to heat the ground in daytime and (2) the net exchange of infrared radiation at the ground surface at night, directly affect the mean vertical temperature gradient and, therefore, the vertical gradient of refractive index in the boundary layer. Wind speed and its vertical distribution affect not only the magnitude of the mean vertical temperature gradient but, in concert with it, produce the turbulent fluctuations in refractive index that cause optical turbulence. Profiles of wind and temperature in the boundary layer, however, are not routinely available. Although the estimates of optical turbulence with relationships from conventional variables are less accurate than those with similarity relationships from vertical profiles, they have the advantage of enabling operational estimates to be made when and where they could not be made otherwise.

The research is primarily analytical, and the results are obtained from an analysis of optical and meteorological measurements made by others in various locations. It is guided by knowledge gained in similar work here several years ago. Data sets consisting of boundary-layer measurements of the structure function parameter for refractive index, C_n^2 (measured optically or calculated with various methods of estimating the temperature structure parameter C_T^2), and meteorological variables, including solar radiation are analyzed. The work concentrates on describing optical turbulence only for sky conditions known to produce the largest values of $C_n^2(C_T^2)$ in the boundary layer, both in daytime and

at night, in that only conditions with a cloudless sky or with scattered clouds (half or less of the sky cloud-covered) are analyzed. In addition to the restriction in terms of cloudiness, the results are applicable mainly to optical turbulence conditions over land surfaces with small amounts of soil moisture.

Acknowledgments

The experimental nature of the research caused heavy reliance to be placed on data obtained by others in several locations. The authors wish to express their thanks to John Gaynor of the NOAA/ERL Wave Propagation Laboratory, Boulder, CO, for data from the 300-m tower at the Boulder Atmospheric Observatory and, in his absence, to Ms. Nancy Dirkes who gave direct assistance to one of the authors (JAB) in transferring data from the file tape. Jerrold Foster (Captain USAF) and others at the Rome Air Development Center cooperated enthusiastically in providing 1982 data tapes for the Optical Test Facility near Verona, NY. The suggestions and research results of Dr. Edmond M. Dewan, James Brown, and Dr. Earl Good of the AFGL Atmospheric Optics Group and their help in providing meteorological and optical turbulence data for field experiments at White Sands, NM and other locations are much appreciated.

At the University of Michigan, Dr. Donald J. Portman gave valuable ideas, comments and general consultation regarding all aspects of the research. Ms. Suyin Liang capably handled office and administrative matters in addition to all technical and routine typing. The authors express their thanks to both.

Contents

Contents (continued)

List of Figures

List of Figures (Continued)

List of Figures (Continued)

List of Tables

1. INTRODUCTION

The propagation of optical and infrared radiation through the atmosphere is often seriously limited by commonplace atmospheric characteristics. In addition to obvious effects of absorption and scattering by precipitation, clouds or turbidity constituents, there are the more subtle clear-air diffraction and refraction effects caused both by turbulent fluctuations of atmospheric density and by average vertical density gradients. To an observer viewing a distant object, for example, these effects may appear as changes in the object's brightness, position, size and color. Brightness fluctuations are termed scintillation, the motion effect is called shimmer and optical turbulence refers to the phenomenon in general. In the atmospheric boundary layer, optical turbulence is usually most pronounced in cloudless conditions when, except for attenuation by atmospheric turbidity constituents, optical propagation and the transmission of visible contrast between objects and their background would be optimum. In cloudless weather, therefore, this phenomenon often limits the performance of electro-optical tracking and homing systems such as high energy laser systems, long-range reconnaissance systems, laser communications systems and compensated imaging systems.

An Air Force need for a method to characterize optical turbulence with conventional meteorological variables led to the work described herein. The objective of the work is to model the dependence of optical turbulence, as parameterized by the refractive index or temperature structure function parameters $C_n^2(C_T^2)$, in the atmospheric boundary layer in terms of standard meteorological and terrain information. The structure function concept is treated comprehensively by Tatarski (1961), and

its physical meaning in relation to optical turbulence is developed and interpreted by Dewan (1980). The temperature structure parameter is defined as

$$C_T^2 = \overline{[T(x) - T(x+r)]^2}\, R^{-2/3} \quad , \tag{1}$$

where T is temperature, x and r are position vectors, R is the scalar magnitude of r and the overbar indicates an ensemble average. R is a constant in the inertial subrange of turbulence eddy sizes. If the turbulence is homogeneous and isotropic, C_T^2 depends not on r, but only on R. Equivalently, C_T^2 can be defined as the amplitude coefficient for the variance spectrum of temperature, $\phi_T(k)$, in the inertial subrange as:

$$\phi_T(k) = 0.25\, C_T^2\, k^{-5/3} \quad , \tag{2}$$

where k is wavenumber for turbulent fluctuations, usually calculated as $2\pi f/\bar{u}$, where f is frequency and $\bar{u}$ is horizontal wind speed.

The refractive index structure parameter C_n^2 can be calculated with (Kohsiek, 1985):

$$C_n^2 = \frac{A_T^2}{T^2} C_T^2 + \frac{A_Q^2}{Q^2} C_Q^2 + 2 \frac{A_T A_Q}{TQ} C_{TQ} \quad , \tag{3}$$

where A_T and A_Q are given by Hill et al. (1980), T is temperature (K) and Q the absolute humidity (g cm^{-3}). C_T^2, C_Q^2 and C_{TQ} are the structure parameters for temperature, humidity and correlated temperature-humidity fluctuations, respectively, and can be calculated with measured temperature and humidity fluctuations (Kohsiek, 1985). Because the present work is concerned with optical wavelengths and a continental environment only,

effects of humidity fluctuations are assumed to be small compared to effects of temperature fluctuations, especially for values of $C_T^2 \geq 10^{-3} K^2 m^{-2/3}$ (Kunkel and Walters, 1982); (Wesely, 1976) and (Kunkel et al., 1981). For this condition C_n^2 can be written as:

$$C_n^2 = \left(\frac{79 \times 10^{-6} p}{T^2}\right) C_T^2 \quad , \tag{4}$$

where p is station pressure in millibars and T is temperature (K).

1.1 C_n^2 boundary layer model variables

The atmospheric density fluctuations responsible for optical turbulence are the result of incomplete turbulent mixing of thermally stratified layers, a condition that is common in the lower atmosphere because the ground usually becomes warmer than the air in daytime (lapse condition) and colder at night (inversion condition). In general, thermally neutral stability in the first several meters over homogeneous surfaces exists only in very cloudy and windy conditions and for very brief periods near sunrise and sunset when the vertical temperature gradient changes sign (Portman et al., 1962). As a result, optical turbulence in the boundary layer varies in a complex manner with thermal stability, but it is at a minimum in thermally neutral (adiabatic) conditions and at a maximum, dependent on wind and surface roughness conditions, for maximum vertical temperature gradients.

The variables affecting C_n^2 in the boundary layer and the relationships among them that are used as a framework to model the variation of C_n^2 with conventional meteorological and surface information are shown in Fig. 1. In Fig. 1, potential temperature fluctuations (θ') are the

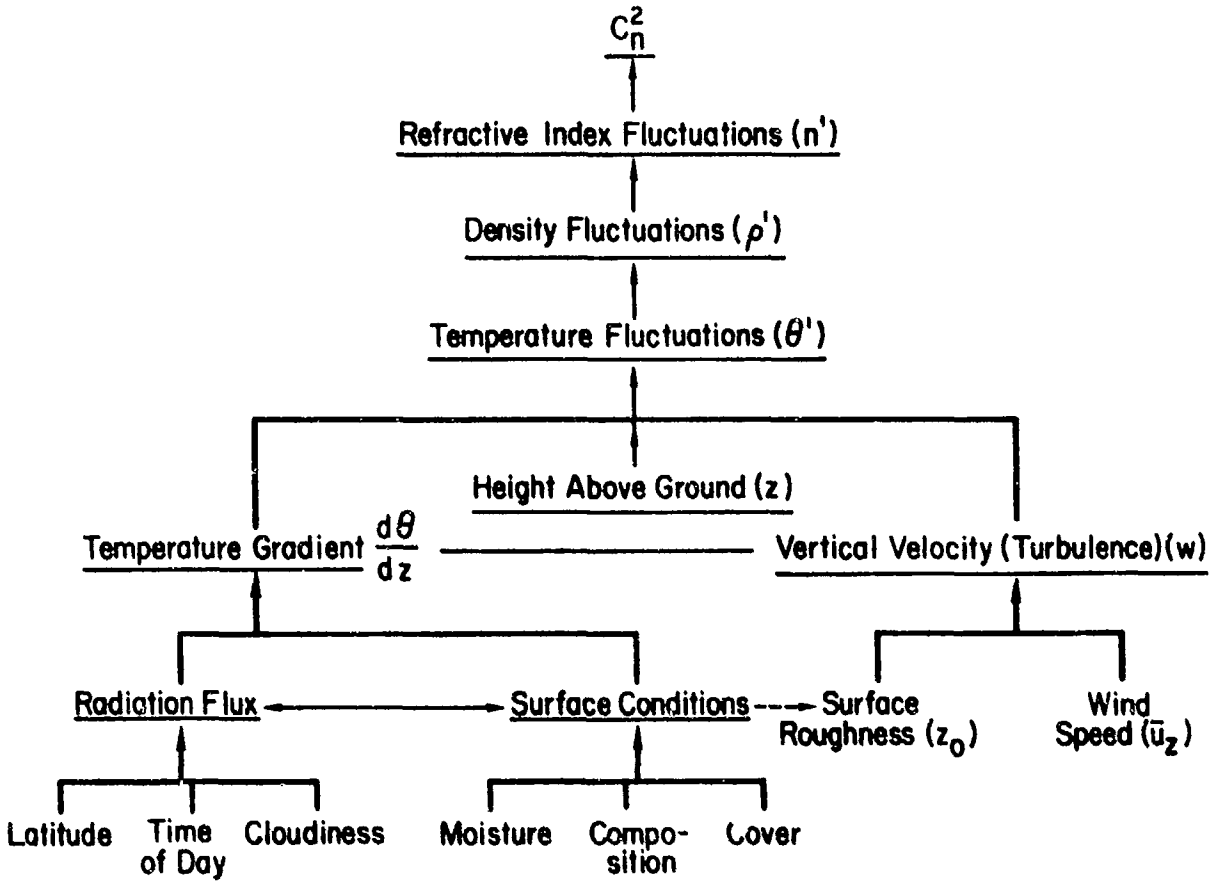

Fig. 1. Optical turbulence variables and relationships

difference between the actual (θ) and average ($\bar{\theta}$) potential temperature and can be expressed as:

$$\theta' = \theta - \bar{\theta} = f_1(d\theta/dz, w', z) = f_2(d\theta/dz, du/dz, z, z_0) = f_3(d\theta/dz, u_z, z_0). \quad (5)$$

As given by f_1, temperature fluctuations at a height z depend on the mean temperature gradient ($d\theta/dz$) and vertical wind speed fluctuations (w'). As given by f_2, the structure of the wind and its effects on w' at a height z depend on: (1) buoyancy effects ($d\theta/dz$), (2) vertical wind shear (du/dz), and (3) the transfer of momentum by the drag of surface elements, or roughness (z_0). Finally, as given by f_3, assuming (1) that the wind speed is zero at the roughness scale height (z_0), (2) that a

wind profile (du/dz) can be expressed for any height interval ($z-z_0$), and (3) that z_0 can be determined from the wind profile when $d\theta/dz \approx$ 1°C/100m, the structure and strength of turbulent fluctuations that determine optical C_n^2 in the boundary layer can be considered dependent on the mean vertical temperature gradient, the average wind speed at a given height (u_z), and the surface roughness, z_0.

Wind, roughness, and height can be regarded as secondary factors affecting both the temperature profile and turbulence. They are mechanical effects relatable through wind shear, and can be combined with buoyancy effects in terms of the vertical temperature gradient as the Richardson number, a non-dimensional ratio that is a measure of the relative intensity of turbulence. Portman et al. (1962) showed that the intensity of optical turbulence for a given mean temperature gradient at 2 m could be characterized by the Richardson number (Ri). They showed that for inversion conditions, there was an apparent discontinuity near Ri $\sim$ +0.35 that indicated a transition from turbulent motion to a more wave-like air motion for larger Ri.

The relationships diagrammed in Fig. 1 show that the behavior of C_n^2 is traceable to effects of unique combinations of cloudiness and wind speed near the ground. An increase in cloudiness, by inhibiting radiative heating or cooling of a surface, decreases the vertical temperature gradient if horizontal advection effects are minimal. Similarly, an increase in wind speed also acts to decrease the vertical temperature gradient through mixing action. Cloudiness and wind speed, therefore, are the main conventional meteorological variables used for the C_n^2 model development discussed below.

1.2 Relevant boundary-layer characteristics

1.2.1 Unstable stratification

Most boundary-layer models for unstable stratification partition the atmosphere's first 1-3 km according to the physical processes that determine mean and turbulent properties in particular regions (Webb, 1984; Carson and Smith, 1974). A daytime convective boundary layer (CBL) is usually considered to be that region within which strong vertical mixing occurs as a result of net upward heat transfer caused by solar heating of the surface. It is usually capped by a comparatively non-turbulent stable layer. Results of three-dimensional numerical calculations (Deardorff, 1972, 1974), atmospheric measurements (Kaimal et al., 1976) and laboratory experiments (Deardorff et al., 1969), show that the two most important variables controlling mean and turbulent properties in particular regions of the mixed layer, or CBL, are w_*, the convective velocity scale and z_i, the depth of the mixed layer, according to:

$$w_* = [g/T\ (\overline{w\theta})_o z_i]^{1/3}\ , \qquad (6)$$

in which g/T is a buoyancy parameter (g is gravitational acceleration, and T is ambient temperature), $(\overline{w\theta})_o$ the surface kinematic heat flux and z_i the height of the mixed layer. The large convective eddies scale with z_i and the turbulence velocity scale is proportional to w_*. Both w_* and z_i undergo diurnal variations that start at zero near sunrise and reach midday values of about 2 ms^{-1} and 1-3 km, respectively.

Several definitions of z_i that have appeared in the literature are summarized here because although the primary maximum of $C_n^2(C_T^2)$ is near the ground, the region around z_i is a region

with a secondary maximum. Scaling theory, furthermore, indicates that $C_n^2(z)$ and $C_T^2(z)$ can be approximated with universal functions of z/z_i (Kukharets and Tsvang, 1980). Kaimal et al. (1976) and Caughey and Palmer (1979) define z_i as the height of the inversion base capping the mixed layer and Wyngaard and LeMone (1980) define it as the minimum of virtual temperature flux ($\overline{w\theta}_v$). As pointed out by Zhou et al. (1985), in most cases the two definitions yield comparable values, but in those cases with shallow and highly baroclinic boundary layers that were analyzed by them, the inversion base had undulating motions above it and turbulent motion below, indicative of the top of the mixed layer. The height of minimum temperature flux, however, did not have these characteristics and it was about 30% higher.

Kukharets and Tsvang (1977) and Gamo et al. (1976) independently found that a reliable and physically sound experimental determination of z_i could be made from measurements of the turbulent energy dissipation rate, ε. They measured $\varepsilon(z)$ with aircraft and found that in unstable stratification $\varepsilon(z)$ showed little variation with height until, at a height usually above 1 km, it decreased 2-3 orders of magnitude in a layer about 200-400 m thick. The subsequent model of Kukharets and Tsvang (1980) of $C_n^2(z)$ was based on this finding.

It is evident from the definitions of z_i given above that detailed measurements of various meteorological variables are required to determine z_i accurately. Smith (1977), however, through an analysis of data from well-known micrometeorological field experiments in England (Malvern Experiment, 1976), the United States (The Minnesota 1973 Experiment and the Kansas 1968 Experiment), and Australia (The 1967 Wangara

Experiment) developed a practical method for estimating z_i with conventional variables. The variables were time of day, month, cloud amount and wind speed at 10 m. His method consists of the stepwise procedure shown in the nomogram in Fig. 2 , which was modified slightly for the present work. As discussed below, reasonable estimates of z_i were obtainable in many cases, but in others, large disparities between estimated and measured values were observed.

The CBL can be divided into three regions in terms of z_i: the surface, mixed, and interfacial (entrainment) layers. The surface layer is within the first few meters. Its mean and turbulent properties are determined by surface fluxes of momentum, sensible heat and latent heat and hence by air-to-ground (bulk) differences of wind speed, temperature, and vapor pressure, respectively. In the surface layer, the assumption that the fluxes are nearly constant with height has been studied experimentally and confirmed, for the most part, for sufficiently long ($\sim$ 1 hour) averaging times (Haugen et al., 1971). Similarity theory allows relevant micrometeorological properties, including structure parameters, in the surface layer to be represented in terms of height, appropriate scaling parameters, and the Monin-Obukhov (1954) stability length (Wyngaard and LeMone, 1980). From the work of Wyngaard et al. (1971), for the free convection case, C_T^2 close to the ground scales according to $z^{-2/3}$, but rapidly approaches $z^{-4/3}$.

The mixed layer extends from the top of the surface layer to near the base of the capping inversion, $0.1\ z_i \lesssim z \lesssim 0.8\ z_i$. Average wind speed and potential temperature are nearly invariant in the mixed layer. Its properties are determined by fluxes in the surface layer

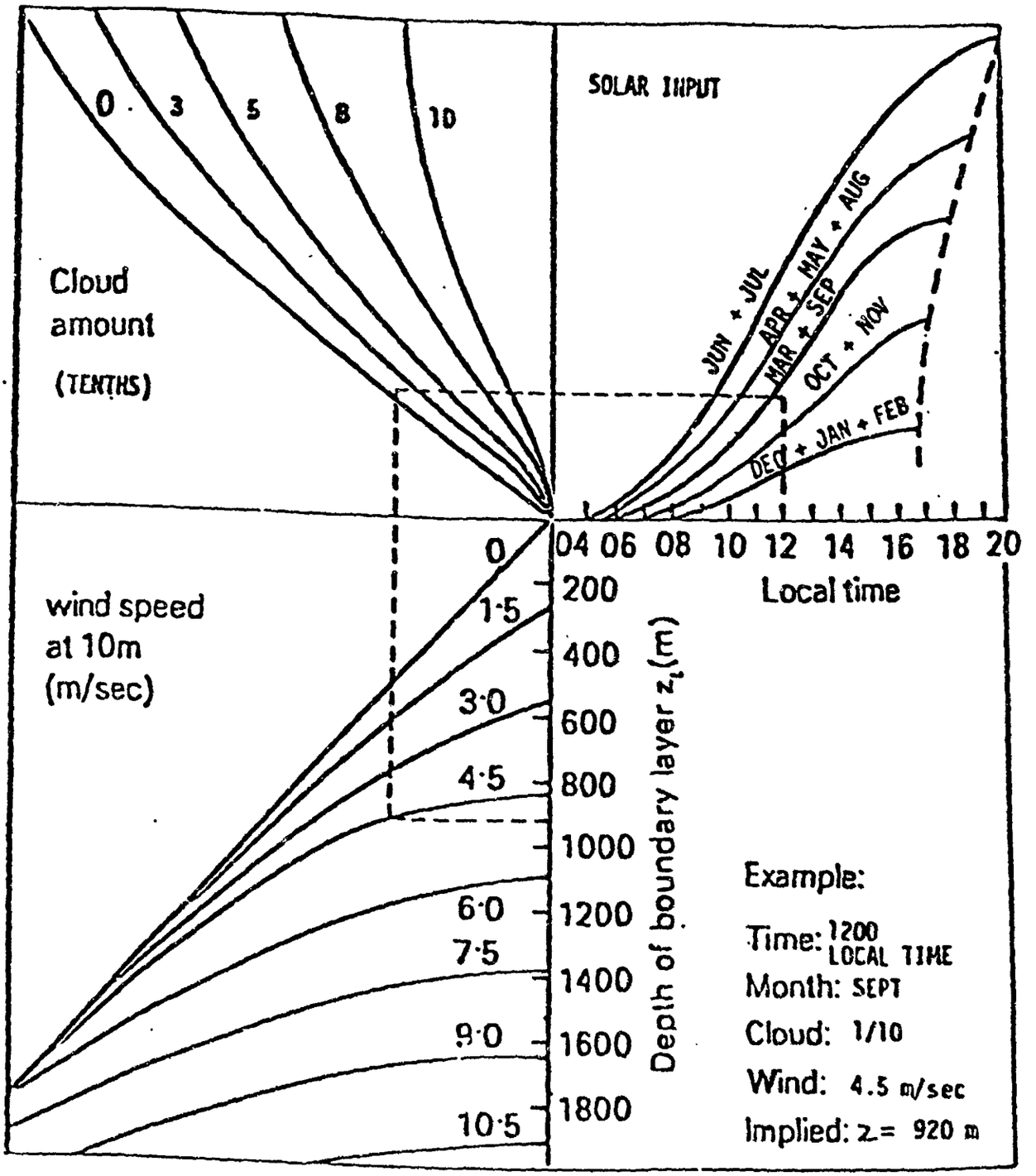

Fig. 2 A nomogram for estimating the depth of the boundary layer in the absence of marked advective effects or basic changes in weather conditions. The marked example shows how the diagram is to be used. Adapted from Smith (1977).

and entrainment processes in the interfacial layer above. In its lower half, C_T^2 scales according to $z^{-4/3}$, Obukhov (1960). In a transition layer beginning near 0.5 z_i, this scaling begins to break down at heights dependent mainly on the value of z_i because of effects of turbulent heat transfer across the interfacial layer (Fairall et al., 1982).

The interfacial layer at the top of the mixed layer ($0.8\ z_i \lesssim z \lesssim 1.2\ z_i$) separates the turbulent boundary layer from the less turbulent, thermally stable air of the free atmosphere. Turbulent processes at work in the interfacial layer erode it by entrainment at a rate that depends on the intensity of turbulence and the work it must do to erode the layer. The former depends on surface fluxes and w_*, and the latter depends primarily on the increase in temperature through the layer and the lapse rate above it. Having a direct effect on entrainment processes are thermal plumes or updrafts that are surrounded by larger downdraft regions, both of which extend from near the ground into the interfacial layer (Webb, 1984). Because of the mixing of the warm dry air from above the inversion with cooler and moister air from below, secondary maxima of C_T^2 and C_n^2 are usually observed within the interfacial layer (Kukharets and Tsvang, 1980; and Kaimal et al., 1976).

1.2.2 Stable stratification

Thermally stable conditions in the boundary layer are usually caused by nocturnal infrared radiation loss from the ground and atmosphere, if the sky is relatively cloud-free, but they can also be caused by advection of air that is warmer than the surface, regardless of cloudiness or time of day. The advection of air above freezing over a snow or ice surface is an example of the latter. In contrast to the combined effects of positive buoyancy and vertical wind shear that

enhance vertical motions and optical turbulence in a CBL, there are negative buoyancy effects in a stable boundary layer (SBL) that inhibit vertical motion and reduce the length scale of turbulent fluctuations. When the length scale becomes much smaller than the height above the surface, effects of the ground on turbulent motion decrease to the point that there is no longer an explicit dependence on height (Nieuwstadt, 1984). Wyngaard (1973) expresses the behavior of surface-layer profiles for stable conditions in terms of local z-less stratification.

Results of field measurements made here (Ryznar et al., 1971) and observations reported by Garrat (1982) are among those that show that a SBL becomes quite well established within about 2 hours after a transition from upward to downward net heat flux. Quite often, a layer of maximum wind speed, commonly called the nocturnal low-level jet, develops near the top of the SBL (Bonner, 1968). As discussed by Blackadar (1957) and Thorpe and Guymer (1977), the jet represents an overshoot in the increase of wind speed after the daytime drag by turbulent coupling with the ground surface is removed.

As Webb (1984) points out, there is no unique way of defining the top of the SBL, denoted here as z_n. In numerical models of the SBL z_n is usually defined either in terms of a flux criterion as the height at which the heat or momentum flux decreases to a small fraction ($\sim$ 5%) of its surface value (Brost and Wyngaard, 1978) or as the height at which a critical gradient Richardson number, usually between 0.2 and 0.3, is reached. In terms of a temperature profile, z_n can be defined by the height to which a ground-based inversion extends, above which the potential temperature changes little with height. In comparing these methods of defining z_n, Nieuwstadt and Driedonks(1979) point out

that a turbulence-limit height for z_n, if defined by Ri $\sim$ 0.2, for example, tends to level off, but a temperature-related height usually continues to increase to well above the jet maximum because of radiational cooling.

In later work, Nieuwstadt (1984a, b) develops local scaling methods to describe profiles and turbulence structure above the surface layer, where the constant flux assumption and similarity theory lose their validity. Local scaling involves the local kinematic stress, τ, and the local temperature flux $\overline{w\theta}$ rather than the surface layer variables u_* and θ_* contained in the Monin-Obukhov similarity theory. With measurements of z_n obtained with an acoustic sounder, furthermore, Nieuwstadt (1984) found that z_n on cloudless nights could be estimated well with a diagnostic relationship involving only measurements of the wind speed at 10 m as:

$$z_n = 28\ u_{10}^{3/2} \quad , \tag{7}$$

The coefficient is probably representative only for the region in which the measurements were made, but as discussed below, this relationship seems to have more general applicability. It is a practical means of obtaining information on z_n in cloudless nocturnal conditions where only wind speed at 10 m is measured.

1.3 Observations and models for $C_n^2(\sigma_r^2)$ in the boundary layer

Work by Wyngaard et al. (1971); Kaimal et al. (1976); Caughey et al. (1979); Wyngaard and LeMone (1980); Burk (1980); Davidson et al. (1981); Walters and Kunkel (1981); Fairall et al. (1982); Kunkel (1982); Kunkel and Walters (1982 and 1983) and Kohsiek (1985) shows that in general, the height variation of C_T^2 or C_n^2 in the CBL fits within the framework of Monin-Obukhov similarity theory. A $z^{-2/3}$ near-ground dependence and $z^{-4/3}$ mixed layer dependence are corroborated by experimental results, but both exponents have been observed for $z \lesssim 2m$, depending largely on vertical wind shear. Near z_i, however, uncertainties regarding entrainment energy (buoyancy, surface wind shear, inversion wind shear and waves on the inversion layer itself) and interface thickness can cause large errors when model results are compared with experimental results (Fairall et al., 1982).

Davidson et al. (1981) and Kunkel (1982) had success in describing C_n^2 at one height in relation to external factors such as surface-to-air temperature difference and wind speed. Kunkel's experimental work considers both terrain and stability effects and in a later work, Kunkel and Walters (1983) modelled the diurnal dependence of C_n^2 by solving an extremely detailed energy balance equation for ground surface temperature for a clear sky, dry soil condition. The solution yields fluxes of sensible and latent heat with which C_n^2 is calculated near the ground. The model simulates the processes quite well for both thermally unstable and stable conditions and is designed for surfaces with little or no vegetation. Similarly, Wesely and Alcaraz (1973) calculated C_n^2 with estimates of sensible and latent heat flux components of the surface energy balance.

Many experimental and theoretical results of investigations of the height variation of C_n^2 are presented and discussed in detail in Gurvich et al. (1976). Fig. 3 is taken from their book and shows a summary of these results, with our translation of the legend given below it. In Fig. 3, values of C_n^2 are on the ordinate and height in meters is on the abscissa. Roman numerals I-IV on the C_n^2 axis are categories based on the findings of Voyt et al. (1973), who measured C_T^2 and temperature with aircraft at heights from 50 m to 5000 m over various types of terrain in conditions from very unstable to near adiabatic stratification. They found that $C_T^2(z)$ in the 50-m to 600-m layer was determinable more from the magnitude of C_T^2 at 50 m than from the temperature lapse rate. For example, in terms of their 3 categories of $C_T^2(50)$, they found that:

I for $C_T^2(50) \gtrsim 100\times10^{-6}(°C)^2cm^{-2/3}$, $C_T^2(z) \sim z^{-4/3}$;

II for $C_T^2(50) \approx 10\text{-}80\times10^{-6}(°C)^2cm^{-2/3}$, $C_T^2(z) \sim z^{-2/3}$

up to about 500-800 m; and

III for $C_T^2(50) \lesssim 10^{-6}(°C)^2cm^{-2/3}$, $C_T^2(z) \sim$ constant.

Their calculations of the total atmospheric modulation transfer function for the 50-5000 m layer showed that for category I, the contribution of the 50m-100m layer alone was 77% of the total, for II it was 22% and for III it was 2%.

Two models that describe $C_n^2(z)$ in a CBL with z_i scaling are those of Kaimal et al. (1976) and Kukharets and Tsvang (1980). The Kaimal model was developed in terms of surface heat flux but Walters and Kunkel (1981) modified it for more practical use by establishing experimentally that for sufficiently unstable stratification,

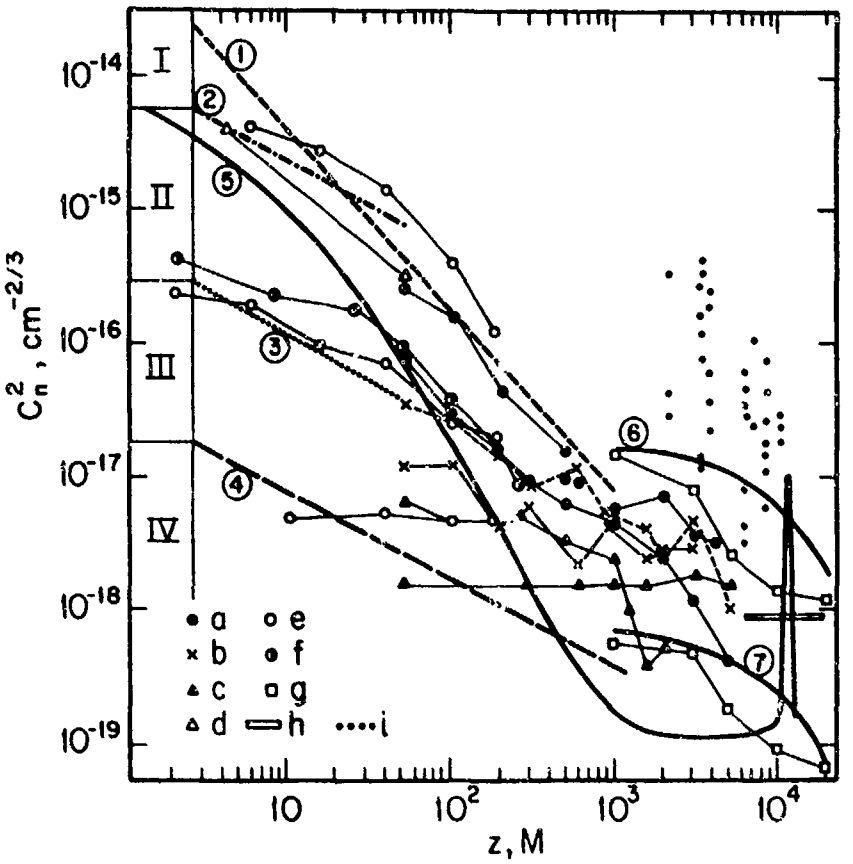

Fig. 3 Experimental data on the vertical profile of the structural characteristics of the index of refraction in the atmosphere (taken from Gurvich et al., 1976).

a, b and c - outer curves corresponding to groups I, II and III of the data of Voyt et al., (1973);

d - neutral data (Kallistratova, 1966) obtained from simultaneous surface (z = 4m) and aircraft (z = 50m) measurements;

e - measurements with resistance thermometers suspended from a tethered balloon (Coulman, 1969);

f - data obtained on a meteorological tower (Byzova and Vyal'tseva, 1970) from micropulsation measurements of temperature;

g - data from Bufton et al. (1972) obtained from measurements of micropulsations of temperature from a balloon in free flight;

h - estimate of C_n^2 from astronomical observations (Tatarski, 1967);

i - aircraft optical measurements (Morris, 1973);

1 - $C_n^2(z) \sim z^{-4/3}$;

2, 3, 4 - $C_n^2(z) \sim z^{-2/3}$;

5 - calculated from the dissipation of turbulent kinetic energy (Hufnagel, 1966), and

6, 7 - $C_n^2 \sim \exp\left[-(z-z_2)/z_3\right]$.

a knowledge of C_n^2 at one height near the ground and information on z_i are sufficient for describing $C_n^2(z)$ in the following regions:

$$\frac{C_n^2(z)}{C_n^2(z_1)} = \begin{cases} (z/z_1)^{-4/3} & \text{for } z_1,\ z \leq 0.5\ z_i \\ (0.5\ z_i/z_1)^{-4/3} & \text{for } 0.5\ z_i \leq z \leq 0.7\ z_i, \text{ and} \\ 2.9\ (0.5\ z_i/z_1)^{-4/3}(z/z_i)^3 & \text{for } 0.7\ z_i \leq z \leq z_i\ . \end{cases} \quad (8)$$

It can be noted that the validity of the Kaimal model extends only as high as z_i and in terms of C_n^2, the model shows an increase with height near z_i.

The model of Kukharets and Tsvang (1980), hereafter referred to as K-T, is based on an analysis of 2 years (1976 and 1977) of measurements of $C_T^2(z)$ and meteorological variables in the CBL over steppe and forested surfaces in the Soviet Union. They normalized their measurements of C_T^2 to $C_T^2(0.1)$, which corresponds to a dimensionless height $\zeta = z/z_i = 0.1$, where z_i was determined from the abrupt decrease in the turbulence energy dissipation rate. An empirical equation was developed to fit a composite of observed variations of a dimensionless structure parameter $\psi_{C_T^2} = C_T^2(\zeta)/C_T^2(0.1)$ through a secondary maximum near $z/z_i \tilde{\sim} 1.1$ without a height-dependent breakdown as in the Kaimal model. Their equation is

$$\psi_{C_T^2}(\zeta) = k_1\ \zeta^{-4/3} + k_2 \exp^{-k_3(\zeta-1.1)^2}\ , \quad (9)$$

with the values of the coefficients $k_1 = 4.6 \times 10^{-2}$, $k_2 = 0.6$ and $k_3 = 12$. It can be noted that eq. 9 describes a $z^{-4/3}$ variation at altitudes well below z_i, with a Gaussian-shaped variation of C_n^2 with height through z_i.

The coefficients k_2 and k_3, respectively, determine the amplitude and standard deviation of the Gaussian-type variation through z_i. The larger the magnitude of k_3, for example, the smaller the standard deviation of the Gaussian-shaped variation.

Profiles of $C_n^2(C_T^2)$ calculated with the modified Kaimal model and the K-T model were compared with balloon-borne and scintillometer measurements of profiles for conditions of unstable stratification by Murphy, Dewan and Sheldon (1985). They adapted the K-T model for application to measurements of C_n^2 at a reference height of 14 m. With profile values of z_i, they found reasonable agreement for an average of several profiles, but for single profiles, they found that measured $C_n^2(z)$ in the vicinity of z_i was narrower than the K-T model prediction. They suggested that a value of $k_3 = 580$ instead of $k_3 = 12$ is more applicable to single profiles.

For stable stratification, fewer research results are available and less modeling work has been conducted. Caughey et al. (1979) reported measurements of σ_T^2 for heights from 4 m to 305 m for a site in Minnesota. The behavior of the corresponding structure parameter normalized by the surface value of a scaling temperature θ_* as $C_T^2 z_n^{2/3}/\theta_*^2$ decreased linearly from about 140 for small z/z_n to near unity near the top of SBL (Caughey, 1982). Their results also indicate that for stable conditions, C_T^2 can be described in terms of Monin-Obukhov similarity in the lowest few meters of the boundary layer if it is assumed that the atmosphere is fully turbulent. Wyngaard et al. (1971) found that C_T^2 decreases with height more slowly than $z^{-2/3}$ for stable conditions and approached $z^{-2/3}$ for near neutral conditions.

2. Data acquisition, processing and tabulation

Early in the work, a search was conducted for experimental data that included simultaneous measurements of structure parameters and meteorological variables. A copy of the PRESSURS data base survey (AFWAL-TR-83-1077) conducted for the EO Sensor/Atmospheric Science Group at the Air Force Avionics Laboratory was obtained that led to the identification of data sets considered to be complete enough for analysis and obtainable in a format compatible with computing facilities here. The sources, responsible individuals and types of data are shown in Table 1.

Table 1 Structure parameter and meteorological data: sources, types and responsible individuals

Source	Type and Form
1) Air Force Geophysics Laboratory E.M. Dewan, J. Brown See Brown et al. (1982) and Brown and Good (1984).	a) Balloon-borne C_n^2 (thermosonde) and met variables through troposphere for several locations (mag tape). b) Optical and spaced-probe C_n^2, micrometeorological profiles and radiation variables for field experiments at White Sands, NM (graphs of diurnal variations).
2) Rome Air Development Center Advanced Optical Test Facility J. Foster	a) Optical C_n^2 at 2-m high, 118-m long optical path. b) Met variables and solar radiation at 2 m (3-min averages on mag tape).
3) NOAA/ERL Wave Propagation Laboratory (Boulder Atmospheric Observatory) J. Gaynor	a) Optical C_n^2 at 4 m on 3 legs of triangle, 450-m optical path. b) Temperature spectral densities and met variables for 10, 22, 50, 100, 150, 200, 250 and 300 m on 300-m BAO tower. Also solar radiation, (20-min averages on mag tape).

2.1 Air Force Geophysics Laboratory (AFGL) data

Data for the research were provided by AFGL in the following forms: (1) computer tapes with data for 17 daytime and 19 nighttime soundings of C_n^2, temperature, relative humidity and wind for Westford, MA, Hanscom AFB, MA; and Boulder, CO and (2) similar data plus graphs of optical and meteorological variables at White Sands, NM. Relevant information was obtained from (1), but because of the greater detail and completeness of (2) from heights near the ground through the complete boundary layer, greater emphasis was placed on an analysis and interpretation of the latter set of data.

The meteorological and C_n^2 data for special experiments at the White Sands Missile Range (WSMR) in New Mexico were provided for the research in the following forms: (1) 82 vertical soundings of C_n^2, temperature, relative humidity and wind on magnetic tape (2) graphs of diurnal variations of meteorological and optical variables in the atmospheric surface layer and (3) near-ground measurements of optical variables on magnetic tape. The vertical soundings had 20-m height resolution and were measured with balloon-borne thermosondes (Brown et al., 1982) by personnel from the AFGL Atmospheric Optics Branch, Optical Physics Division, and the ground-based measurements were made by personnel from the US Army Atmospheric Sciences Laboratory, WSMR. The field experiments for which data were obtained were entitled: CRITICAL LASER ENHANCING ATMOSPHERIC RESEARCH (CLEAR), and took place from 27 Aug. to 27 Sept. 1984 (CLEAR I), from 25 Feb. to 10 Mar. 1985 (CLEAR II), and from 29 July to 3 Aug. 1985 (CLEAR III).

A significant effort was devoted to devising a method for programming the University of Michigan computer to accept the format of the CLEAR I

and II sounding data for processing and analysis. Once a method was developed, the C_n^2 data for each sounding were averaged logarithmically within the height-dependent increments shown in Table 2 . This method of averaging reduced the number of sample points in 3000 m from about 150 to 23 and distributed them quite equally on a logarithmic scale. Table 3 shows the averaging method applied to the temperature and humidity data, which were averaged linearly in the height intervals shown. Most boundary layer wind measurements were missing.

For visually evaluating each sounding averaged in these ways, computer graphs were produced with the 21 to 24 values of $\overline{C_n^2}$ plotted against height up to 3000 m, with both variables in logarithmic coordinates, and with 35 to 40 values of temperature and relative humidity up to 3000 m, with both variables in linear coordinates. For nocturnal conditions, profiles with all 30 values up to a height of 600 m values were also graphed to provide improved resolution in determining the top of the stable boundary layer.

Because the vertical soundings for CLEAR I and II were obtained at various times of day, they were representative of various conditions of thermal stability. Stability conditions estimated from the graphs of diurnal temperature profiles measured on HIDL tower 2 at heights of 0.5, 1, 2 and 4 m were used to group only those soundings obtained in steady cloudless or scattered sky conditions into general categories of stable, unstable and near neutral. Table 4 contains (1) a listing of the soundings, (2) the lowest height of the first measurement (z_L), (3) cloud amount and height for the sounding time as estimated from hourly weather observations at C Station, WSMR, and at Holloman AFB, (4) wind

Table 2 Averaging method for log C_n^2 for the AFGL data. z_L refers to the lowest measurement height on each sounding

Height Interval (m)	Number of Values Averaged
z_L-20	1
21-40	1
41-60	1
61-80	1
81-100	1
101-120	1
121-140	1
141-160	1
161-200	2
201-240	2
241-280	2
281-320	2
321-380	3
381-440	3
441-520	4
521-640	6
641-800	8
801-1000	10
1001-1240	12
1241-1560	16
1561-1960	20
1961-2440	24
2441-3000	28

Table 3 Averaging method for temperature and relative humidity for the AFGL data. z_L refers to the lowest measurement height on each sounding

Height Interval (m)	Number of Values Averaged
z_L-20	1
21-40	1
41-60	1
⋮	⋮
to 200 m	1
201-240	2
241-280	2
281-320	2
⋮	⋮
to 600 m	2
601-680	4
681-760	4
761-840	4
⋮	⋮
to 1400 m	4
1401-1560	8
1561-1720	8
1721-1880	8
⋮	⋮
to 3000 m	8

Table 4. Values of meteorological variables, C_n^2 (scintillometer) and lowest sounding heights for thermosoundings of CLEAR I and CLEAR II

CLEAR I	(1)	(2)	(3)		(4)	(5)	(6)	(7)	(8)	(9)
DAY/TIME 1984 (MST)	STAB.	z_L (m)	CLOUD AMT	CLOUD HT	u(4m) ms^{-1}	$C_n^2(4m)$ $x10^{-14} m^{-2/3}$	SOLAR Wm^{-2}	z_i (m)	z_n (m)	REMARKS
AUG 28/1354	u	12	3	60,120		MISDA		1400		no C_n^2
29/1502		22	9	60,120	2.6	1.2	145			
29/1753		513	9	65,100	2.6	1.1	50			
29/2104	s	20	3	80,250	0.9	7.5			180	
31/1404	u	10	3	80,250	2.9	27	745	2600		no C_n^2
SEP 1/1525		12	7	60,120	1.4	9	500			
2/1909	s	22	3	50,100		MISDA			-	COMPLEX T PROFILE
3/2113	s	16	1	100	1.8	4			80	
4/1348	u	17	1	60	1.6	38	830	1800		
4/1716	n	13	1	200	1.8	2.5	220			
5/1319	u	20	0		1.9	51	890	1800		
5/1716	n	21	0		2.9	2.1	190			
6/1311	u	20	0		2.9	44	890	1800		
6/2056	s	18	1	250	1.0	7			110	
7/1417	u	13	1	250	3.5	34	780	2100		
7/1708	n	22	0		2.3	4.4	220			
7/1724	n	28	0		1.3	2.4	140			
7/1945	s	8	0		1.2	18			60	
8/1343	u	25	2	60,250	1.6	46	840	2600		
8/2010	s	4	1	120,250	1.0	6.5			140	
9/1303	u	15	1	120,250	2.1	20	880	1900		
9/1746	n	10	1	80,250	0.6	M				
10/1457	u	15	3	60,250	3.1	17	570	2700		
10/1733	n	1908	4	60,250	1.5	2.8	95			
10/2005	s	12	4	60,250	1.0	13			90	
11/1303	u	37	4	65,200	1.9	47	870	2000		no C_n^2
11/1627	u	10	3	65,120	2.6	5.5	225	2300		
11/1854	s	8	2	65,100	0.9	4			60	
12/1157	u	8	1	60,120	1.5	34	885	1000		
12/2016	s	18	3	60,120	0.6	7			404 300	DOUBLE LAPSE

(Continued on next page.)

(Table 4, continued.)

DAY/TIME 1984 (MST)	(1) STAB.	(2) z_L (m)	(3) CLOUD AMT	(3) CLOUD HT	(4) u(4m) ms^{-1}	(5) $C_n^2(4m)$ $x10^{-14}m^{-2/3}$	(6) SOLAR Wm^{-2}	(7) z_i (m)	(8) z_n (m)	(9) REMARKS
SEP 13/1301	u	11	2	70,100	1.7	46	865	2000		
13/1931	s	21	3	60,120	1.3	7			190	
14/1258	u	26	2	60,120	2.4	44	854	2000		
14/1609	u	16	2	60,250	3.1	7.8	411	2700		
15/2019	s	17	5	60,120	MISDA				560	
16/1243	u	17	1	70	2.5	41	750	{200 1500		DOUBLE z_i
16/1851	s	17	2	70,100	1.7	4.8			60	
17/1854	s	18	3	50,250	0.9	3.7			100	
18/1253	u	19	3	60,120	1.8	46	750	2600		
18/1851	s	7	2	60,120	0.8	7			100	
20/0321	s	7	0		1.5	5.8			50	
20/1034	u	22	3	60,110	2.2	48	810	2800		no C_n^2
21/0302	s	22	2	100,200	1.5	9.1			{60 180	DOUBLE LAPSE
21/0751	n	14	3	120,200	1.0	12	380			
24/1239	u	22	1	60,250	2.6	19		2400		
24/1908	s	8	1	60,250	0.9	1.7			120	
25/1232		77	7	60,120	6.0	22	830			
26/0658		930	10	12,20	2.6	0.02	35			
26/1236		39	10	8,22	2.0	0.8	180			
27/1155		3	5	40	1.6	15	920			

(1) Stability category: unstable (u), neutral (n), stable (s) for soundings with cloud amount < 6/10.
(2) z_L: lowest sounding height.
(3) Cloud amount (tenths) and height (hundreds of feet) for Holloman AFB (CLEAR I).
(4) u(4m): 4-meter wind speed for Tower I, HIDL.
(5) C_n^2(4m): 4-meter scintillometer value, Tower I, HIDL.
(6) SOLAR: direct plus diffuse irradiance on a horizontal surface, Tower I, HIDL.
(7) z_i: top of mixed layer.
(8) z_n: top of nocturnal boundary layer.

Table 4 (Continued.)

CLEAR II (no ground-based meteorological or C_n^2 data available.)

DAY/TIME 1985 (MST)	(1) STAB.	(2) z_L (m)	(3) CLOUD AMT	(3) CLOUD HT	(7) z_i (m)	(8) z_n (m)	(9) REMARKS
FEB 26/1429		9	10	280			
26/1759		201	8	160,260			
27/0938	u	12	3	220	450 1000		DOUBLE INVERSION
27/1538		12	7	80,220			
27/1805		13	10	110,220			
27/2106	s	4	4	120		400	
28/1403		3	6	120,220			
28/1815	s	12	2	60,250		70	
28/2104	s	10	1	60		80	
MAR 1/0950	u	13	1	60	1700		
1/1527	n	0	2	65,250			
1/1807	s	14	4	65,240		40 160	DOUBLE LAPSE
1/2059	s	14	5	250		50 230	DOUBLE LAPSE
2/0856		7	10	150,250			
2/1736		3	8	80,250			
4/0904	n	35	CLR				
4/1756	s	15	"			I	
4/2050	s	4	"			70	
5/0901	n	1	"				
5/1441	u	44	1	250	1100		HIGH z_L
5/1746	s	159	3	150,250		-	HIGH z_L
6/0850		9	10	120,250			
6/1731		204	10	150,200			
6/1959		31	9	150,250			
7/0846		31	10	150,200			
7/1452		16	10	120,200			
7/1735		3783	10	150,200			
7/2002		6	9	150,220			
8/1311		8	8	120,200			
8/1721		13	10	150,250			
9/0854		17	10	100,200			
9/1928	s	8	5	120		-	COMPLEX T PROFILE

speed, and (5) scintillometer measurements of C_n^2. The values of wind speed and C_n^2 shown in Table 4 are those measured at 4 m on HIDL Tower 1. Because the height of first measurement varied with each sounding, values of C_n^2 obtained with the thermosonde were not available for a standard height. Such a measurement would have been useful in permitting a grouping of the soundings not only according to stability criteria but also according to values of C_n^2 at one height.

Also shown in Table 4 are estimates of z_i, the top of the mixed layer for unstable stratification, and z_n, the top of the nocturnal boundary layer for stable conditions. Values of z_i and z_n were determined by inspecting graphs of profiles for height intervals with changes in temperature, relative humidity and C_n^2. For many profiles, z_i was detectable as a temperature inversion above an adiabatic layer, but a more reliable indicator was a marked decrease in relative humidity, even for cloudless conditions. A cloudless example is given in Fig. 4 , which shows profiles of C_n^2, temperature, and relative humidity for 1417 MST, 9/7/84, at WSMR for which a z_i of 2100 m was determined. A temperature profile with a -1°C/100m slope, corresponding to adiabatic conditions(r), is drawn near the measured temperature profile for comparison. It can be noted that the measured profile is nearly adiabatic above about 300 m, with a small change in stability above 2200 m. Relative humidity, however, (1) increases gradually from 19 to 26% from 13 m to 1000 m, (2) increases sharply to a maximum of 47% between 1000 and 2100 m and (3) decreases sharply to about 20% between 2100 and 2400 m. A secondary maximum of C_n^2 can also be noted near 2000 m.

Reasons for the marked changes in relative humidity (R.H.) may be

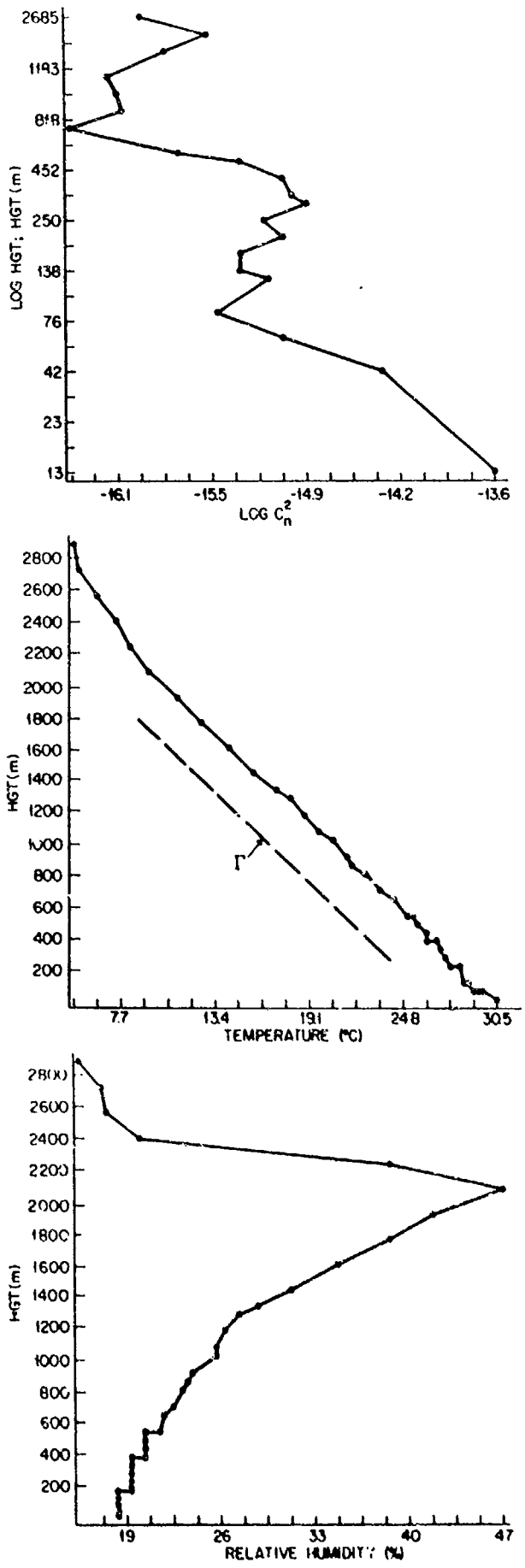

Fig. 4 Profiles of C_n^2, temperature and relative humidity for 1417 MST, 9/7/84 at White Sands, NM.

accounted for by considering its definition in percent as

$$R.H. = \frac{w}{w_s} (100) \ , \qquad (10)$$

which is the ratio of the actual mixing ratio (w) to the mixing ratio of air saturated at the same temperature (w_s). The actual and saturation mixing ratios are the mass of water vapor per unit mass of dry air and saturated air, respectively. The value of w depends on dew point, which is a single-valued function of the amount of water vapor per unit volume, and w_s depends on temperature only. Dew point is less than temperature except in completely saturated conditions, such as dense fog for which it can equal temperature, and RH $\approx$ 100%. Because the temperature change was small at the height corresponding to the change in relative humidity, w_s changed very little, but the actual amount of water vapor (w) must have decreased sharply above 2100 m to cause the decrease in relative humidity. Physical processes responsible for such a large change in cloudless conditions involve the structure of thermals and complex thermodynamics that are beyond the scope of the present research.

For stable stratification, values of z_n were detectable as the height at which a ground-based temperature increase with height changed to a near-adiabatic decrease that was coincident with an increase in relative humidity. By graphing all values recorded within only 600 m above ground instead of average values up to 3000 m, it was possible to obtain adequate resolution to allow z_n to be reliably determined for most soundings.

2.2 Rome Air Development Center (RADC) data

Magnetic tape recordings of 3-minute averages of (1) C_n^2 measured with an optical scintillometer ($m^{-2/3}$), (2) air temperature (°C), (3) dew point (°C), (4) wind speed (mph), (5) wind direction (°az.), (6) station pressure (mb), and (7) global (direct plus diffuse on a horizontal surface) solar irradiance (Langley min^{-1}) were processed and analyzed for selected days in 1982. The measurements were made by Air Force personnel at the Advanced Optical Test Facility of the Rome Air Development Center (RADC), Verona, NY (Fragapane, et al., 1983).

The scintillometer system used at RADC was based on the design of Ochs et al. (1977) and consisted of a quartz-iodine light source located 118 m from a receiver. The receiver had two 5-cm diameter apertures spaced 13.5 cm apart. Fluctuations in refractive index cause variations in light intensity at the two apertures and C_n^2 is proportional to the difference in light intensity. The system responded to values of C_n^2 between about 10^{-17} and 10^{-12} $m^{-2/3}$ and was sensitive primarily to turbulent refractive index scale sizes of about 5 cm. The optical path had a north-south orientation and, like the meteorological sensors, was at a height of 2 m. Voltage signals from the C_n^2 and meteorological sensors were sampled 50 times each minute, digitized, and each 3-minute average was entered onto magnetic tape.

Hourly weather observations for 1982 were obtained for Griffiss Air Force Base, located 23 km from the test facility, and were used to select daytime and nighttime periods for analysis. Because the largest values of C_n^2 ($\sim 10^{-12} m^{-2/3}$) occur with a cloudless sky and light wind, the criterion for selecting periods for analysis was that the observed sky condition at Griffiss AFB be either cloudless or that it

have only scattered clouds (half or less of the sky covered with clouds) and that the visibility exceed 10 miles, with both conditions lasting for at least 2 hours. Daytime was taken to be from one hour after sunrise to one hour before sunset, and nighttime was taken to be from one hour after sunset to one hour before sunrise.

It was assumed that average meteorological conditions, such as surface visibility, humidity and the type, height and amount of clouds observed at Griffiss AFB were representative of those at the test site 14 miles away. Limited information obtained concerning the test site, however, indicated that it was located at a lower elevation and had a greater than average soil moisture, so this assumption was probably not valid for certain conditions. For several cloudless nights, for example, temperature, dew point and wind conditions were conducive to the formation of ground fog at Griffiss AFB but none was reported. If it had occurred at the test site, attenuation of the scintillometer light beam could render C_n^2 data useless. As a criterion in screening data, therefore, if the temperature-dew point difference measured at the test site was less than 2°C, the data were not used. In addition, differences in cloudiness between the two sites could also occur and are probably responsible for some of the scatter in the relationships of C_n^2 to meteorological variables. The chance of occurrence of different cloudiness conditions at the two locations could have been minimized by selecting periods only with a cloudless sky observed at Griffiss AFB, but then (1) the sample size would have been severely reduced and (2) important effects of variable cloud conditions on C_n^2, such as the large changes that can occur in short time intervals when there are occasional shadows

from scattered cumulus clouds on snowless ground, would not have been disclosed.

Periods from winter months when there was at least 3" of snow and the air temperature was above 0°C were also selected for analysis, regardless of cloudiness. As discussed below, these are special cases that can produce large values of C_n^2 because a snow surface temperature remains near 0°C, regardless of how much the air temperature exceeds 0°C. C_n^2 for daytime conditions over snow with $T_{air} < 0°C$, on the other hand, was found to be small ($\lesssim 10^{-15} m^{-2/3}$) and quite steady. As a result, periods with these conditions were not selected for analysis.

In summary, RADC data were analyzed separately for the following conditions:

1) Nighttime
   a) No snow cover, cloudless or scattered clouds, regardless of air temperature;
   b) With snow cover, cloudless or scattered clouds, but restricted to $T_{air} < 0°C$; and
   c) With snow cover, regardless of cloudiness, but restricted to $T_{air} > 0°C$.
2) Daytime
   a) No snow cover, cloudless or scattered clouds, regardless of temperature; and
   b) With snow cover, regardless of cloudiness but restricted to $T_{air} > 0°C$.

The nighttime periods are listed in Table 5 , together with average cloud amount and height and the maximum and minimum 3-minute values of C_n^2,

TABLE 5 Maximum and minimum values of C_n^2 and relevant meteorological variables for nighttime periods analyzed from the RADC Optical Test Facility, for a 2-meter measurement height

1982	TIME (GMT)		$C_n^2 \times 10^{-14} (m^{-2/3})$		CLOUD[1]	WIND (mph)		TEMP (°C)		DEW PT (°C)	
MO/DAY	BEG.	END	MIN	MAX	(AMT.) HT.	MIN	MAX	MIN	MAX	MIN	MAX
1/22	0554	1124	0.006	20.3	(1) 200	*	2.0	-29.0	-20.2	-30.9	-23.0
1/27	0154	1121	0.005	103	(0)	*	3.8	-29.0	-18.6	-31.1	-20.0
2/10	2354	0954	0.001	41.4	(0)	*	6.7	-22.3	-13.6	-24.3	-18.5
2/25	2345	1042	0.001	32.7	(0)	*	10.3	-17.3	-8.7	-19.1	-15.1
3/1	0654	1039	0.0007	1.2	(0)	*	2.9	-10.1	-6.7	-12.2	-9.0
3/3	0654	1033	0.06	5.9	(0)	1.9	5.6	-16.7	-8.6	-20.1	-14.1
3/3	2351	1033	0.001	3.5	(0)	*	8.1	-22.7	-13.1	-25.4	-17.0
3/15	0006	0954	0.08	0.70	(1) 200	1.6	16.0	-2.0	2.3	-6.0	-3.8
3/16	0254	0754	0.0009	0.50	(2) 200	*	4.0	-4.9	-1.5	-10.9	-5.4
3/24	0015	0957	0.008	0.14	(1) 250	*	5.5	-1.6	2.5	-7.0	-2.3
3/25	0454	0954	0.003	0.24	(2) 250	*	9.1	1.8	7.8	-1.8	1.3
3/28	0154	0951	0.025	0.16	(0)	3.9	19.3	-8.8	-6.6	-16.4	-12.6
3/29	0021	0948	0.001	0.26	(2) 200	*	4.7	-8.7	-2.1	-11.1	-7.5
3/30	0024	0948	0.0006	0.46	(2) 100	*	5.0	-1.2	2.3	-5.7	-3.1
4/8	0033	0930	0.0005	0.0007	(1) 200	8.2	19.5	-4.8	-2.8	-15.2	-8.5
4/15	0042	0818	0.006	293	(0)	*	2.4	-1.4	4.8	-4.3	-2.0
4/19	0045	0912	0.01	6.4	(0)	*	10.2	-0.5	5.9	-2.4	-0.9
4/23	0051	0906	0.009	13.8	(0)	*	3.6	-1.9	3.0	-9.9	-4.4
4/24	0051	0906	7.4	16.5	(0)	2.4	11.2	8.1	14.0	0	1.0
4/25	0054	0903	0.003	23.0	(0)	*	4.5	3.4	13.6	0.7	4.4

* < 0.5 mph

** $C_n^2 < 1 \times 10^{-17} m^{-2/3}$

1. CLOUD AMOUNT IN TENTHS OF SKY COVERED; HEIGHT IN HUNDREDS OF FEET

TABLE 5 (Continued.)

1982	TIME (GMT)		$C_n^2 \times 10^{-14} (m^{-2/3})$		CLOUD[1]	WIND (mph)		TEMP (°C)		DEW PT (°C)	
MO/DAY	BEG.	END	MIN	MAX	(AMT.) HT.	MIN	MAX	MIN	MAX	MIN	MAX
4/29	0057	0857	0.94	12.1	(0)	*	7.7	1.0	10.6	-6.8	-2.5
4/30	0057	0857	0.006	11.9	(0)	*	3.7	2.1	13.6	-2.8	0
5/15	0115	0836	**	14.5	(0)	*	3.5	4.7	12.6	1.7	7.0
5/19	0118	0833	0.051	14.0	(5) 250	*	4.4	14.2	19.4	6.1	13.5
6/15	0142	0821	0.001	1.5	(5)	*	1.9	9.7	15.1	8.0	11.0
7/2	0145	0824	0.0006	2.8	(0)	*	2.9	8.5	13.5	4.1	7.8
7/5	0145	0827	0.0002	3.2	(1) 250	*	2.1	7.9	13.2	5.6	7.7
7/24	0133	0842	**	11.4	(0)	*	3.2	9.0	21.0	5.9	11.6
8/7	0118	0600	0.002	9.0	(1) 250	*	3.0	12.3	21.3	9.0	15.8
8/26	0051	0915	0.49	6.5	(0)	1.0	7.1	13.3	18.6	9.7	14.3
9/19	0009	0942	0.01	6.6	(1) 30	*	6.5	7.7	15.2	5.4	7.3
9/29	2348	0954	**	6.6	(2) 150	*	3.6	11.6	15.9	6.0	11.8
10/2	0157	0957	0.24	10.6	(1) 40	0.5	7.8	6.1	15.5	-8.0	7.3
10/3	0054	0606	0.0005	0.84	(1) 80	*	2.6	2.3	6.4	-10	2.6
10/4	2339	0954	0.0006	4.5	(0)	*	2.9	2.6	12.1	-5.5	4.0
10/6	2336	0854	0.0004	6.6	(0)	*	3.9	8.1	12.8	5.0	7.7
10/18	2354	0854	0.0006	5.7	(1) 90	*	5.4	1.2	7.2	-1.0	-0.1
11/15	2254	1054	**	3.5	(1) 40	*	5.8	-6.3	1.0	-8.7	-6.3
12/7	0654	1118	2.1	3.6	(1) 50	*	1.3	2.6	3.8	-4.5	-2.4
12/9	2254	1054	0.002	0.39	(1) 20	*	0.8	-15.0	-12.0	-18.9	-16.5
12/11	2254	0254	**	0.86	(2) 40	*	7.6	-9.7	-5.3	-14.4	-12.2
12/13	0454	1121	**	0.16	(0)	*	*	-17.4	-13.4	-20.2	-17.4
12/17	2230	1118	**	0.45	(0)	*	*	-10.5	-7.0	-13.0	-11.2

* < 0.5 mph

** $C_n^2 < 1 \times 10^{-17} m^{-2/3}$

1. CLOUD AMOUNT IN TENTHS OF SKY COVERED; HEIGHT IN HUNDREDS OF FEET

wind speed, temperature and dewpoint for each period. The cloudiness values are those obtained from the Griffiss AFB observations and are representative averages for each period. Values of C_n^2 less than $1 \times 10^{-17} m^{-2/3}$ were not used, and if the measured wind speed was less than 0.5 mph, it is noted with a single asterisk. Periods are listed for 43 nights that met the above criteria and in addition, had most equipment operating. After final screening, 4041 3-minute values comprised the nighttime RADC data set.

The daytime periods are listed in Table 6 together with average cloud amount and height, estimates of the top of the mixed layer (z_i) at 1800 GMT with the Smith (1977) nomogram, and maximum and minimum values of C_n^2, solar irradiance and wind speed. Periods from 20 days, or about 213 hours with 4267 3-minute values, comprise the daytime RADC data set.

TABLE 6 Maximum and minimum values of C_n^2 and relevant meteorological variables for daytime periods analyzed from the RADC Optical Test Facility, for a 2-meter measurement height

1982	TIME (GMT)		$C_n^2 \times 10^{-14}$ ($m^{-2/3}$)		CLOUD[1]		SOLAR (LY/MIN)		WIND (mph)		Z_i (m)
MO/DAY	BEG.	END	MIN	MAX	(AMT.)	HT.	MIN	MAX	MIN	MAX	18 GMT
4/19	1115	2248	0.059	38.4	0-4	40	0.23	1.22	*	14.9	1200
4/23	1109	2251	0.051	33.9	1-5	40	1.31	1.42	1.3	21.2	1700
4/28	1100	2257	0.052	53.8	0-1	200	0.19	1.40	2.9	12.7	1200
5/15	1042	2315	0.001	32.4	0-5	250	0.17	1.36	*	11.7	1100
6/2	1024	2333	0.054	9.51	0-1	200	0.08	1.49	5.2	16.5	2000
6/24	1024	2342	0.004	12.6	2-5	30	0.07	1.53	2.5	13.0	1250
6/30	1024	2345	0.03	8.74	1-4	30	0.15	1.64	1.4	14.9	1350
7/1	1027	2345	0.02	12.2	1-4	30	0.16	1.49	2.5	13.8	1250
7/4	1027	2342	0.001	22.7	3-5	35	0.06	1.48	*	10.1	650
7/6	1027	2342	0.002	13.6	0-4	40	0.09	1.42	*	8.0	1150
7/24	1024	2333	0.0002	30.8	0-2	30	0.18	1.44	*	6.7	1250
8/7	1057	2315	0.006	26.2	1-4	35	0.15	1.46	1.1	7.9	1100
9/11	1136	2221	0.005	40.6	0-2	40	0.15	1.17	*	5.2	800
9/13	1136	2218	0.02	31.4	0-3	40	0.11	1.10	*	6.2	800
10/4	1729	2139	0.09	16.4	2	40	0.19	1.04	7.3	10.3	950
10/5	1203	2136	0.02	30.8	0-6	250	0.19	1.02	*	5.1	500
11/17	1257	2036	**	14.9	0-6	100	0.13	0.65	*	5.6	450
12/7	1351	2024	0.004	2.54	2-5	35	0.14	0.58	2.4	14.9	700
12/17	1533	2018	0.01	2.09	1	200	0.18	0.58	*	5.2	350
12/18	1336	2024	0.002	1.33	1-3	120	0.12	0.62	*	11.3	800

* < 0.5 mph

1. CLOUD AMOUNT IN TENTHS OF SKY COVERED; CLOUD HEIGHT IN HUNDREDS OF FEET

2.3 NOAA/ERL Boulder Atmospheric Observatory (BAO) data

Information on the variation of $C_n^2(C_T^2)$ and meteorological variables between 10 m and 300 m above ground was obtained from measurements made at the Boulder Atmospheric Observatory (BAO), CO. The facility is operated by the NOAA/ERL Wave Propagation Laboratory and is located about 25 km east of the foothills of the Rocky Mountains in Colorado. The profile measurements were made on a 300-m tower there and are unique in their type, detail and format for analysis (Kaimal and Gaynor, 1983).

The BAO tower instrumentation for the measurement of C_T^2 and meteorological profiles was (1) a 3-axis sonic anemometer for wind component fluctuations, (2) a propeller-vane anemometer for average wind velocity, (3) quartz (slow response) and platinum-wire (fast response) temperature sensors and (4) a cooled mirror dew point hygrometer. This combination of sensors was located at heights of 10, 22, 50, 100, 150, 200, 250 and 300 m above ground. In full operation, mean and fluctuation measurements of temperature, wind and humidity and other variables were automatically recorded in 20-minute segments. Otherwise, only mean quantities were recorded. Coincident ground-based measurements included solar irradiance on a horizontal surface and C_n^2 obtained with scintillometers at a height of 4 m in three 450-m optical paths in the shape of a triangle. The purpose of this scintillometer arrangement was to enable wind convergence characteristics to be measured optically (Kjelaas and Ochs, 1974).

The processing and analysis of BAO data were carried out on the University of Michigan AMDAHL 470 V/8 computer. The tape-recorded 20-minute values of mean temperature, dew point, wind speed and temperature

fluctuation spectral data for the 8 heights were printed out and graphed. Values of C_T^2 for each height were calculated from spectral densities for 22 frequencies between 10^{-3} and 4 Hz. With graphs of successive spectra, it was possible to determine limits of the inertial subrange from the -2/3 slope relationship (Kaimal, 1973). Values of C_T^2 were calculated with the spectral density corresponding to a particular frequency in the inertial subrange with the following relationship:

$$C_T^2 = 13.6\ (n/\bar{u})^{2/3}\ n\ S_T(n)\ , \qquad (11)$$

where $S_T(n)$ is the spectral density of temperature fluctuations ($°C^2Hz^{-1}$) at n = 2.03 Hz and $\bar{u}$ is the corresponding mean 20-minute wind speed measured at each height of C_T^2. The coefficient 13.6 results from the transformation from frequency to wave number. Profiles of $\ln C_T^2$ vs $\ln z$ were graphed by computer and compared with a $z^{-4/3}$ variation for correlation with meteorological conditions. Values of C_T^2 were also converted to C_n^2 with eq. (3) for comparison with corresponding scintillometer measurements of C_n^2. Data for that scintillometer with an optical path oriented in a northeast-southwest direction were used.

Twenty-minute data for daytime and nighttime conditions were obtained for (1) 11 days from a month-long intensive field experiment conducted in September 1978 called Project PHOENIX (Hooke, 1979), (2) those periods closest to the launch times of thermosondes by AFGL personnel from Table Top Mountain near Boulder on 7 days in March 1983 and (3) 23 days selected from June through September, 1983. As much as possible, the data were selected only for a cloudless sky or one with scattered clouds. The PHOENIX periods were documented with detailed weather

observations and other meteorological data, but for the remaining periods, cloudiness conditions at the BAO location were inferred from weather maps and hourly observations made at the National Weather Service Station at Denver's Stapleton Airport, about 40 km south of Boulder. For most days conditions were similar, but it is likely that for some periods, the sky may have been overcast at Denver and cloudless at BAO, or vice versa.

The daytime periods are listed in Table 7 in a format similar to that used for the RADC data. There were 227 sample 20-minute periods for the 1978 PHOENIX daytime data and 325 samples for the 1983 data. The C_n^2 values are scintillometer measurements and the values of wind speed are those at 10 m on the tower. Also shown for several days in the September 1978 PHOENIX data are values of z_i reported by Kaimal (1982) from measurements with various active and passive sensing equipment. They are listed with values estimated from the Smith (1977) nomogram. For the 1983 data, only values estimated with the Smith nomogram are available. Nighttime periods and relevant data for the BAO data set are given in Table 8 . A total of 360 20-minute periods comprise the nighttime BAO data set.

Table 7 Values of C_n^2 and relevant meteorological variables for daytime periods analyzed from the Boulder Atmospheric Observatory Tower

DATE	TIME (MST)		$C_n^2 \times 10^{-14}$ ($m^{-2/3}$)[1]		CLOUD[2]		SOLAR (LY/MIN)		WIND[3] (ms^{-1})		Z_i (m)(13MST)	
	BEG	END	MIN	MAX	AMT	HT	MIN	MAX	MIN	MAX	MEA	EST[4]
SEPT 1978												
5	0720	1300	6.9	28.5	0		0.46	1.15	0.4	3.8	630	750
6	0800	1120	9.3	28.0	1	60	0.64	1.14	1.0	1.9	680	700
	1200	1300										
9	0840	1440	8.9	28.3	0-2	60	0.76	1.12	1.8	3.2		900
11	0640	1700	0.001	14.7	3-5	60	0.23	1.18	0.5	18.7	> 2000	
12	0640	0800	0.67	12.6	3	60	0.25	0.63	1.2	2.2		650
18	0720	0940	0.34	28.5	4-9	50	0.20	1.12	0.8	9.1	-	
	1020	1340										
	1420	1540										
19	0940	1100	0.99	26.3	7-10	40	0.39	1.10	3.9	4.9	-	
21	0740	1640	0.13	42 5	0-1	250	0.22	1.15	0.3	2.8	850	750
22	0740	1640	0.03	33.1	0-2	250	0.19	1.10	0.3	3.3	480	650
26	0700	1620	0.38	28.9	0-2	60	0.25	1.06	0.6	4.8	650	900
27	0700	1640	0.05	32.4	0-7	60	0.11	1.04	0.4	4.0	680	800
MAR 1983												
21	1400	1420	0.19		7	250	1.06		1.0			450
29	1340	1400	12.9		5	40	0.80		3.1			750
JUNE 1983												
14	0280	1800	0.72	19.8	0-3	70	0.22	1.49	1.9	5.3		1200
JULY 1983												
4	0540	1800	0.54	34.2	0		0.16	1.01	1.4	3.3		1250
AUG 1983												
20	1020	1440	18.0	23.8	0-4	75	0.94	1.31	0.6	2.6		1200

[1] C_n^2 values from scintillometer, northwest-southeast orientation, 4 m height, 400 m path length.

[2] Cloud amount in tenths of sky covered, height in hundreds of feet estimated for BAO from NWS observations, Stapleton Airport, Denver.

[3] Wind at 10 meters.

[4] Z_i for 1300 wind and cloud conditions estimated from Smith (1977) nomogram; measured only in September 1978.

Table 7 Values of C_n^2 and relevant meteorological variables for daytime periods analyzed from the Boulder Atmospheric Observatory Tower (continued)

DATE	TIME (MST)		$C_n^2 X10^{-14} (m^{-2/3})^1$		CLOUD^2		SOLAR (LY/MIN)		WIND^3 (ms^{-1})		Z_i (m) (13 MST)	
	BEG	END	MIN	MAX	AMT	HT	MIN	MAX	MIN	MAX	MEA	EST^4
AUG 1983												
21	0840	1840	14.5	20.4	0-4	80	0.01	1.38	0.7	4.1		1300
27	1120	1440	11.9	31.7	3	80	0.14	1.29	1.1	3.1		1100
28	1000	1320	16.4	28.4	0		0.62	1.29	0.9	2.5		1250
	1400	1540			2	70						
31	0840	1300	16.3	28.7	0		0.26	1.25	0.6	2.3		1250
	1340	1700			2	70						
SEP 1983												
1	0720	1140	11.5	52.9	0		0.27	1.26	1.1	3.8		1100
	1220	1240										
	1340	1420			2	90						
	1520	1700										
5	0840	1700	23.3	91.9	0		0.26	1.28	4.2	11.4		1550
6	0640	1300	1.73	46.1	0				0.9	3.1		900
	1340	1700										
7	0720	1400	1.14	30.2	0		0.08	1.26	0.4	4.9		950
	1440	1700			6	90						
9	0820	1120	1.19	26.3	0		0.16	1.21	0.9	4.0		950
	1220	1700			2	90						
22	0640	0920	1.06	40.7	2	250	0.20	1.24	0.4	3.0		850
	1000	1100										
	1140	1340										

Table 8 Values of C_n^2 and relevant meteorological variables for nighttime periods analyzed from the Boulder Atmospheric Observatory Tower

DATE	TIME (MST)		$C_n^2 \times 10^{-14}$ ($m^{-2/3}$)[1]		CLOUD[2]		WIND[3] (ms^{-1})		TEMP (°C)		DEW PT (°C)	
	BEG	END	MIN	MAX	AMT	HT	MIN	MAX	MIN	MAX	MIN	MAX
SEP 1978												
11-12	1920	0420	0.15	4.1	0		3.0	11.0	9.7	17.2	-1.3	0.2
26-27	1900	0440	0.08	1.5	0		1.2	3.2	12.1	22.5	-4.1	1.9
MAR 1983												
19	2040	2100	12.3		5	30	0.7		-7.9	-7.8	-7.9	-6.3
	2300	2320	0.25		6	30	2.1					
20	2140	2200	3.5		0		2.9		-7.4		-10.1	
25	2000	2020	1.3		7	45	3.9		-2.3		-9.8	
26	2020	2040	0.28		10	65	7.6		-1.5		-6	
28	1920	1940	0.44		7	25	5.0		0.8	3.7	-2.6	-0.6
	2140	2200	1.2		8	250	3.4					
JUN 1983												
14-15	2020	0340	1.03	30.3	0		1.1	4.0	11.1	16.3	2.7	6.8
JUL 1983												
4-5	2020	0200	0.67	20.9	0		0.2	4.1	13.1	20.1	3.8	6.7
AUG 1983												
19-20	2000	0300	3.0	8.9	10	140	0.9	10.9	17.0	21.7	9.7	13.3
21-22	1940	0340	4.1	20.8	0-10	80	1.1	7.9	15.2	24.6	8.9	12.9
24-25	1940	0340	4.7	13.6	0-10	100	1.8	5.4	18.9	23.0	8.8	12.1
26-27	2000	0320	4.6	8.8	4-10	120	2.3	5.6	16.2	20.7	11.4	13.2
28-29	1940	0340	7.3	15.7	4-8	140	0.6	5.3	17.9	24.5	7.6	10.1
30-31	1920	0340	8.9	21.1	0-10	85	1.3	5.4	14.8	21.2	9.2	12.2
31-1 SEP	1940	0000	12.4	24.7	0		0.9	5.1	20.8	24.7	10.9	12.5
SEP 1983												
1	0000	0340			0		3.1	5.4	17.1	20.0	10.9	11.8
	1920	2200	21.3	30.7								

[1] C_n^2 values from scintillometer, northwest-southeast orientation, 4 m high, 450 m path length.

[2] Cloud amount in tenths of sky covered, height in hundreds of feet, estimated for BAO from NWS observations, Stapleton Airport, Denver.

[3] Wind, temperature and dew point at 10 meters.

Table 8 Values of C_n^2 and relevant meteorological variables for nighttime periods analyzed from the Boulder Atmospheric Observatory Tower (continued)

DATE	TIME (MST)		$C_n^2 X10^{-14} (m^{-2/3})^1$		CLOUD^2		WIND^3 (ms^{-1})		TEMP (°C)		DEW PT (°C)	
	BEG	END	MIN	MAX	AMT	HT	MIN	MAX	MIN	MAX	MIN	MAX
SEP 1983												
5-6	1920	0340	19.8	24.5	0		2.0	6.9	14.1	22.9	1.5	4.1
8-9	1920	0400	0.65	19.7	0-3	80	2.2	5.4	19.5	24.5	4.2	11.1
16-17	1900	0420	1.8	27.8	0		1.3	6.1	15.7	23.8	-2.3	2.5

2.4 Compatibility of various C_n^2 measurements

Because estimates of C_n^2 were made from measurements with various optical and temperature fluctuation equipment in different locations, it is reasonable to expect C_n^2 data sets that are internally consistent but somewhat different from each other because of differences in (1) physical, electrical and optical characteristics of the equipment used and (2) thermal, roughness and radiative characteristics of the measurement sites and (3) methods of data acquisition and processing.

As pointed out by Kunkel and Walters (1982), scintillometer measurements tend to converge to a mean very rapidly compared with point measurements made with either a single probe or with 2 spaced probes. The main reason is that because scintillometer measurements are path averaged, a single sample in time is already an ensemble average. In addition, the sensitivity of a scintillometer primarily to small turbulent eddy sizes ($\sim$ 5 cm) causes the statistical uncertainty to decrease rapidly with time because effects of a large number of eddies can be measured. A fast convergence of these measurements allowed Kunkel and Walters to measure rapid changes in flow characteristics.

With regard to the C_n^2 relationships obtained with the scintillometers at RADC and BAO, even though their optical and electrical characteristics were very similar, their different physical characteristics alone resulted in different values of C_n^2 for similar meteorological conditions. The differences could have been caused by the 2-m height of the RADC optical path as opposed to the 4-m height of the BAO path because of the exponential decrease of C_n^2 with height in the first few meters. For

similar meteorological conditions in unstable stratification, for example, effects on C_n^2 of the 2-m path height at RADC and the 4-m height at BAO alone should cause C_n^2 at BAO to be less by a factor between about $(4/2)^{-4/3}$ = 0.39 and $(4/2)^{-2/3}$ = 0.63, depending mainly on the thermal and wind structure in the first few meters. Even though the scintillometer path length is 118 m at RADC and 400 m at BAO, a path length effect alone should not cause C_n^2 at BAO to be significantly greater at BAO as it would be if measured with a single receiver and light source (Portman et al., 1962).

Quantifying effects of these inherent physical differences separately was not possible with the information available, especially since thermal, roughness, and radiative characteristics of the measurement sites were also different. An indication of combined effects on scintillometer values of C_n^2, however, can be noted in Fig. 5, which compares data from RADC with the BAO relationship shown in Fig. 7. It shows that for a given solar irradiance, C_n is at least 50% greater at BAO than at RADC. Apparently, effects of the different scintillometer type at BAO in increasing C_n significantly exceed effects of the higher path in decreasing it, assuming that average effects of other meteorological variables that determine C_n are taken into account by the large sample sizes.

Values of C_n^2 obtained from temperature fluctuation spectra as point measurements can also be expected to be somewhat different from the integral-path measurements with scintillometers, depending on meteorological conditions. A conflicting result that occurred in the BAO data is that for a given solar irradiance, $\overline{C_n^2}$ obtained from temperature spectra at 10 m was about 38% greater than $\overline{C_n^2}$ from the scintillometer measurements at 4 m, whereas it would be expected to be less by a factor between

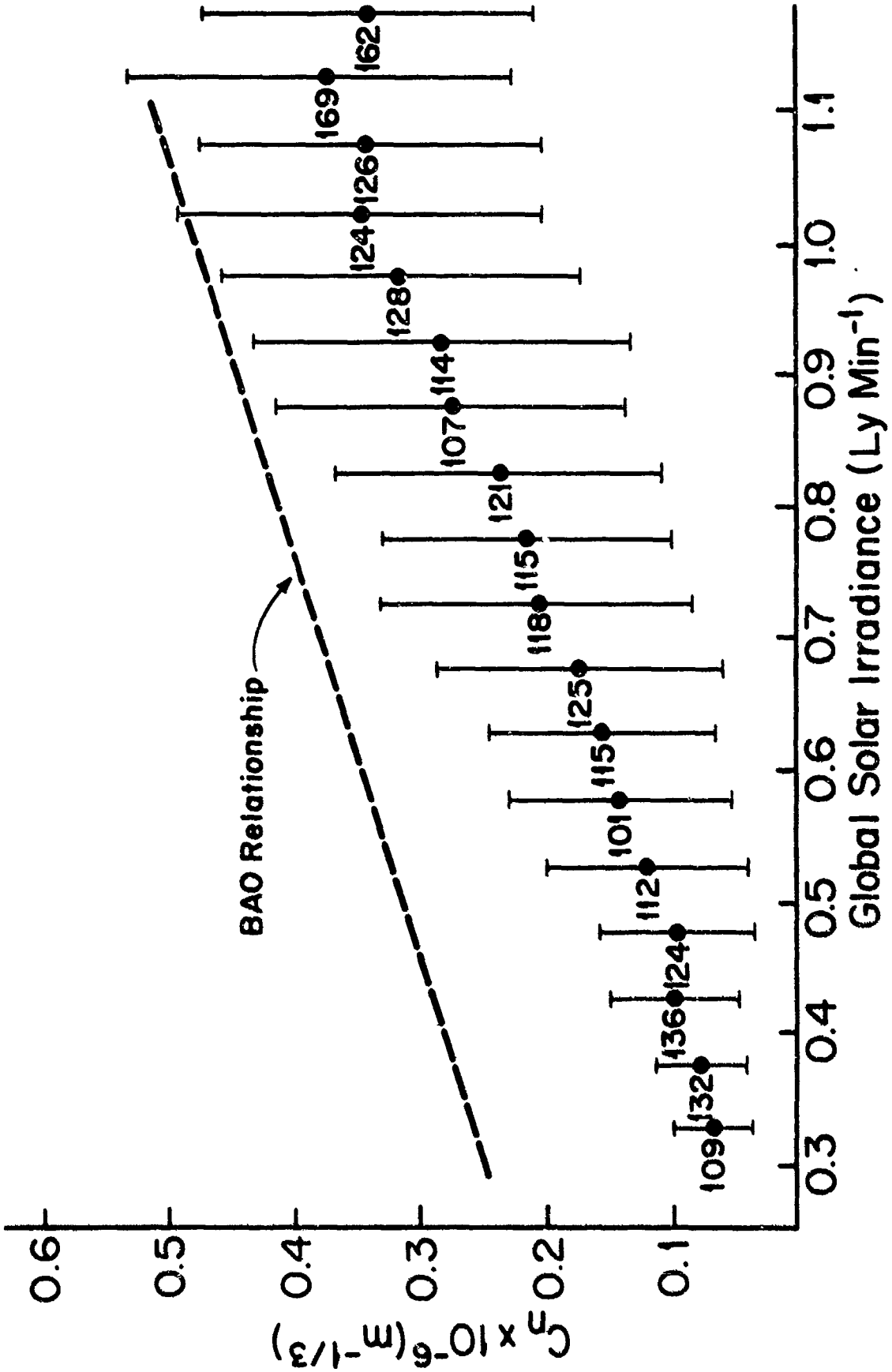

Fig. 5 C_n versus global solar irradiance for RADC and BAO data for irradiances between 0.3 and 1.2 Langley min^{-1}. The points are C_n averages in 0.05 Langley min^{-1} irradiance categories. Sample sizes and standard deviations are shown for the RADC data.

about $(10/4)^{-4/3} = 0.29$ and $(10/4)^{-2/3} = 0.54$. Reasons for this difference were not determined, but in addition to those given above, they involve questions regarding the accuracy of spectra at low wind speeds, assumptions regarding the isotropy of turbulence and possible effects of a tower structure on temperature spectra for certain wind directions. For these reasons, values of C_n^2 obtained from BAO temperature spectra were analyzed independently of those obtained from the scintillometer.

A comparison was also made between scintillometer and temperature probe estimates of C_n^2 at heights of 4 and 14 m for 2 cloudless days (7 and 8 Sept. 1984) at White Sands, NM. The 4-m and 14-m scintillometers had path lengths of 400 m and 1 km, respectively. With the temperature difference sensors, the temperature structure parameter C_T^2 was determined with the expression:

$$C_T^2 = \overline{(\Delta T)^2}\, R^{-2/3} , \qquad (12)$$

where ΔT is the rms value of the temperature difference and R is the distance between sensors, assuming isotropy of turbulence and that R is within the inertial subrange. A listing of daytime values of meteorological variables and C_n^2 for every hour on the hour for the 2 days is given in Table 9. Occasional large differences are evident for a given height that could be due to the factors discussed above in addition to the visual-manual method used to abstract the values, but in general, acceptable agreement for these and other days was found.

Table 9 Values of meteorological variables and C_n^2 on the hour for 2 cloudless days at White Sands, NM

DATE	TIME (MST)	$T_{SFC}-\bar{T}_{AIR}$[1] °C	WIND[2] DIR.	WIND[2] SP(ms^{-1})	SOLAR[3] Wm^{-2}	$C_n^2 \times 10^{-14}$ ($m^{-2/3}$) SCINT.[4] 4m	SCINT.[4] 14m	ΔT PROBES[5] 4m	ΔT PROBES[5] 14m
9/7/84	07	3.3	360	0.7	200	5.7	1	14	40
	08	8.9	280	0.7	413	15	0.4	9.7	7
	09	11.1	290	2.8	640	19	5	7	3.6
	10	13.9	360	2.2	813	29	6.7	11	6.2
	11	18.9	330	1.8	884	38	7.4	35	9.6
	12	19.4	310	3.8	917	38	11	37	8.1
	13	18.3	320	4.5	891	35	11	34	10
	14	17.2	300	3.5	815	38	8.5	30	7
	15	15.0	310	3.6	660	28	6.7	24	6.1
	16	7.8	300	2.6	451	17	3.4	12	3.6
	17	1.7	290	2.3	227	4.8	0.8	1.7	0.6
9/8/84									
	07	3.3	360	0.6	180	5.2	1.2	8	6.5
	08	8.3	360	0.4	412	14	2	14	13
	09	12.8	360	1.4	635	25	5.3	18	17
	10	16.7	350	1.4	804	35	6.3	42	42
	11	20.0	230	1.3	892	45	7.5	41	12
	12	21.1	210	1.3	917	50	10	45	10
	13	20.6	220	1.6	895	48	8.6	45	17
	14	19.4	360	1.6	809	45	7.2	39	15
	15	15.6	300	2.2	667	28	6.7	28	11
	16	7.8	290	1.7	457	15	3.3	13	3.5
	17	1.7	310	2.5	224	2.4	0.7	1	0.2

1 $\bar{T}_{air}$ is average of temperatures at 0.5, 1, 2, 4 m estimated from curve drawn through graphed diurnal variation, tower 2(HIDL).

2 Wind velocity at 4m, tower 1 (HIDL).

3 Global solar irradiance at 14 m, tower 1 (HIDL).

4 Scintillometer path length is 400 m at 4 m and 1 km at 14 m (HIDL).

5 Horizontal temperature difference probes, tower 1 (HIDL).

3. Data analysis

The approach in the analysis was to develop and test relationships that will (1) provide estimates of $C_n^2(C_T^2)$ for one height in the atmosphere's first few meters, (2) estimate the depth of the daytime convective boundary layer with solar radiation, cloud and wind speed information and (3) apply an expression similar to that of Kukharets and Tsvang (1980) to obtain $C_n^2(z)$. It is assumed that because the magnitude of C_n^2 near the ground is determined by thermal and mechanical turbulence processes linked by similarity principles, the value of C_n^2 at one height can, in most cases, be a reliable indication of its profile above or below that height. As an extreme example, with adiabatic conditions throughout the boundary layer, minimum values of C_n^2 can be expected. Not until C_n^2 reaches a certain value at a given height should it reflect the thermal and wind structure described by similarity theory that leads to a particular variation with height.

3.1 $C_n^2(C_T^2)$ in unstable stratification

Determining effects of solar radiation was emphasized for the following reasons: (1) the amount of direct and diffuse solar radiation reaching the ground is the primary determinant of how much heating of the ground takes place and how unstable the lapse rate in the surface layer will become as it is acted on by wind to produce $C_n^2(C_T^2)$, (2) it can be estimated for time intervals as short as an hour if location (latitude, longitude), date, time of day, and cloud type, height and amount are known (Kasten and Czeplak, 1980) and (Turner and Mujahid, 1984), and (3) it is implicitly important in determinations of z_i, as shown in Fig. 2 (Smith, 1977).

In this section, relationships among these variables are developed for the RADC and BAO data for a single height and tested with hourly values of C_n^2 abstracted from graphs for 17 days for CLEAR I. Also, measured boundary layer profiles of C_n^2 for CLEAR I and II are compared with profiles calculated with the K-T model, using C_n^2 measured at a reference height and values of z_i obtained from temperature and humidity profiles.

3.1.1 Single-height relationships

For the RADC data 3-minute values of C_n were graphed against solar irradiance for individual days shown in Table 6. For most days, C_n increased linearly with solar irradiance from an early morning minimum just after sunrise to a midday maximum near solar noon and then decreased linearly to a late afternoon minimum. The afternoon minima of C_n occurred at higher values of solar irradiance than the morning minima and are explainable in terms of energy exchange processes and the time of occurrence of a near adiabatic temperature profile after sunrise and before sunset.

For most of the RADC days analyzed, it was found that for a given solar irradiance either side of solar noon, mid-afternoon values of C_n were commonly half those in mid-morning. An example is shown in Fig. 6, which is a computer graph of values for 15 May 1982, a day with about 2/10 cloudiness and a wind speed of 3 ms^{-1}. It can be noted that a morning increase of C_n to a maximum has values that are about twice those of an afternoon decrease to a minimum. Although less frequent and less pronounced, this difference also occurred for a few days in the BAO scintillometer data and was evident in a sample C_n^2 recording for

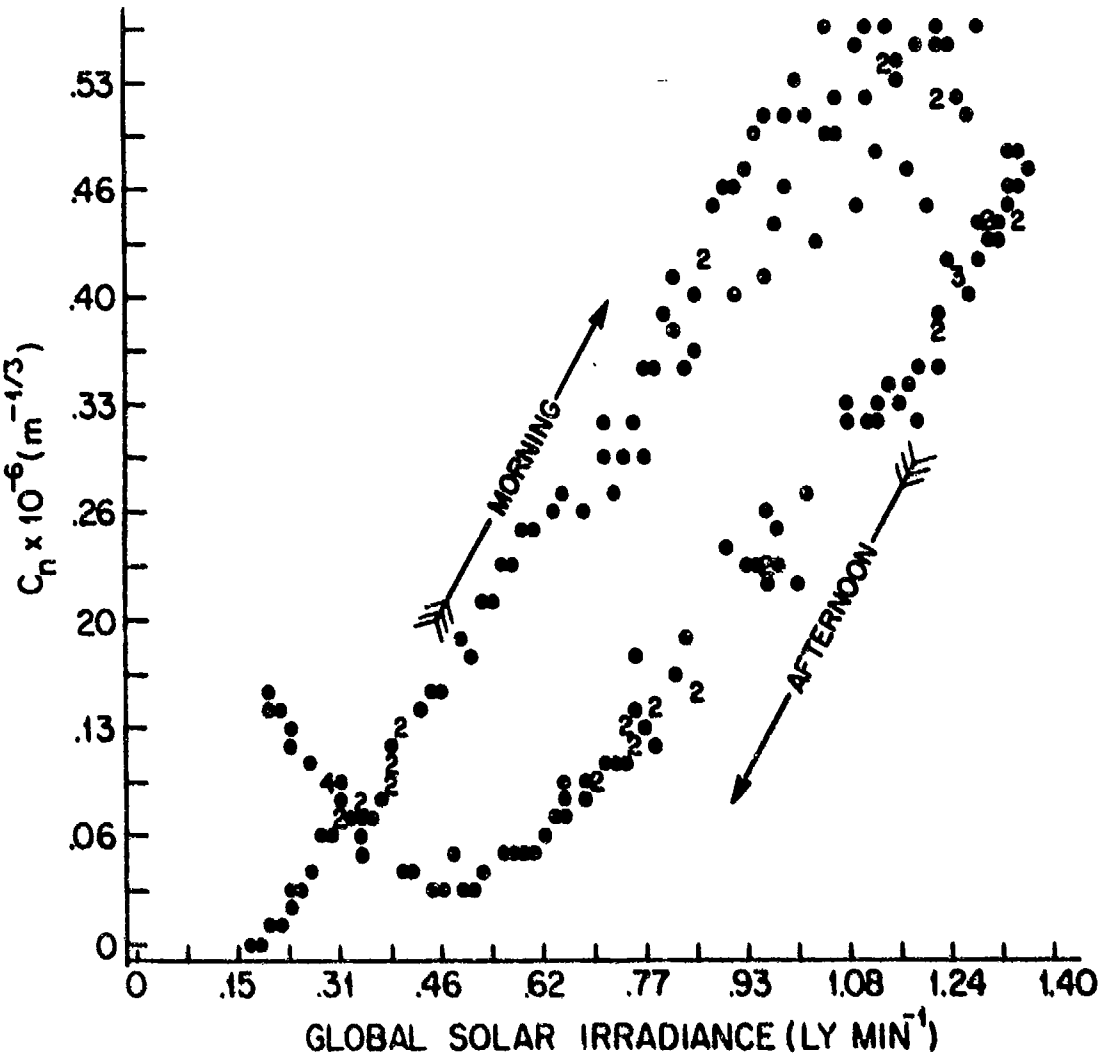

Fig. 6 C_n versus global solar irradiance for 15 May 1982 for the Rome Air Development Center, NY (RADC).

one day for Table Mountain, CO (Ochs, personal cummunication). It was not evident, however, in hourly values abstracted for 7 cloudless days in the CLEAR I data for White Sands, NM.

If the morning to afternoon differences at RADC are accepted as being due to natural causes and not to the equipment used, a reasonable explanation is possible that involves the availability of soil moisture for evaporation. If adequate soil moisture is available, differences in energy exchange processes involving latent and sensible heat transfer, net radiation and soil heat transfer from morning to afternoon result in greater vertical temperature differences before solar noon than afterward, "external" conditions remaining steady. Such a soil moisture condition could be expected most of the time in the moist, grass-covered RADC test site, occasionally at BAO following rain, but seldom at White Sands, where water content (% by weight) in September, 1981, was found to range from near zero to about 7% (Smith, 1984). Profile and other measurements are necessary to test the explanation given above.

Because (1) morning to afternoon differences in C_n were rare and not as pronounced at BAO and (2) C_n was measured at 4 m and the wind speed was measured at a standard height of 10 m, the BAO data were used to develop the final regression equation involving C_n, solar irradiance and wind speed. Fig. 7 shows average values of C_n versus solar irradiance (RAD) for the BAO data that were used to develop the regression equation. Standard deviations are shown as vertical line segements and sample sizes are given below each average.

In Fig. 7 a nearly linear increase of C_n from small values at irradiances less than 0.3 ly min^{-1} to maximum values at irradiances

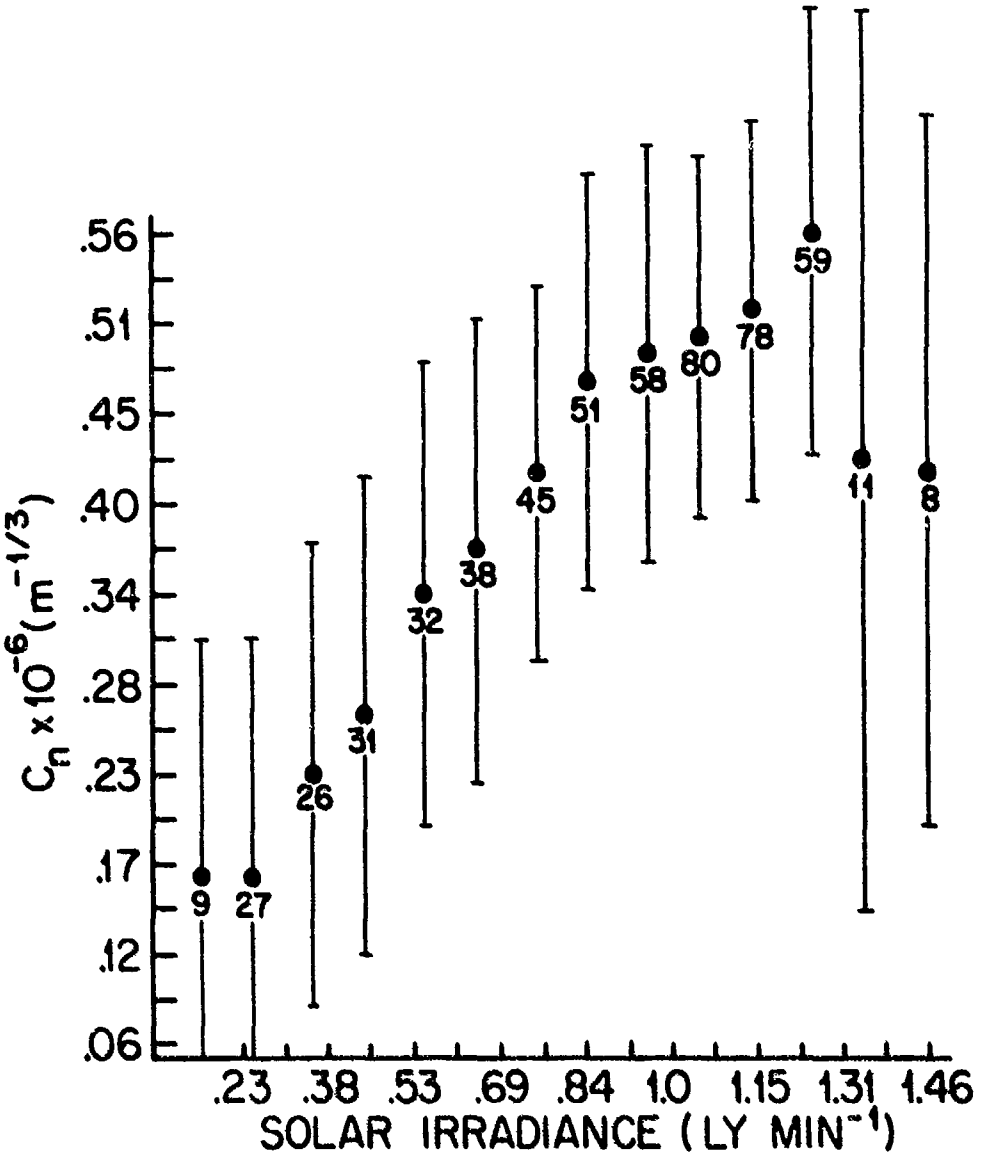

Fig. 7 C_n versus global solar irradiance for the BAO scintillometer data.

near 1.25 ly min^{-1} can be noted, with a decrease in C_n for irradiances between about 1.25 and 1.47 ly min^{-1}. For RAD $\lesssim$ 0.3 ly min^{-1}, the small values of C_n are representative of the morning and afternoon transitions in $\Delta T/\Delta z$, as C_n approaches the noise level of a scintillometer system. For 0.3 $\lesssim$ RAD $\lesssim$ 1.25 ly min^{-1}, a linear increase in C_n reflects the increase in $\Delta T/\Delta z$ with increased solar heating of the surface. For 1.25 $\lesssim$ RAD $\lesssim$ 1.5 ly min^{-1} a decrease in C_n is more difficult to interpret without measurements of $\Delta T/\Delta z$ because the reason for C_n leveling off and then decreasing could be meteorological, within the C_n measurement system or a combination of both. The last 2 data points with fewer samples, for example, are for very high irradiance values that are likely comprised of brief increases that are commonly caused by multiple reflections from well-developed cumulus clouds. In addition, with the large values of $\Delta T/\Delta z$ that probably occur in this region, light source-to-receiver alignment problems could be caused by large mean refraction in the optical path (see also RADC data, Fig. 5).

Wind speed effects were determined from graphs of C_n vs 10-m wind speed (u_{10}) for various categories of solar irradiance, from which it was found that for irradiances greater than about 0.5 ly min^{-1}, $\bar{C}_n$ increased with u_{10}, reached a maximum near u_{10} = 2-3 ms^{-1} and gradually decreased at higher speeds.

The regression equation involving C_n, solar irradiance (RAD) and wind speed (WS) was developed in terms of RAD, RAD^2, and RAD^3 and WS, WS^2, and WS^3. Third-order polynomials were chosen for these variables to account for (1) the two inflection points for C_n vs RAD shown in Fig. 7 and (2) the one inflection point for the C_n vs WS relationship. The equation for the BAO data is:

$$C_n = .12724 \times 10^{-6} + .17314 \times 10^{-6}(RAD) - .33899 \times 10^{-7}(WS)$$
$$+ .62238 \times 10^{-6}(RAD)^2 + .10264 \times 10^{-7}(WS)^2 \quad (13)$$
$$- .39727 \times 10^{-6}(RAD)^3 - .53824 \times 10^{-9}(WS)^3$$

where RAD is solar irradiance in ly min^{-1}, WS wind speed in ms^{-1}, and C_n in $m^{-1/3}$.

The equation is valid for irradiances between 0.07 and 1.49 ly min^{-1} and for 10-m wind speed from about 0.3 to 19 ms^{-1}. It can be noted that a value of $C_n < 0$ is possible for certain values of irradiance and wind speed. This is a consequence of the method of regression. A value of C_n on the order of $10^{-8} m^{-1/3}$ can be assumed for a calculated $C_n < 0$.

3.1.2 Boundary layer profiles

Fig. 8 shows average profiles of C_T^2 for 8 heights between 10 m and 300 m for 5 daytime periods of the 1978 PHOENIX experiment. Because height is on the ordinate, the line with the -3/4 slope shown for reference actually corresponds to $C_T^2 \propto z^{-4/3}$. It can be noted that except for values of C_T^2 at heights between 200 and 300 m on 26 September, a $z^{-4/3}$ relationship is followed quite closely. For all the profiles in Fig. 8, measurements of z_i were made with various methods (Kaimal et al., 1980 and 1982) and showed that z_i was above the 300-m height. On 26 September, however, it was not well-defined and could not be detected as an increase in temperature with conventional radiosonde temperature measurements. z_i, as a capping inversion and having other properties detectable by all methods, was most pronounced on 21 September, when it increased from 500 m to approximately 850 m during the period represented by the C_T^2 profile.

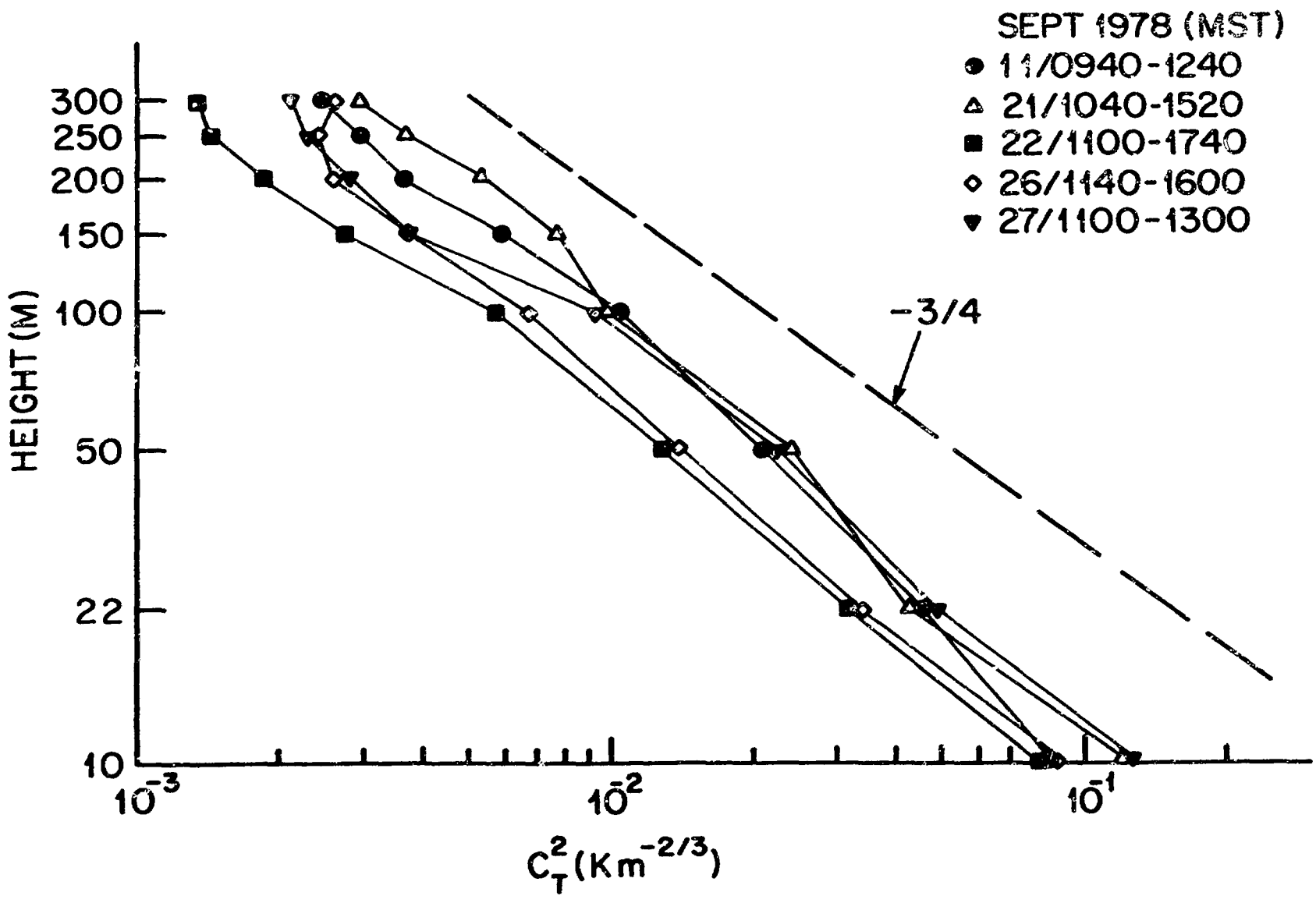

Fig. 8 Average profiles of C_T^2 for 5 daytime periods from the NOAA Boulder Atmospheric Observatory for the 1978 PHOENIX experiment.

A comparison was made between available measurements of z_i reported by Kaimal and estimates of z_i from the Smith (1977) nomogram shown in Fig. 2. Results for 21, 22, 26 and 27 September are shown in Table 10.

Table 10 Measured and estimated values of z_i for 1300 MST for BAO data from PROJECT PHOENIX

Date (Sept. 1978)	Cloudiness	u_{10} (ms^{-1})	z_i(m) Meas.	Calc.
21	clear	1.0	850	750
22	2/10 cirrus	1.3	480	650
26	clear	3.0	650	900
27	clear	1.5	680	800

Comparisons were made between profiles of C_n^2 obtained with the K-T model and values of C_n^2 measured with thermosondes during CLEAR I & II and height-averaged with the method given in Table 2. The results of the comparisons made for soundings with convective conditions and less than 0.5 cloudiness are shown in Fig. 9a through 9i. In each figure, the coordinates are logarithmic and the abscissa scale for log C_n^2 is the same ($\sim 10^{-19}$ to 10^{-13}). The numbers on the ordinate are actual heights that correspond to the logarithmic height scaling by computer. The solid line is the C_n^2 profile calculated with the K-T model and the dots are measured values. Values of $C_n^2(z)$ were calculated with the K-T model equation as modified by Murphy, Dewan, and Sheldon (1985), hereafter referred to as MDS, to be applicable to any reference height, z_r, instead of $z_r = 0.1$ as in Eq. 9: The expression for $C_n^2(z)$ used in the calculations was:

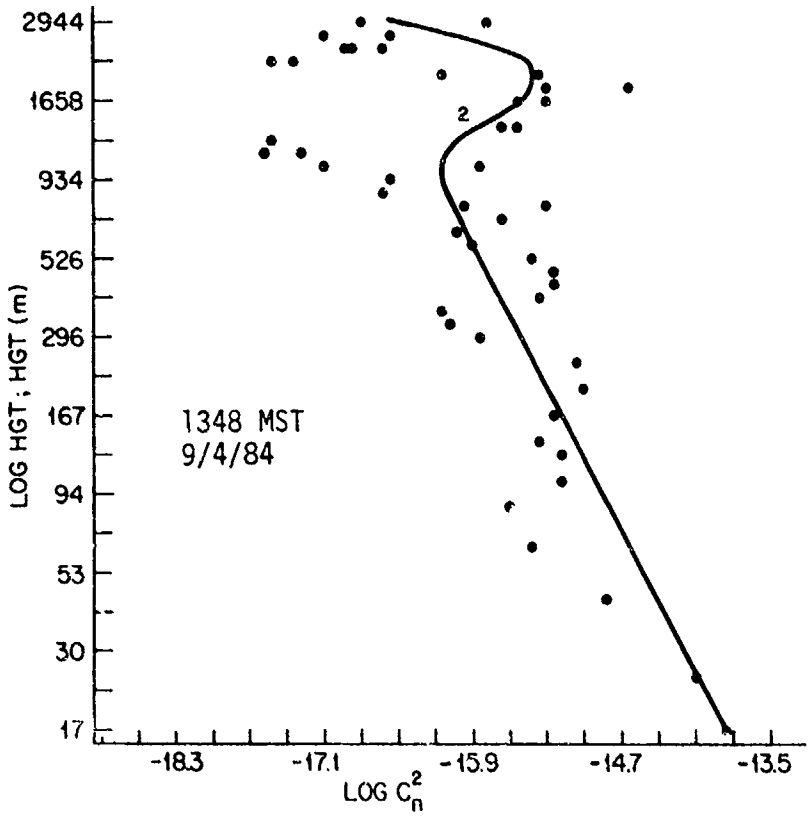

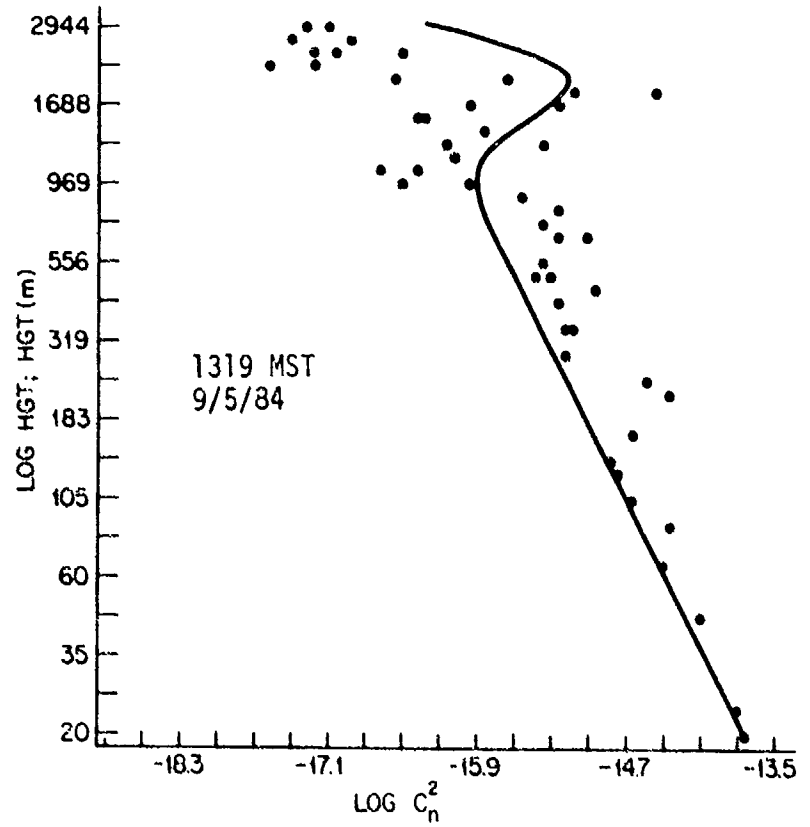

Fig. 9a Comparison of C_n^2 profile calculated with the Kukharets and Tsvang model and measured values for unstable stratification at White Sands, NM for 1348 MST, 9/4/84 and 1319 MST, 9/5/84. Measured values are height-averaged as in Table 2.

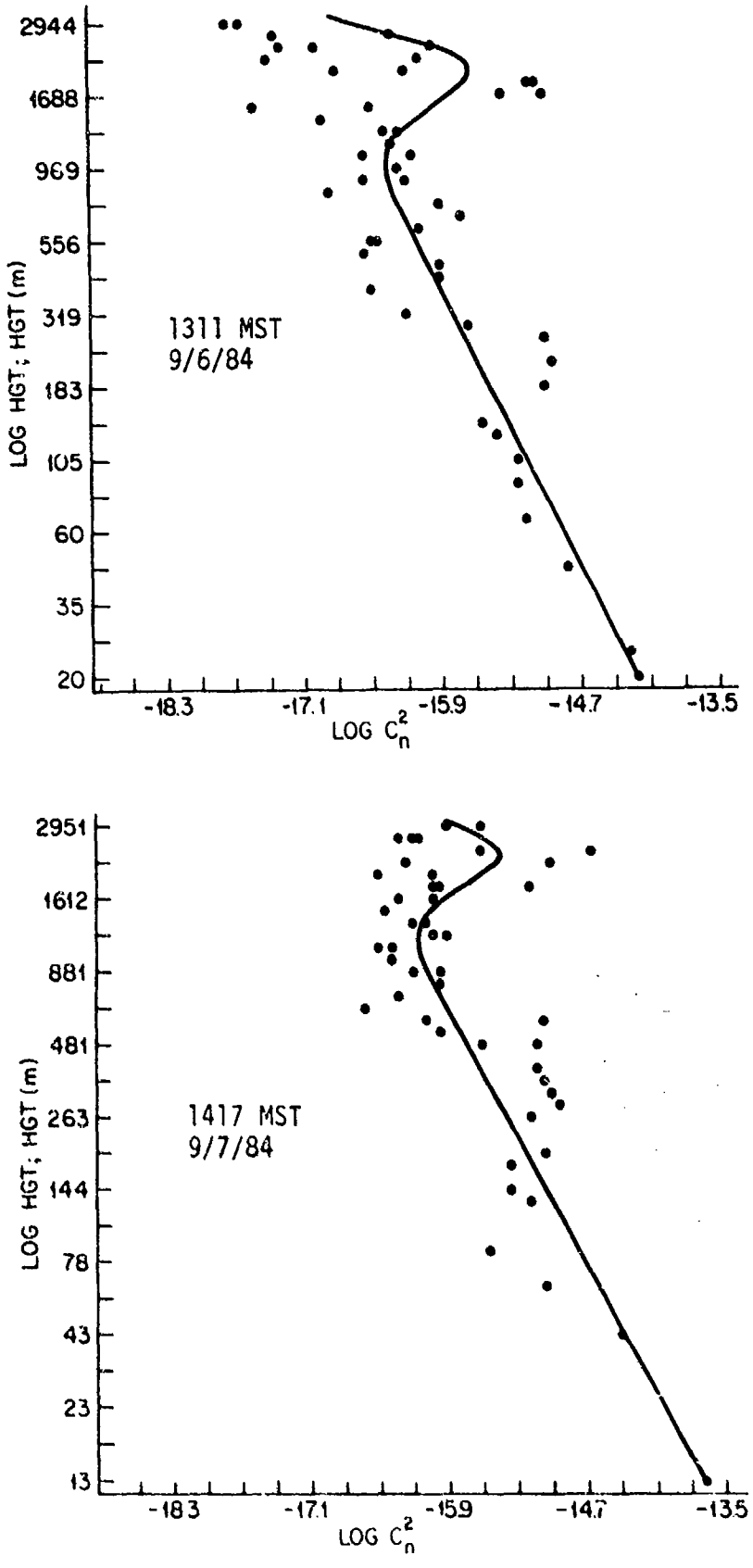

Fig. 9b Same as 9a, but for 1311 MST, 9/6/84 and 1417 MST, 9/7/84.

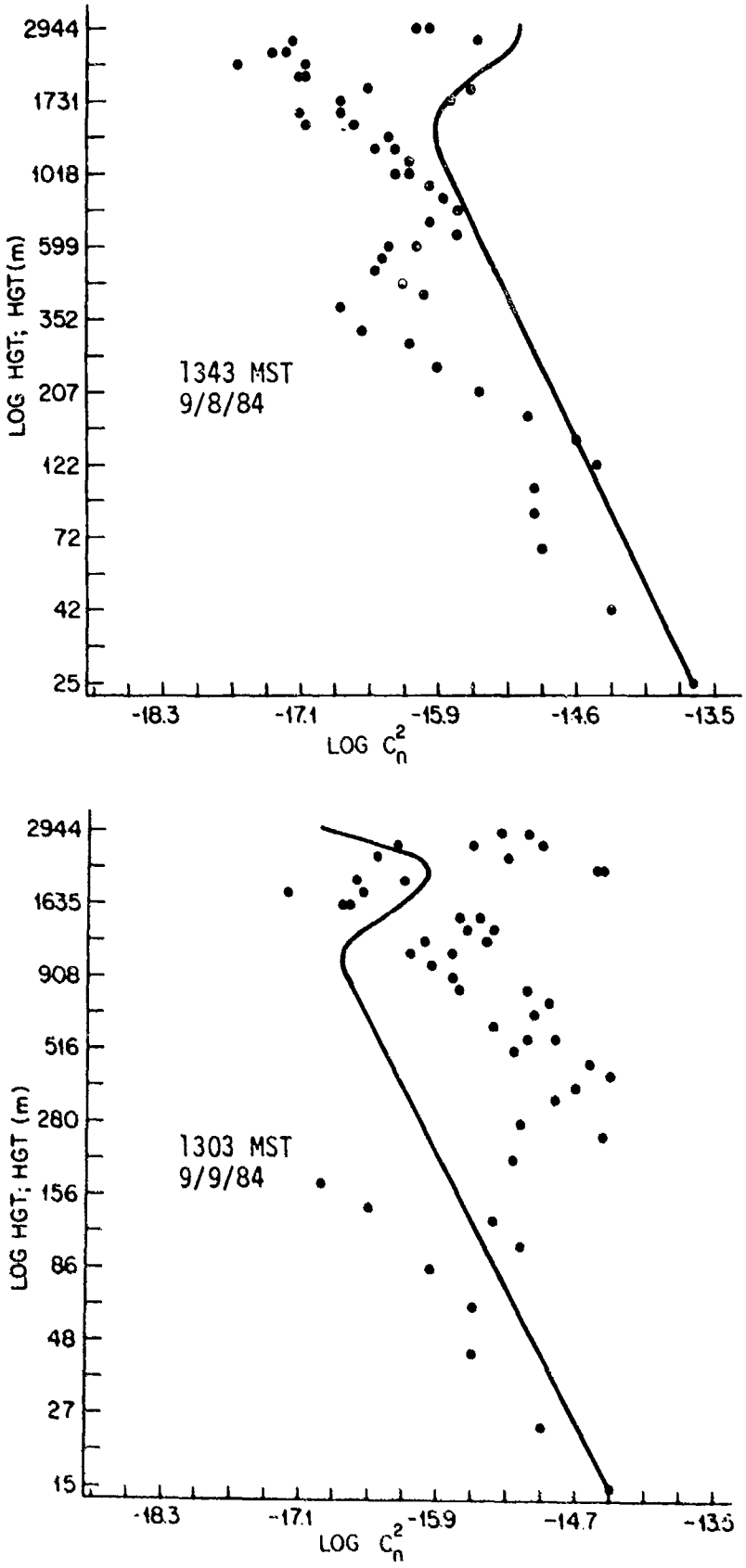

Fig. 9c Same as 9a, but for 1343 MST, 9/8/84 and 1303 MST, 9/9/84.

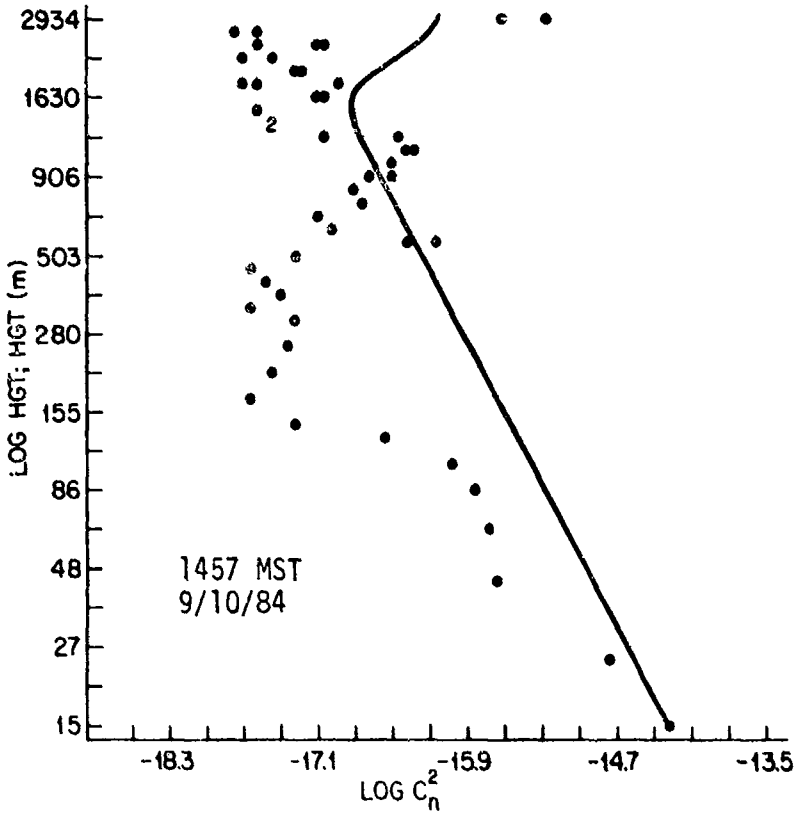

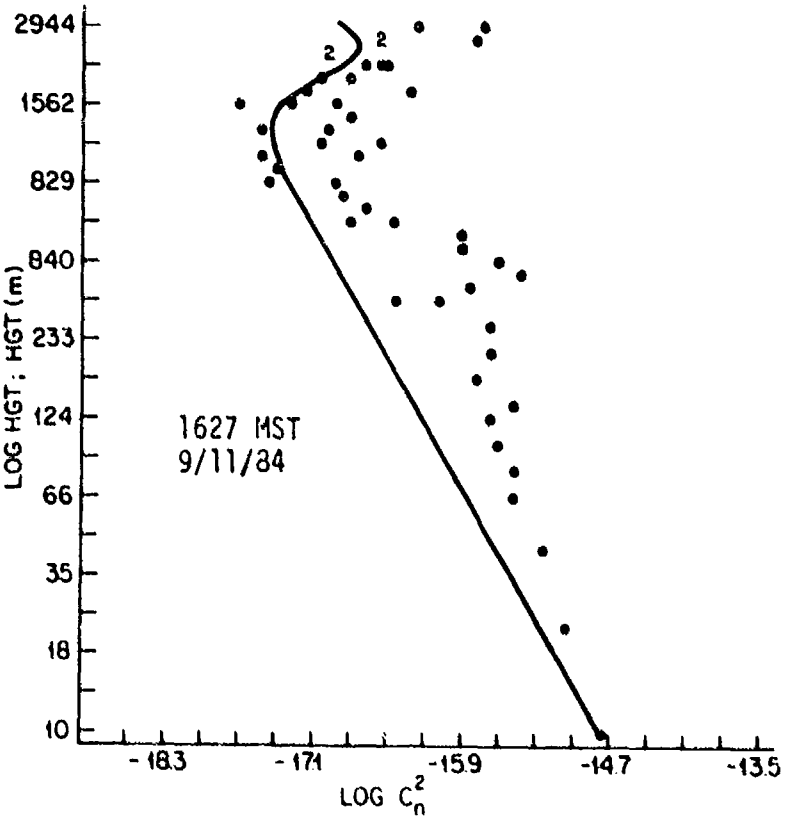

Fig. 9d Same as 9a, but for 1457 MST, 9/10/84 and 1627 MST, 9/11/84.

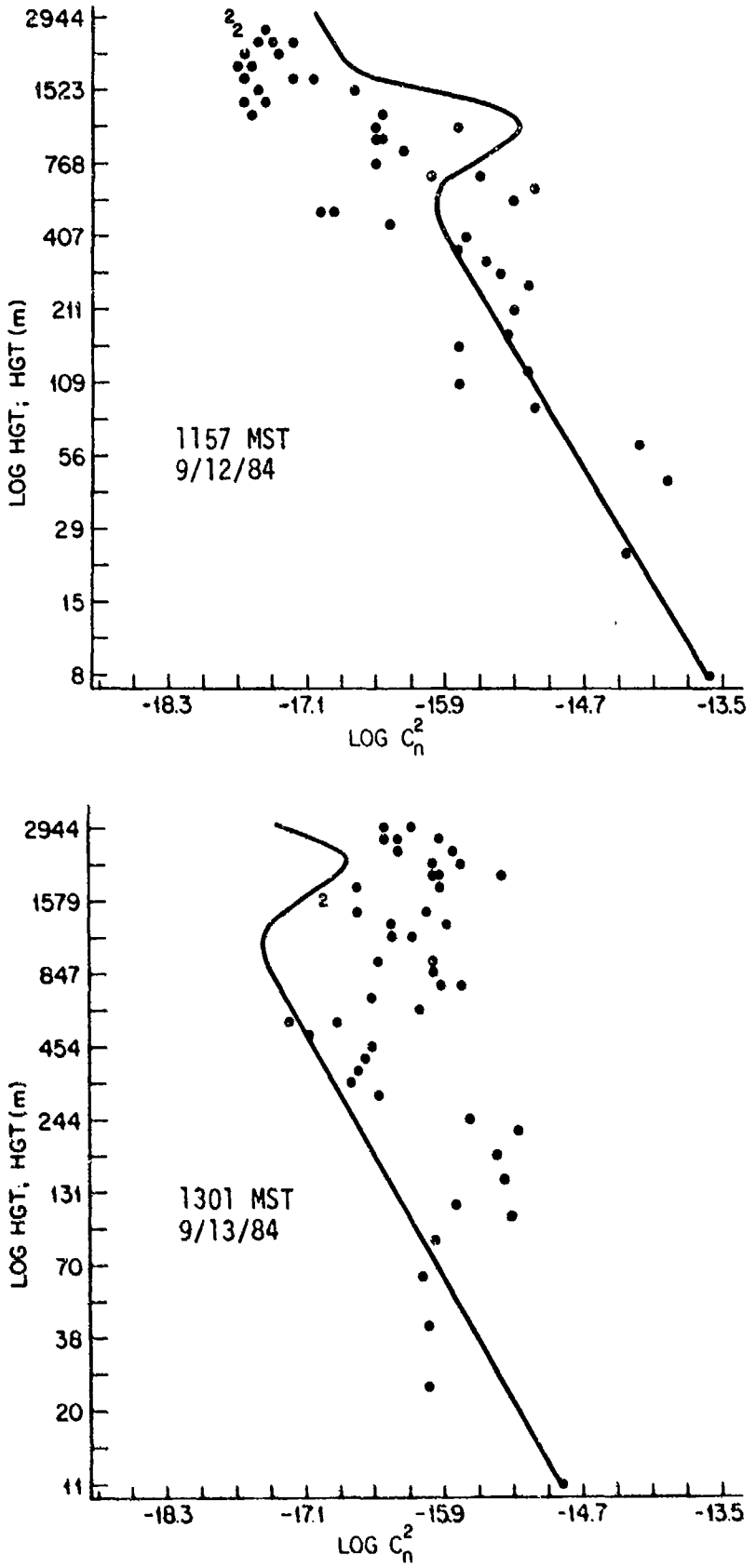

Fig. 9e Same as 9a, but for 1157 MST, 9/12/84 and 1301 MST, 9/13/84.

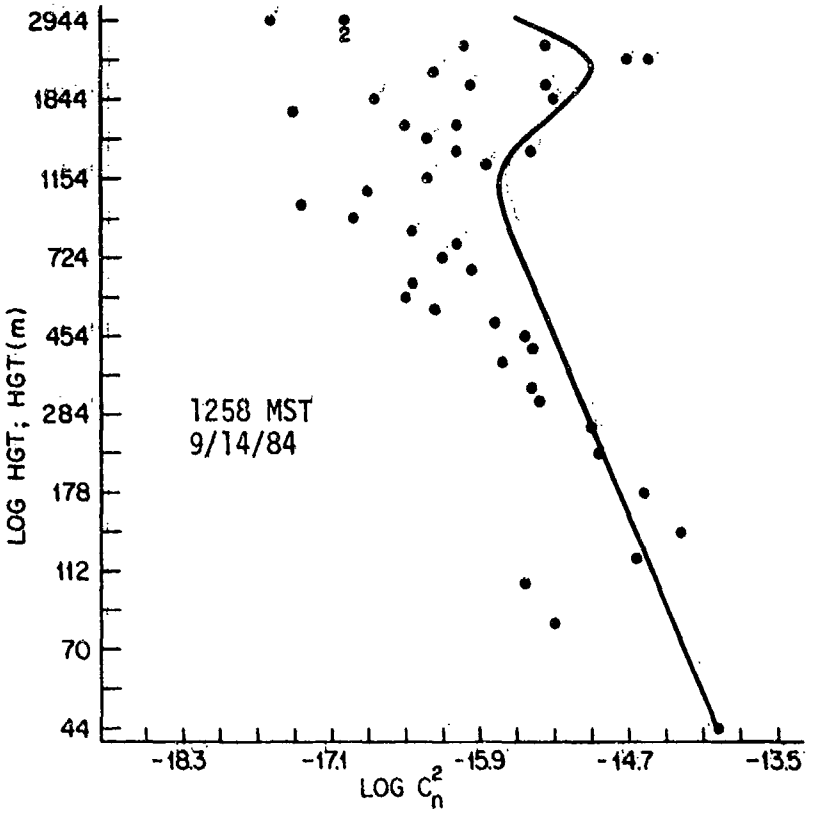

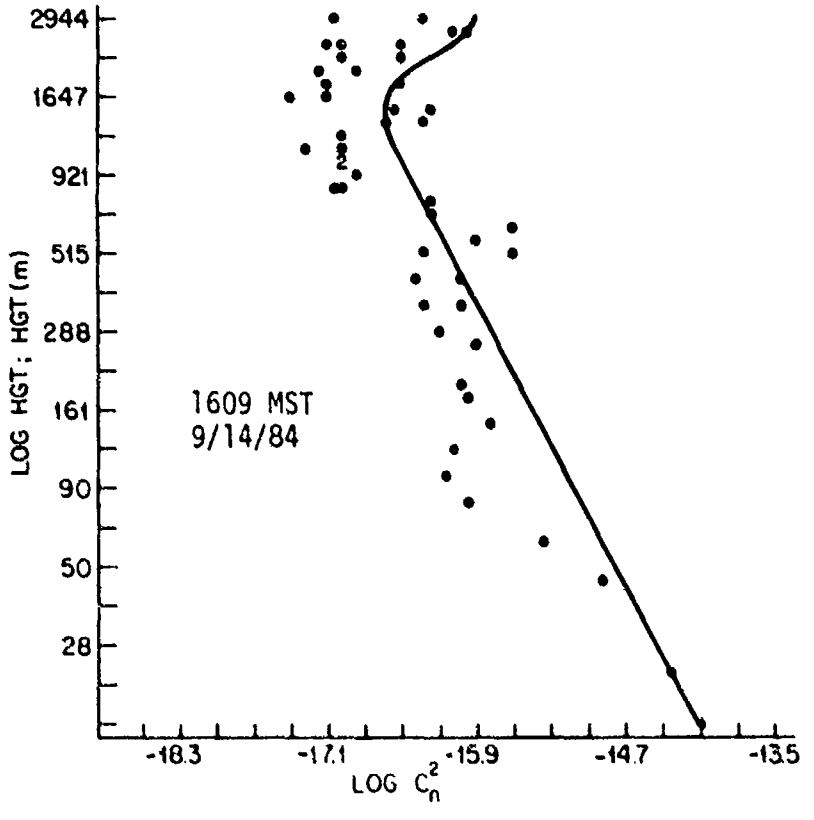

Fig. 9f Same as 9a, but for 1258 MST, 9/14/84 and 1609 MST, 9/14/84.

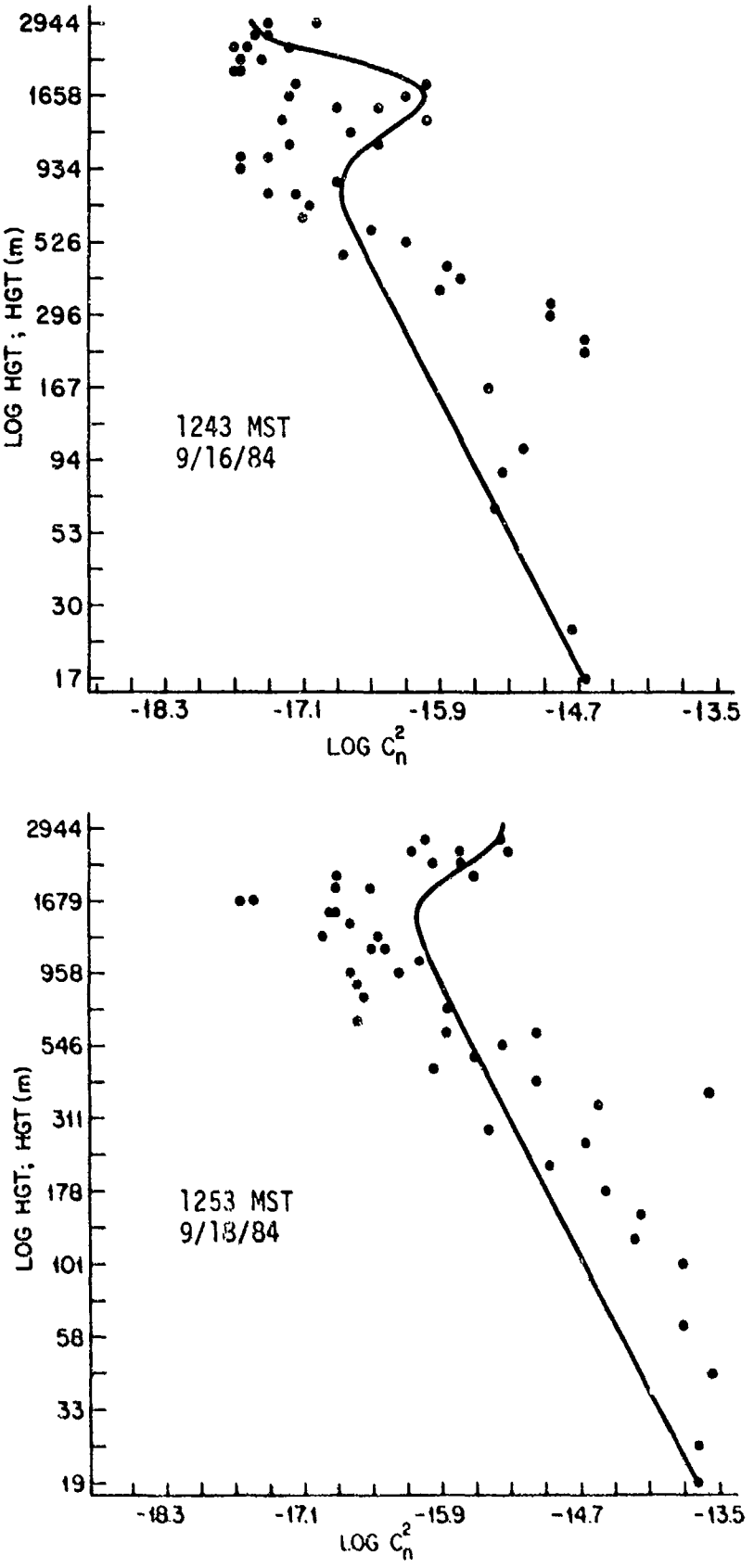

Fig. 9g Same as 9a, but for 1243 MST, 9/16/84 and 1253 MST, 9/18/84.

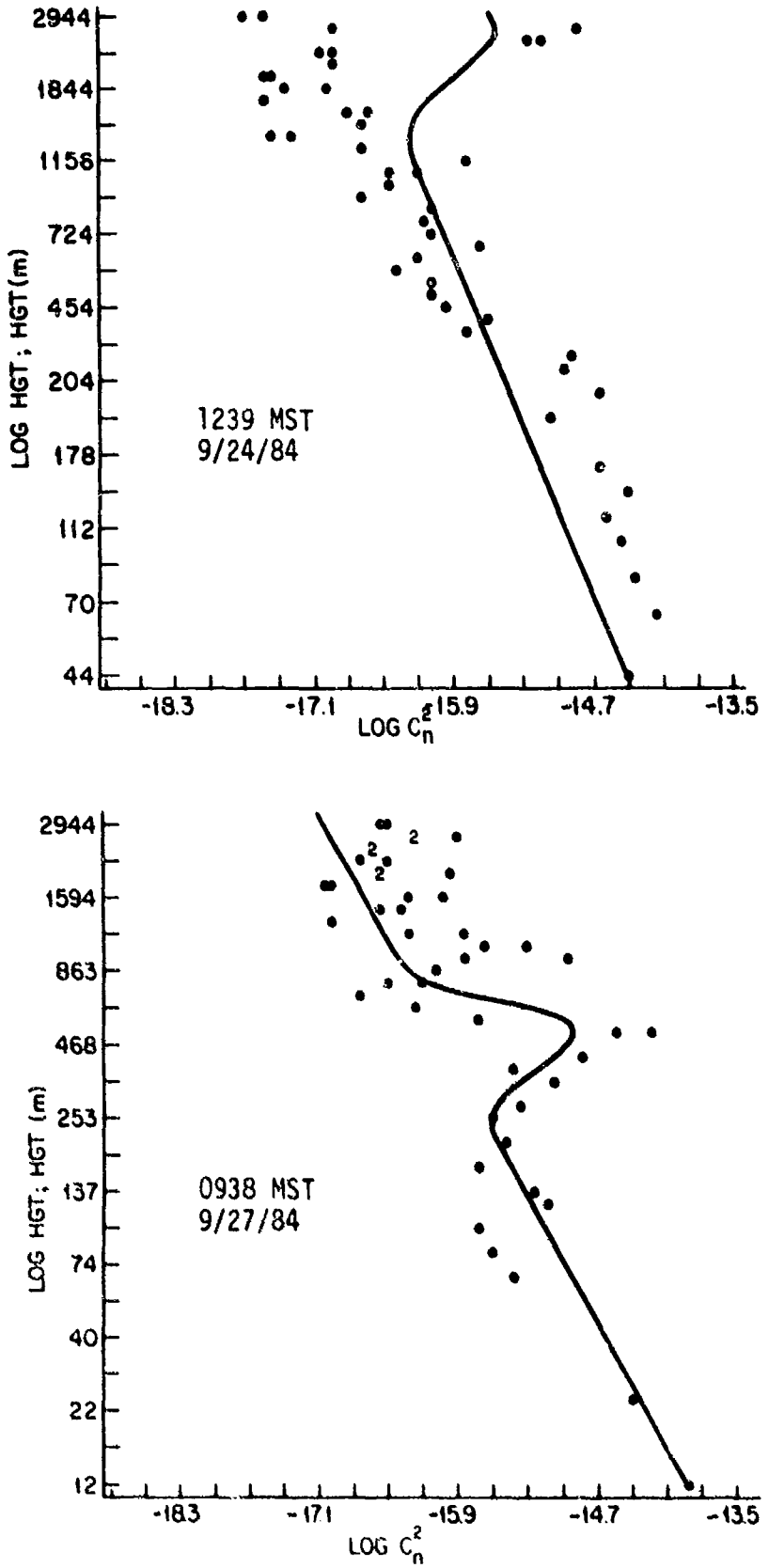

Fig. 9h Same as 9a, but for 1239 MST, 9/24/84 and 0938 MST, 2/27/85.

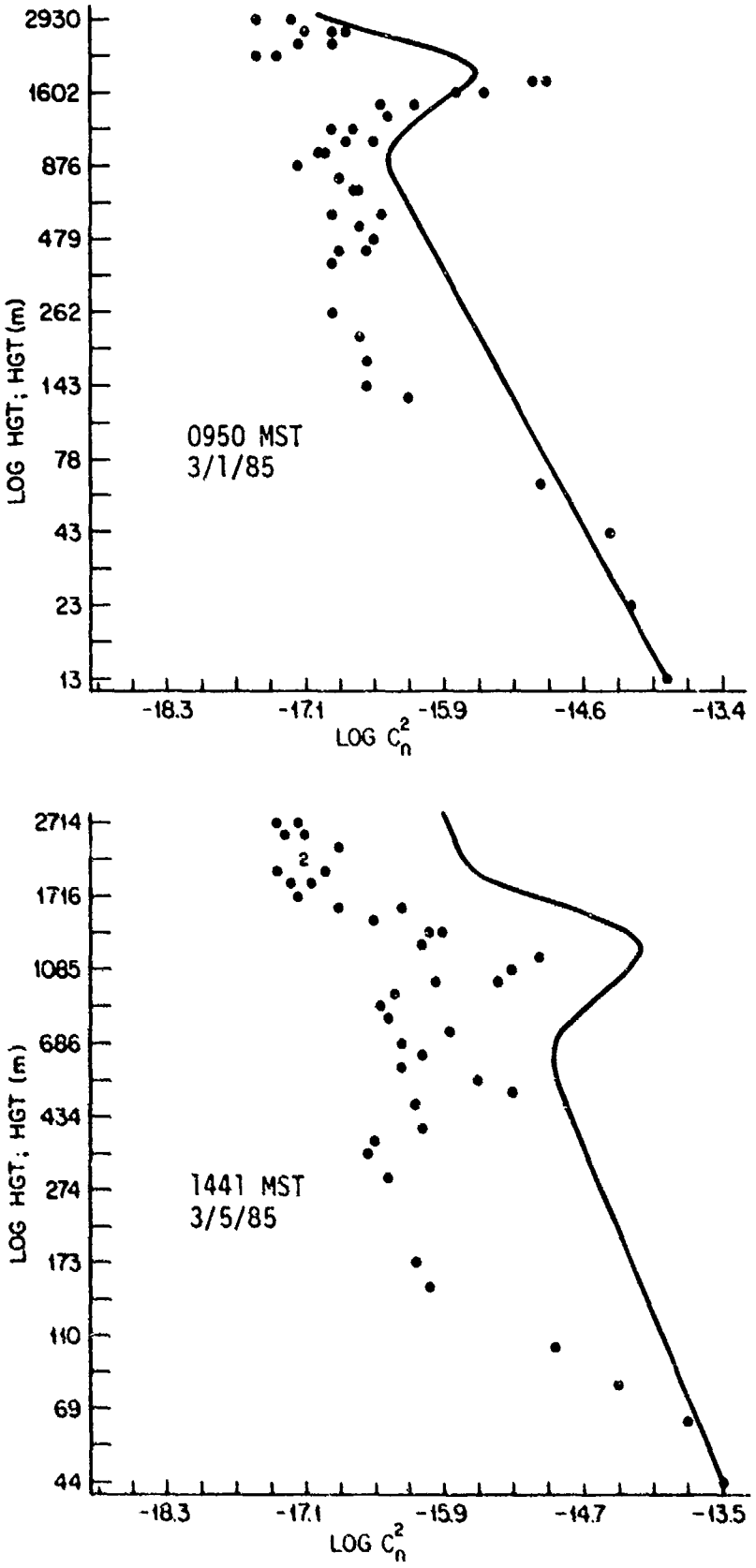

Fig. 9i Same as 9a, but for 0950 MST, 3/1/85 and 1441 MST, 3/5/85.

$$C_n^2(z) = C_n^2(z_0) \frac{0.046\ (z/z_i)^{-4/3} + 0.6\ \exp^{-12(z/z_i - 1.1)^2}}{0.046\ (z_0/z_i)^{-4/3}} , \quad (14)$$

where z_0 is a reference height, taken here to be the height of lowest measurement of C_n^2, T and R.H. for each sounding (excluding occasional "surface" measurements), z is height, and z_i is the top of the mixed layer obtained from profiles of temperature and relative humidity. Actual values of z_i and z_0 for each sounding are given in Table 4 .

Reasonably good agreement between the K-T model results and measurements of C_n^2 is evident, including the region with the secondary maximum of C_n^2 near z_i. The use of the C_n^2 value at the lowest height of measurement as a reference value for the model profiles worked well except for the profile on 1441 MST, 3/5/85. For this profile, the reference value of $C_n^2 \approx 4 \times 10^{-14}\ m^{-2/3}$ for z_0 = 44 m is unusually large for 44 m compared to values at the same height for other soundings and caused all calculated values to be larger than actual. There was no clear evidence that the distribution of C_n^2 in the region of z_i was narrower than the K-T model prediction as found by MDS, at least not enough narrower to support their value of k_3 = 580 instead of 12. Somewhat different results, however, could be expected because (1) different averaging techniques were applied by MDS to the C_n^2 data, and (2) in the work here, the values of z_i that were used in the calculations were also probably somewhat different.

The results support other findings that a knowledge of C_n^2 at z_0 is sufficient information, in most cases, to enable a profile of C_n^2 in a CBL to be described. With the single-height relationships involving C_n^2, solar irradiance and wind speed discussed in the previous section, estimates of C_n^2 at z_0 can be made that lead to boundary layer profiles with the MDS modification of the K-T model.

3.2 $C_n^2(C_T^2)$ in stable stratification

3.2.1 Single-height relationships

In contrast to the combined effects of positive buoyancy and vertical wind shear that enhance turbulence and $C_n^2(C_T^2)$ in a convective boundary layer, negative buoyancy and viscosity in a thermally stable boundary (SBL) act to suppress turbulence. In a SBL, mechanical turbulence is maintained by vertical wind shear alone, which acts on an increase in temperature with height to produce $C_n^2(C_T^2)$. At the air-ground interface, there is usually a nocturnal loss of heat from the surface by infrared radiation and a gain of heat by (1) a downward transfer of infrared radiation and sensible and latent heat from air to ground and (2) an upward transfer of heat by conduction through the soil. If the net heat exchange is negative, the surface becomes colder than the air and temperature increases with height.

Because of their pronounced effects on radiative and turbulent exchange processes in the boundary layer regardless of time of day, cloudiness and wind speed are the primary standard meteorological variables that determine nocturnal temperature and wind structure, and, therefore, values of $C_n^2(C_T^2)$. As clouds become fewer and/or higher (colder), for example, the net radiative exchange and surface temperature decrease and air temperature increases with height. For a completely cloudless sky, radiative loss is optimum and wind speed (shear), through its mixing action, becomes the controlling variable of the magnitude of the inversion in the first few meters. In the absence of large-scale advection of air that is much colder than the surface, the higher the wind speed, the smaller the inversion. For nocturnal conditions with radiative loss,

therefore, because $C_n^2(C_T^2)$ is caused by wind (shear) acting on a vertical temperature gradient, it was reasonable to expect that values of $C_n^2(C_T^2)$ at one height as well as their profiles would be relatable to wind speed. By confining the analysis to periods with a sky condition that was cloudless or scattered ($\leq$ 0.5 cloud-covered), furthermore, a large radiative loss leading to inversion formation could be expected, leaving wind speed alone as the most likely describer of $C_n^2(C_T^2)$ characteristics.

In line with this reasoning, the 4041 3-minute values comprising the RADC nighttime set of data for the periods listed in Table 5 were grouped into 1 mph categories of the wind speed at 2m, and the average values of C_n^2 and wind speed were obtained in each category. Categories with fewer than 30 samples were not retained, which meant that there were no wind speed categories with sufficient samples greater than 7 mph. The results of the grouping are shown in linear coordinates in Fig. 10. Values of $\overline{C}_n^2 \times 10^{-14} m^{-2/3}$ are on the ordinate and wind speed in mph is on the abscissa. It can be noted that $\overline{C}_n^2$ increases from a minimum of $0.5 \times 10^{-14} m^{-2/3}$ at a wind speed of $\sim$ 0.3 mph to a maximum of about $6.2 \times 10^{-14} m^{-2/3}$ at $\sim$ 4.3 mph and decreases sharply at higher speeds. Limited C_n^2 data obtained at higher speeds show that values become progressively smaller as wind speed increases, approaching about $10^{-17} m^{-2/3}$.

The data shown in Fig.10 were fitted with a normal curve shown by the solid line. It describes the RADC relationship quite well for nighttime conditions in the form:

$$\overline{C}_n^2 = 6.2 \times 10^{-14} \exp - \frac{(u_2 - 4.3)^2}{2(1.8)^2} , \qquad (15)$$

where 6.2×10^{-14} is the peak value of $\overline{C}_n^2$ occurring at a 2m wind speed (u_2)

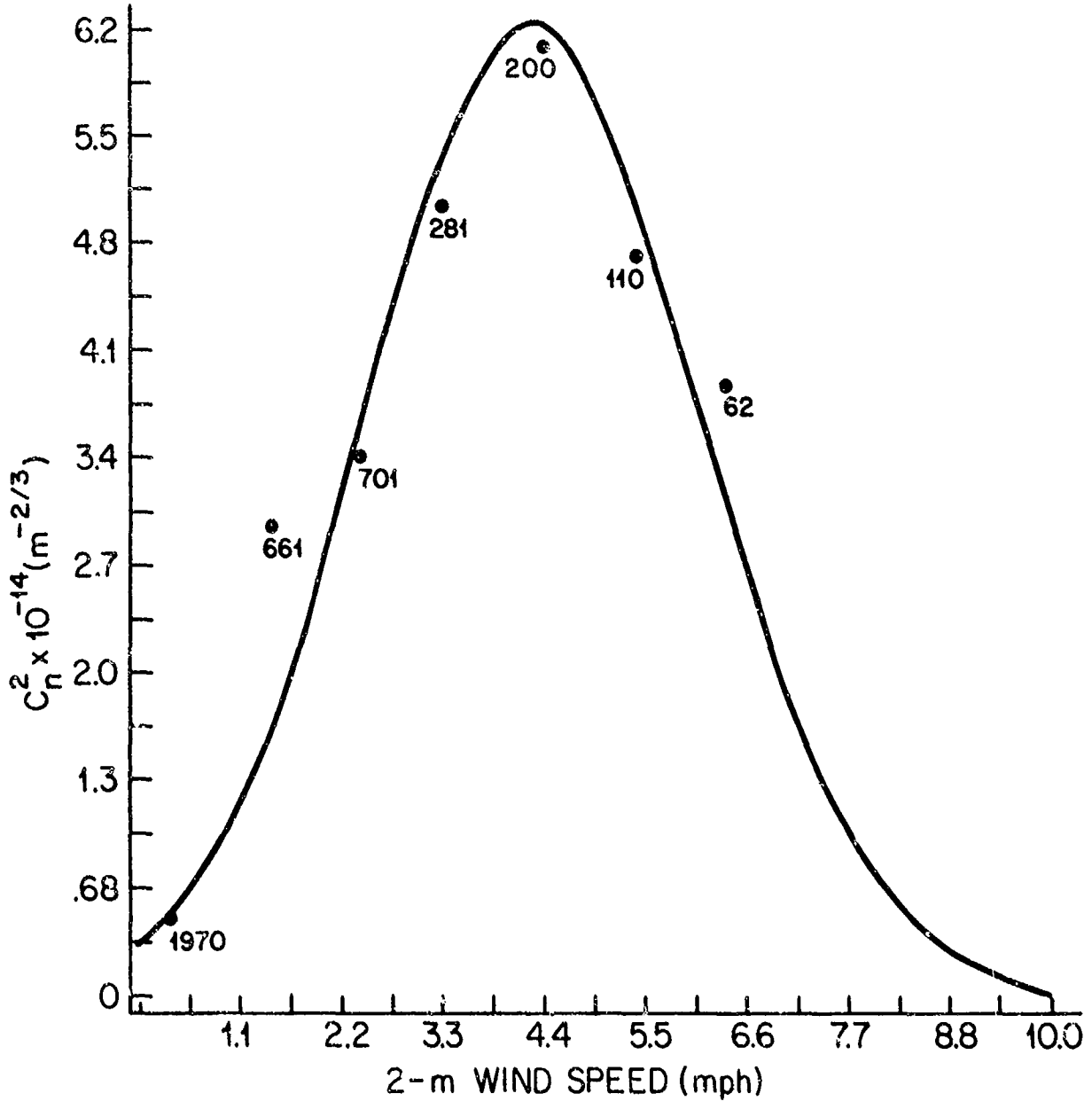

Fig. 10 C_n^2 versus 2-m wind speed on linear scales for nighttime conditions at RADC. The numbers are sample sizes.

of 4.3 mph, and 1.8 mph is the standard deviation of u_2 for the normal curve; about 68% of the area under the curve is between wind speeds of 2.5 and 6.1 mph.

Another portrayal of the RADC data is given in Fig.11 to illustrate sample sizes and standard deviations in the relationship. It has $\overline{C_n^2}$ on a logarithmic ordinate scale and wind speed on a linear abscissa scale. Sample sizes are given alongside each mean and the vertical lines are standard deviations. It can be noted that sample sizes range from 1970 for $\bar{u}_2$ = 3 mph to 62 for $\bar{u}_2$ = 6.4 mph and that the standard deviations are much larger for $\bar{u}_2$ < 3 mph, indicating turbulence intermittency.

Similar results were obtained with the scintillometer data for the BAO facility. In the BAO data, however, optical C_n^2 was measured at a height of 4 m, but the lowest height of wind speed measurement on the 300-m tower was 10 m. Averages of C_n^2 (4 m) and u_{10} in successive 1 ms^{-1} categories of $\bar{u}_{10}$ are shown in Fig.12 together with sample sizes and a normal curve estimated to fit $\overline{C_n^2}$ (4 m) vs u_{10}. It can be noted that compared to the RADC results, which show a peak of $\overline{C_n^2}$ (2 m) = $6.2 \times 10^{-14} m^{-2/3}$ at $\bar{u}_2$ = 4.3 mph (1.9 ms^{-1}), the BAO data have a peak of $\overline{C_n^2}$ (4 m) = $12.8 \times 10^{-14} m^{-2/3}$ near $\bar{u}_{10}$ = 4.0 ms^{-1} ($\sim$ 9 mph). The BAO relationship, fitted with the equation given below, is the nighttime single-height model for C_n^2 used in the profile calculations in Section 4.2.

$$\overline{C_n^2} = 12.8 \times 10^{-14} \exp \frac{-(u_{10}-4.0)^2}{2(2.3)^2} \quad , \qquad (16)$$

where 12.8×10^{-14} is the peak value of $\overline{C_n^2}$ (4 m) occurring at a 10 m wind speed of 4.0 ms^{-1}, and 2.3 ms^{-1} is the standard deviation of u_{10}.

The behavior of C_n^2 shown in Fig.10 and Fig.12 is caused by the interaction of wind speed (shear) with the thermally stable vertical

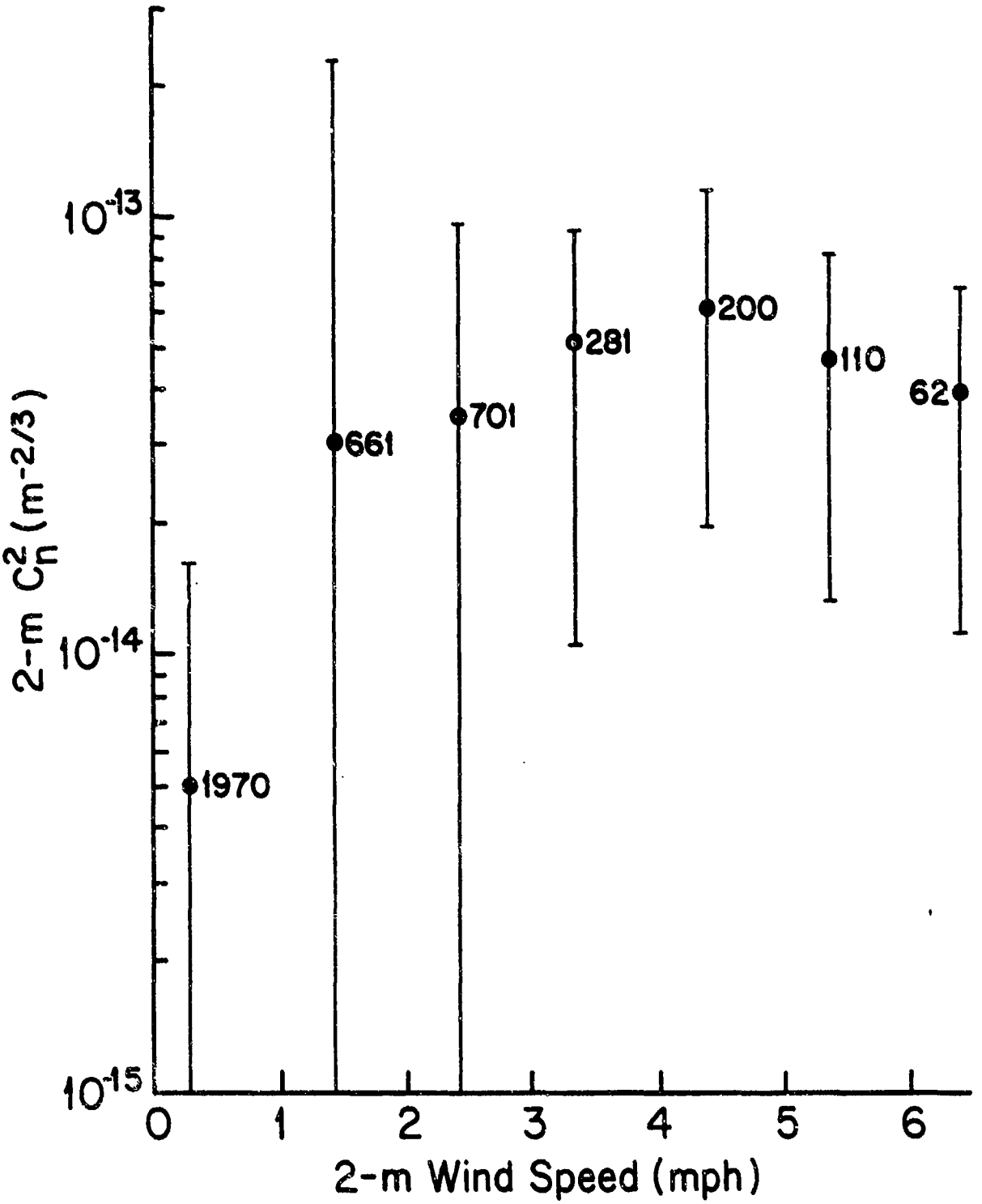

Fig. 11 Same as Fig. 10 but with C_n^2 on a logarithmic scale.

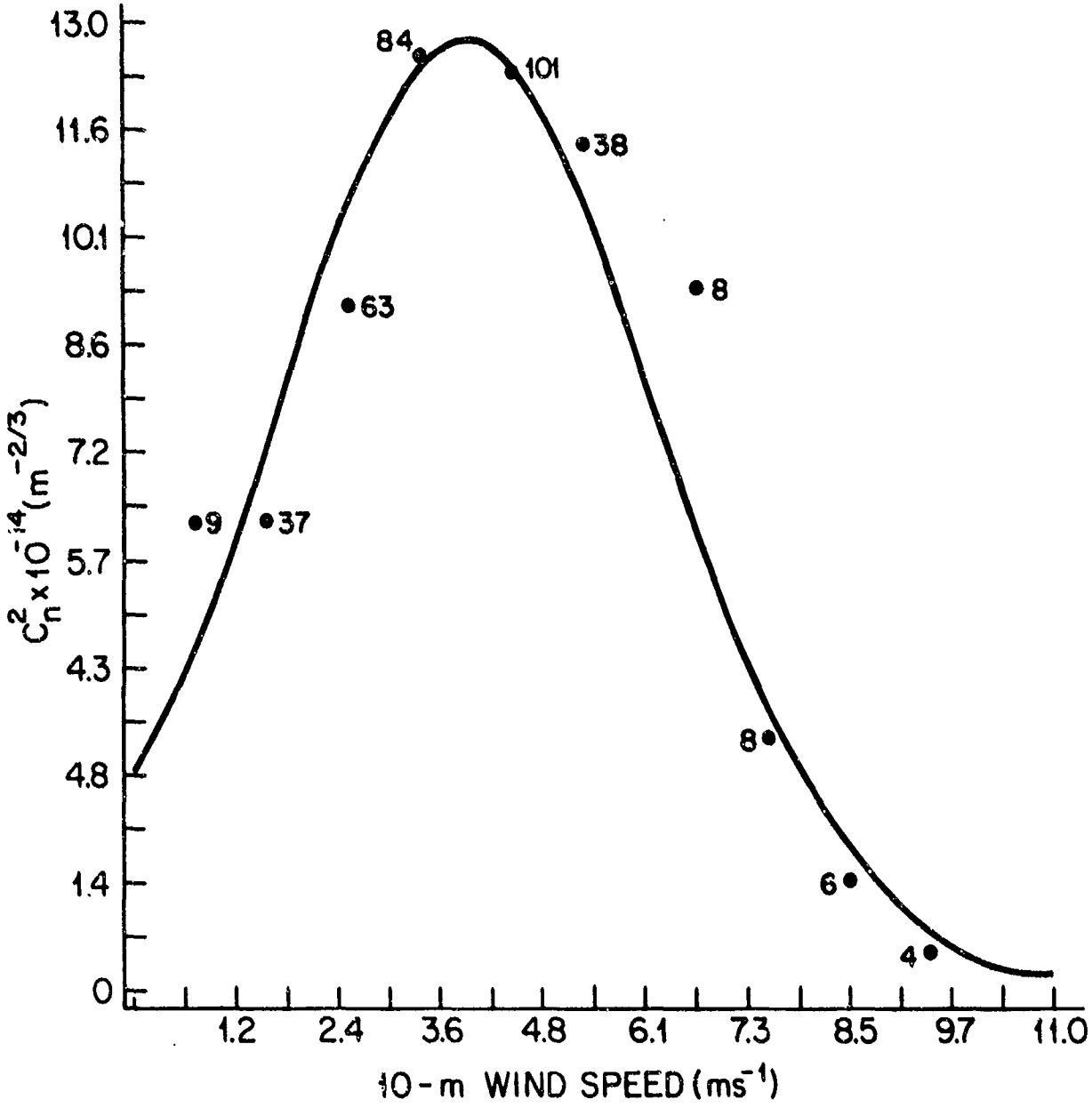

Fig. 12 C_n^2 at 4m versus 10-m wind speed for nighttime conditions at BAO.

temperature gradient. With few or no clouds and no detectable wind speed, the largest inversions are possible. Because vertical motions are suppressed by the large negative buoyancy and viscosity associated with such inversions, air motion is mostly wave-like and laminar, with slow horizontal meandering. Visible evidence of such motion can be seen in the behavior of smoke plumes on a cloudless and windless night. For such a condition, observations show that although mean optical refraction is very large, optical turbulence itself can be very small, with C_n^2 values occasionally approaching those expected for adiabatic conditions. Such small values, however, are usually only temporary. Abrupt increases occur intermittently that are due to "bursts" of turbulence. In the RADC data, for example, on some cloudless nights with zero wind recorded because it was less than an anemometer's starting speed, the 3-minute values of C_n^2 occasionally increased 2 to 3 decades in short ($\sim$ 10 minute) periods and lasted for about 10 minutes before decreasing. Pronounced effects on optical scintillation and visual resolution for this condition occur that have been measured and described by Portman et al. (1962) and by Ryznar (1963). Dewan (1982) presents and discusses reasons for such behavior in terms of a wave interaction and cascade processes.

As RADC wind speed at 2 m increased from nearly calm to about 4 mph, the magnitude of the inversion decreased somewhat, but more importantly, vertical motions increased, causing a large increase in C_n^2. The increase was more evident in the RADC data than in the BAO data because 3-minute values, rather than 20-minute values were available. If conditions were conducive to a steady wind speed of about 3-4 mph at RADC, C_n^2 also remained steady at large values.

As wind speed continued to increase, vertical motions also continued to increase, but the inversion magnitude decreased. As shown in Fig.10 and 12, C_n^2 also decreased. The decrease in inversion magnitude is due primarily to enhanced mixing and downward turbulent heat transfer that inhibit cooling of the surface by radiative loss. A wind speed was eventually reached when (1) the heat lost by the surface was insufficient to keep it colder than the air, (2) the vertical temperature gradient probably approached adiabatic, and (3) C_n^2 decreased to steady minimum values that were near the measurement system's noise level, $\sim 3\ ms^{-1}$ for RADC and $7\ ms^{-1}$ for BAO.

It should be pointed out that in the absence of marked advection of air with different properties, the wind speed at which C_n^2 minima are reached are greater for a daytime cloudless condition than for a nighttime one. The daytime gain of heat by solar radiation at the surface much exceeds that lost by turbulent and radiative heat transfer and keeps the surface significantly warmer than the air at much higher wind speeds. As a result, values of $\overline{C}_n^2$ with 2-m wind speeds between about 3 and 5 ms^{-1}, for example, were near $10^{-13}m^{-2/3}$ on a sunny mid-day, but approached $10^{-15}m^{-2/3}$ on a cloudless night.

Wintertime conditions with a snow cover and with air temperatures above 0°C can cause large values of C_n^2 in stable stratification that are not describable in terms of those cloudiness, solar irradiance and wind speed relationships that apply to conditions with $T_{air} < 0°C$. For $T_{air} < 0°C$ over uniformly fresh deep snow ($\gtrsim 10$ cm) and few or no clouds, the average temperature of a snow surface (1) is usually colder than the air at night due to infrared radiation loss,

(2) is nearly the same as the air temperature in daytime mainly because of its high albedo ($\sim$ 80% for fresh snow) and (3) responds rapidly to air temperature changes as long as $T_{air} < 0°C$, with solar irradiance and wind speed exerting comparatively smaller effects. The RADC data reflect (2) and (3) in that daytime values of C_n^2 at 2m remained quite small. Typically, values were less than $10^{-15} m^{-2/3}$ and had small variability.

For $T_{air} > 0°C$, however, as long as there is a snow cover of substantial depth, its surface temperature remains near 0°C regardless of how much warmer the air temperature becomes. The advection of $T_{air} > 0°C$ produces values of C_n^2 that are proportional mainly to the air temperature alone, with cloudiness and wind speed having secondary effects. In fact, one of the largest increases in C_n^2 in the shortest time period for the RADC data occurred at night in an 18-minute period between 2254 and 2312 GMT on 15 February 1982. The 3-minute values of C_n^2 increased from near $10^{-17} m^{-2/3}$ to near $10^{-12} m^{-2/3}$. There were 31 cm of snow, the 2-m temperature was about +7°C, and the wind speed increased from about 0.5 mph to 2.1 mph when this occurred.

It can be expected that the most common location and time for the above condition to occur are mid-latitude regions with snow and ice that is deep (thick) enough to last well into springtime. It is possible, for example, to have occasional periods with air as warm as about 20°C moving over a snow or ice surface until complete melting occurs. A frequent effect of the cold surface on the warmer air moving over it, however, is to cause condensation as fog in the first few meters. Whether or not fog forms depends largely on temperature and humidity characteristics of the air mass, but if it does form, the meaning and effects of optical turbulence are likely to be obscured.

3.2.2 Boundary layer profiles

The 20-minute averages of profile data for 8 heights on the NOAA BAO tower provide unique resolution in both time and height regarding the behavior of $C_n^2(C_T^2)$ and meteorological variables between 10 m and 300 m. The nocturnal periods with a cloudless sky or scattered clouds listed in Table 8 were used to test the effectiveness of wind speed as a variable to describe $C_n^2(C_T^2)$ variations not only at one height, but also vertical profiles of C_T^2, temperature and wind speed. Averages of these variables for each of the 8 heights were calculated in successive 1 ms^{-1} categories of wind speed measured at 10 m (u_{10}) for categories from 0-1 ms^{-1} to 10-11 ms^{-1}. The results are shown in Fig. 13a through 13k for temperature and C_T^2 and Fig. 14a through Fig. 14e for wind speed. Temperature and wind speed plotted against height (z) are shown with linear scales, and log C_T^2, with the same 5-decade scale for all figures, is shown against log z. The category of u_{10} is given at the top of each figure. In the caption for each figure, the range of sample sizes for that category of u_{10} is given because the sample sizes were limited and varied not only with height but also from one category of wind speed to another. Table 11 lists sample sizes, maximum and minimum values of $\overline{C_T^2}$ at 10 m, $\overline{C_T^2}$ profile slopes and the top of the SBL for each u_{10} category.

A general feature of the BAO tower results is that they show that changes in (1) actual values of $\overline{C_T^2}$ at 10 m, (2) slopes of $\overline{C_T^2}$ profiles, (3) the top of the SBL (z_n), and (4) shapes and slopes of temperature and wind profiles are affected by changes in u_{10} in a consistent manner. For example:

1) $\overline{C_T^2}(10)$ increases from about 0.03°C $m^{-2/3}$ for 0-1 ms^{-1} to

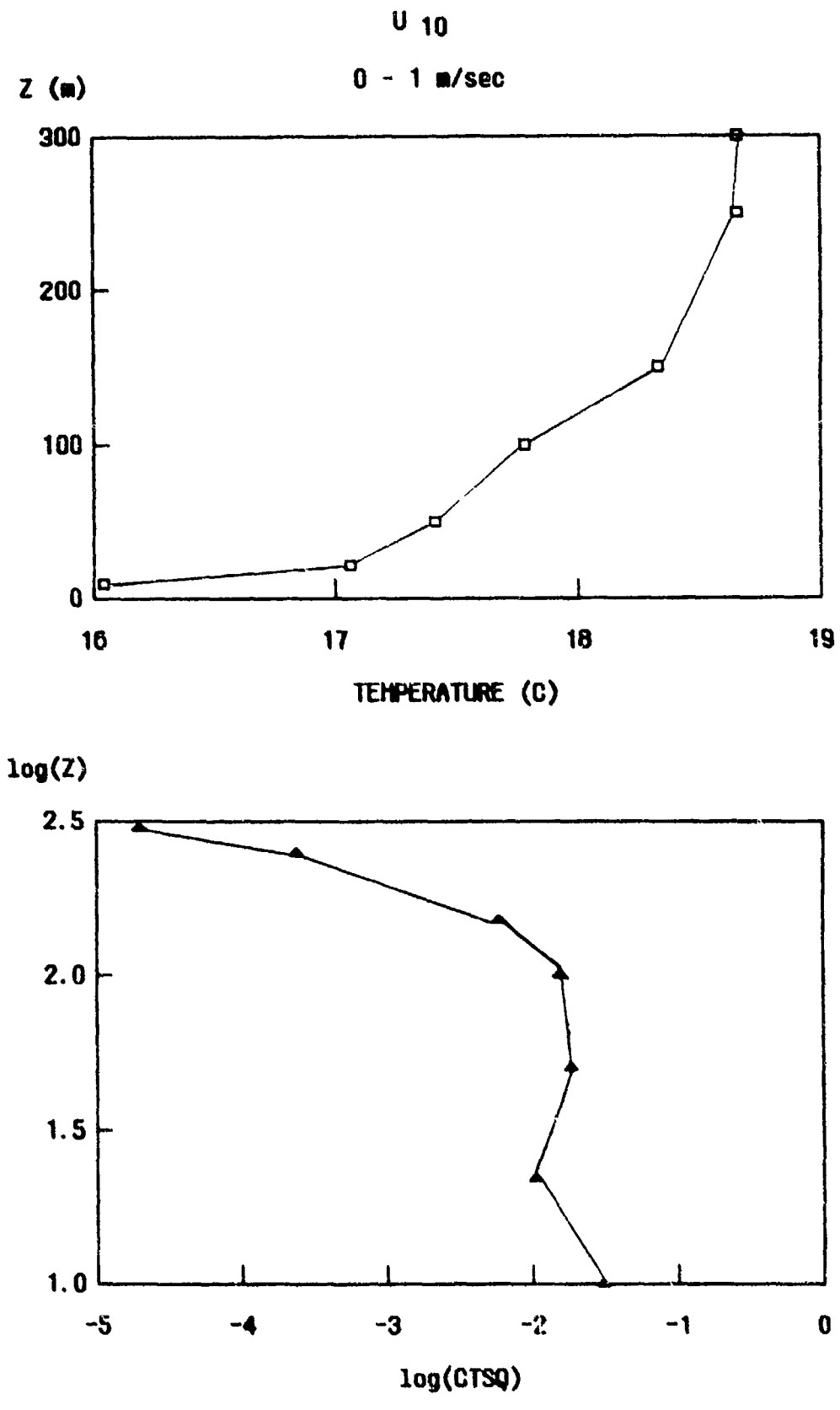

Fig. 13a Temperature versus height (top) and log C_T^2 versus log height (bottom) at BAO for nighttime conditions with a cloudless sky or scattered cloudiness and a 10-m wind speed (u_{10}) category of 0-1 ms^{-1}. Sample sizes range from 2 to 4.

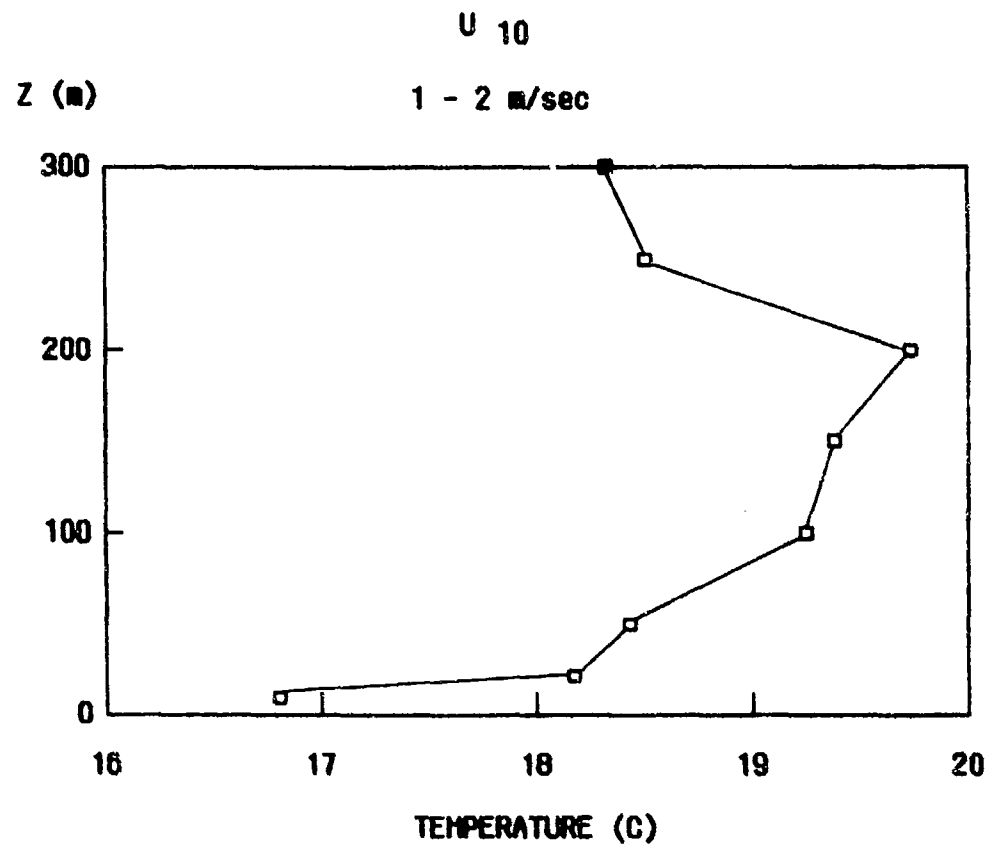

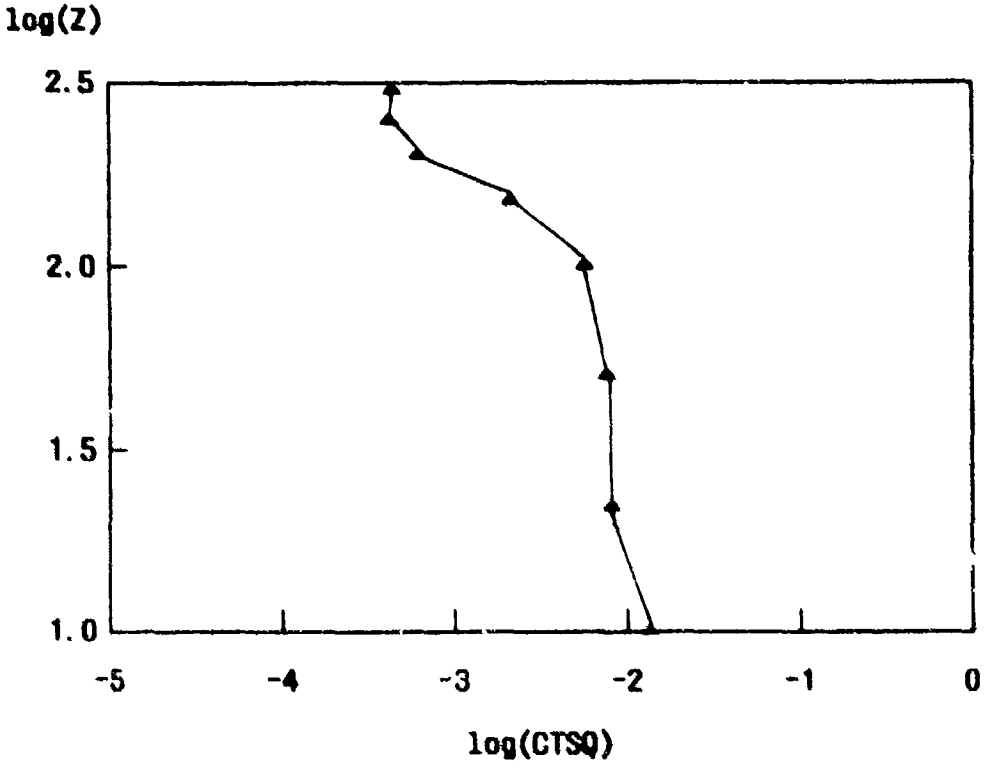

Fig. 13b Same as 13a but with u_{10} = 1-2 ms^{-1} and a range in sample sizes from 13 to 20.

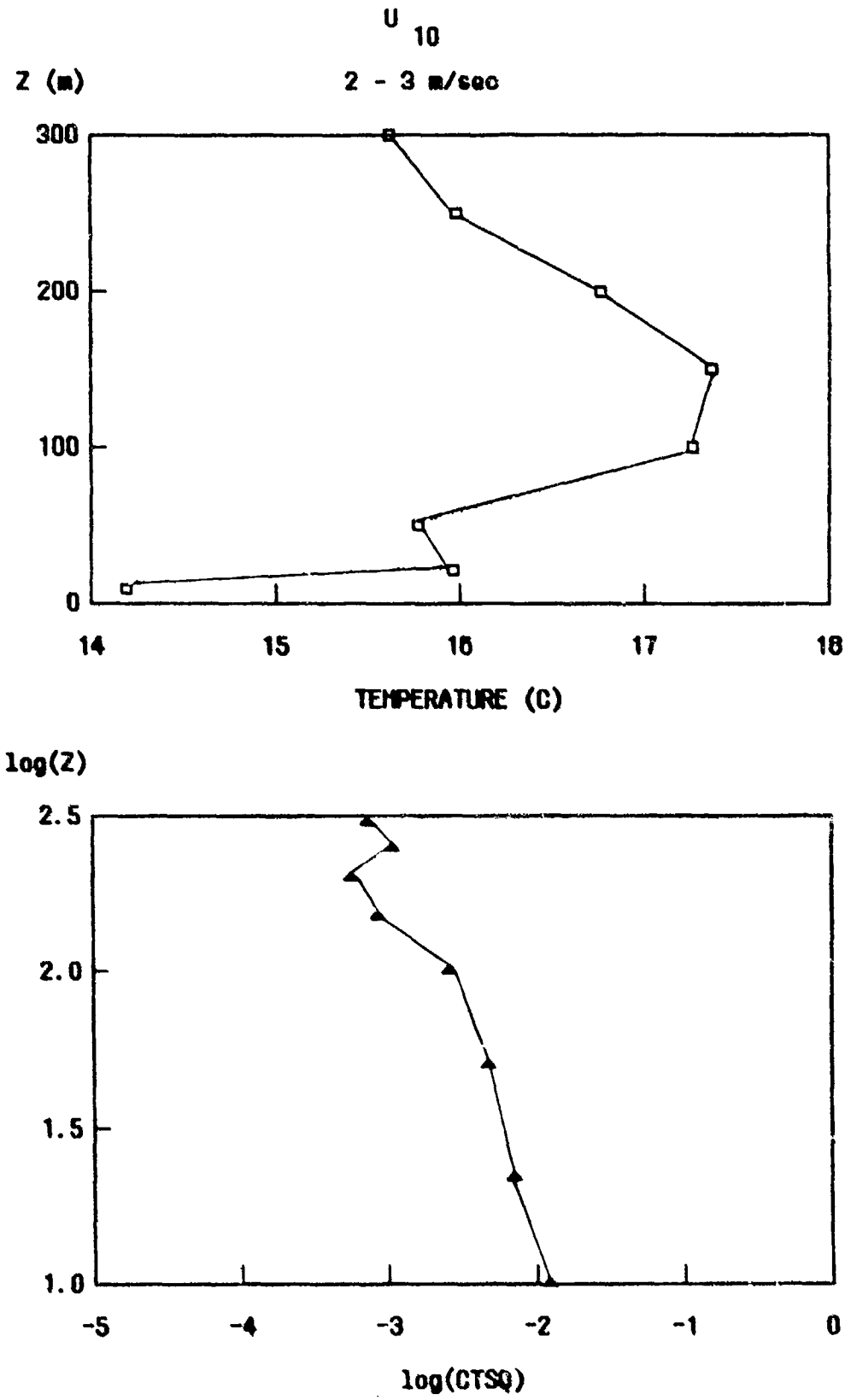

Fig. 13c Same as 13a but with u_{10} = 2-3 ms^{-1} and a range in sample sizes from 17 to 30.

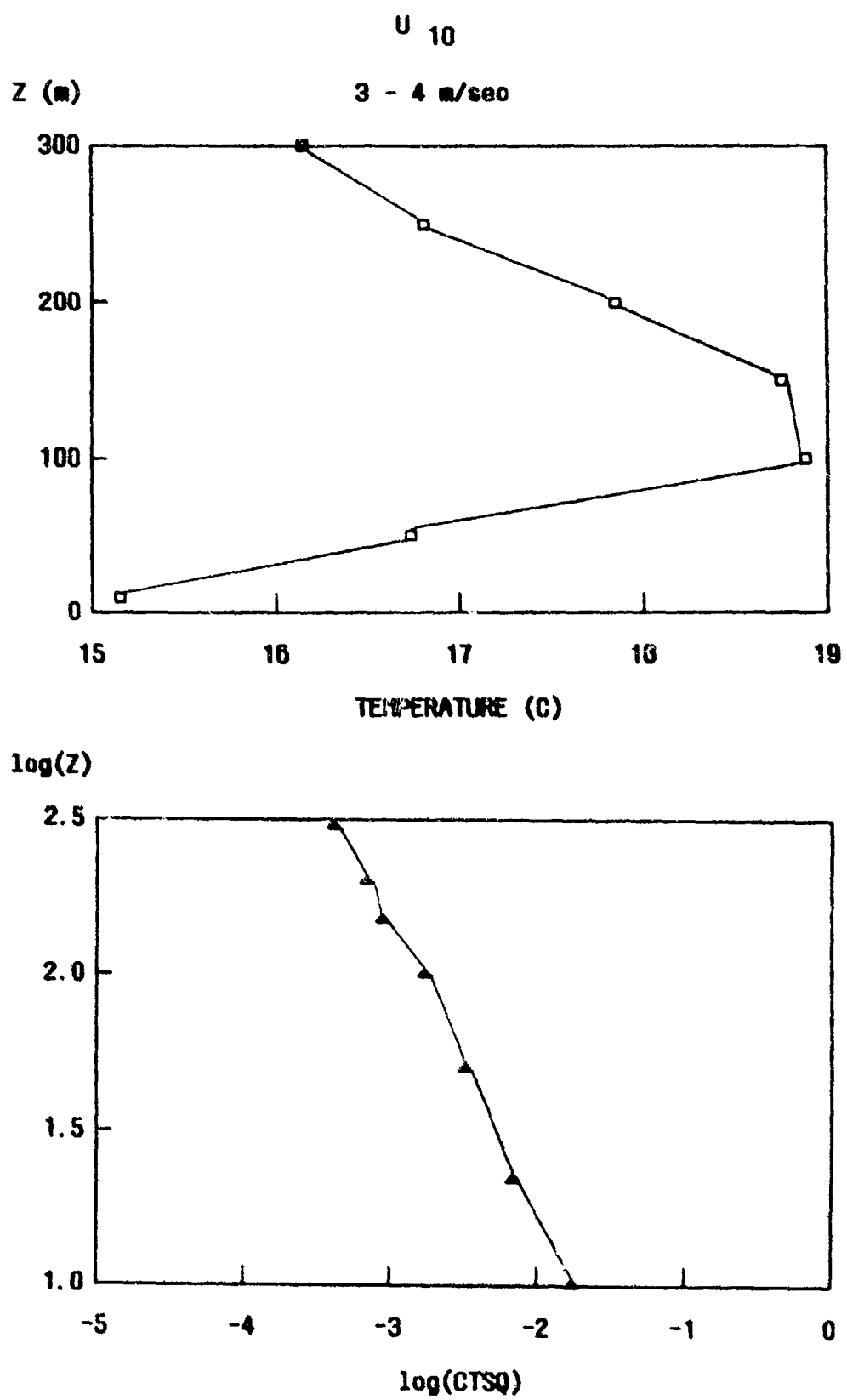

Fig. 13d Same as 13a but with u_{10} = 3-4 ms^{-1} and a range in sample sizes from 13 to 28.

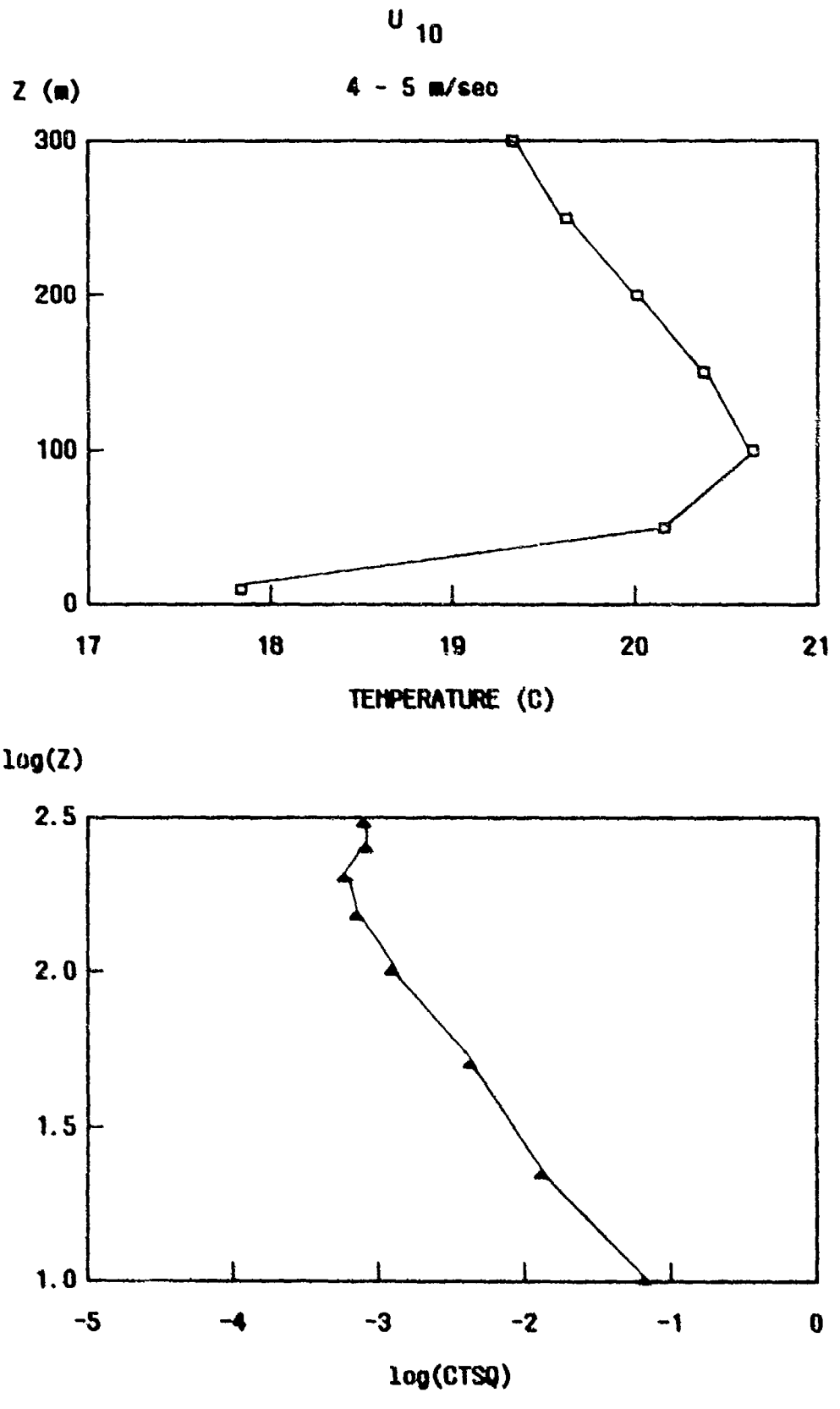

Fig. 13e Same as 13a but with u_{10} = 4-5 ms^{-1} and range in sample sizes from 34-41.

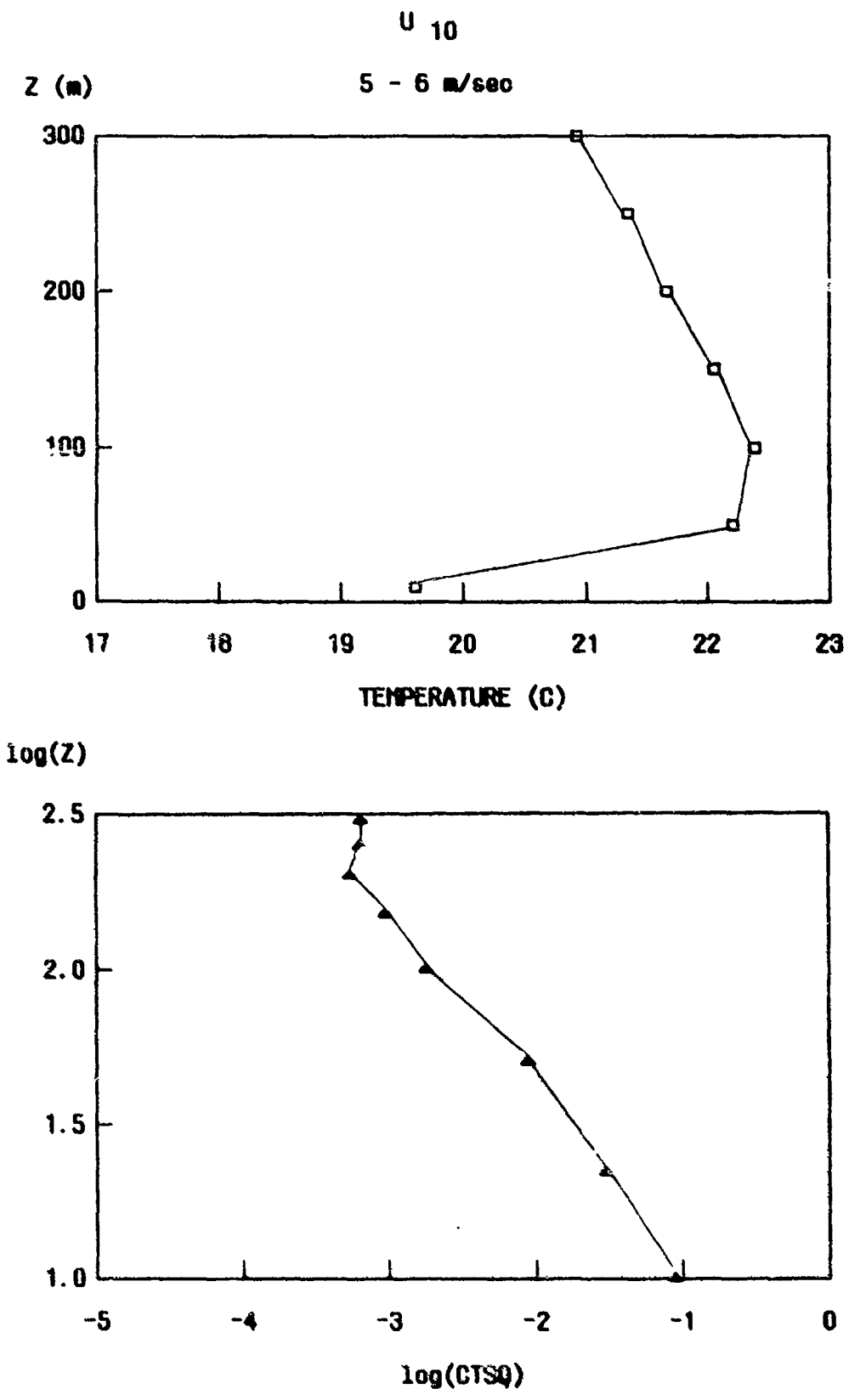

Fig. 13f Same as 13a but with u_{10} = 5-6 ms^{-1} and a range sample sizes from 19-21.

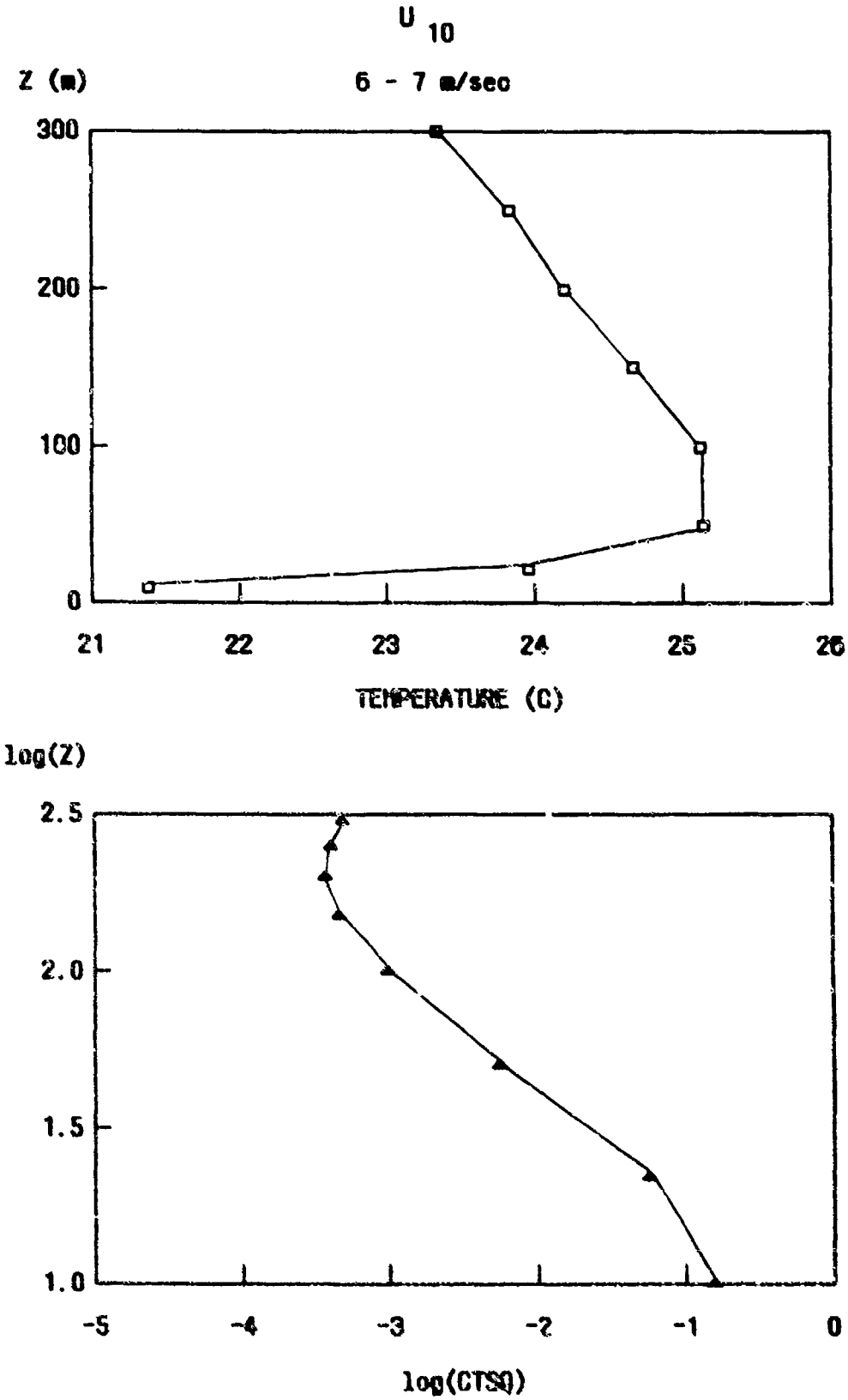

Fig. 13g Same as 13a but with u_{10} = 6-7 ms^{-1} and a sample size of 2.

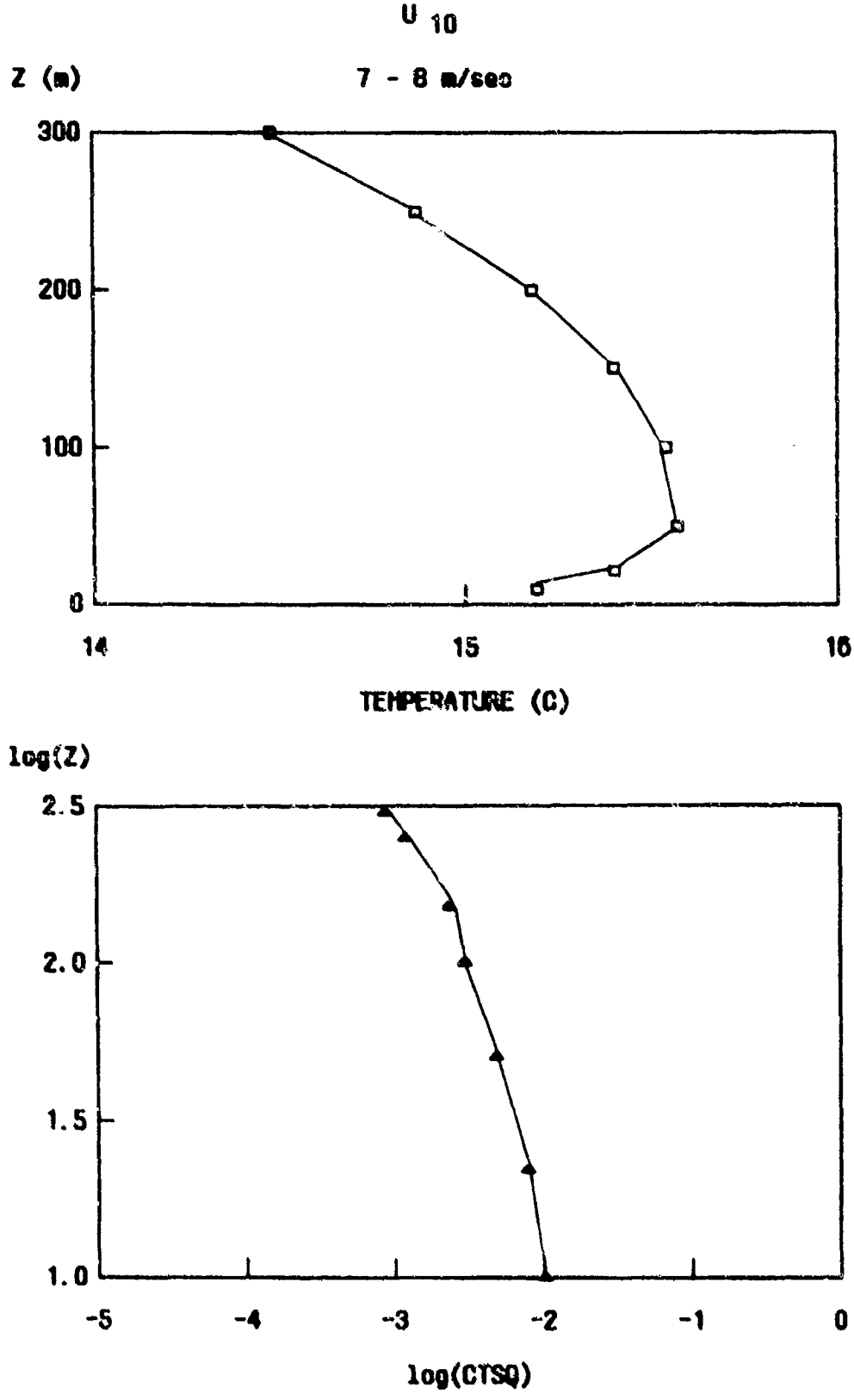

Fig. 13h Same as 13a but with u_{10} = 7-8 ms^{-1} and a sample size of 2.

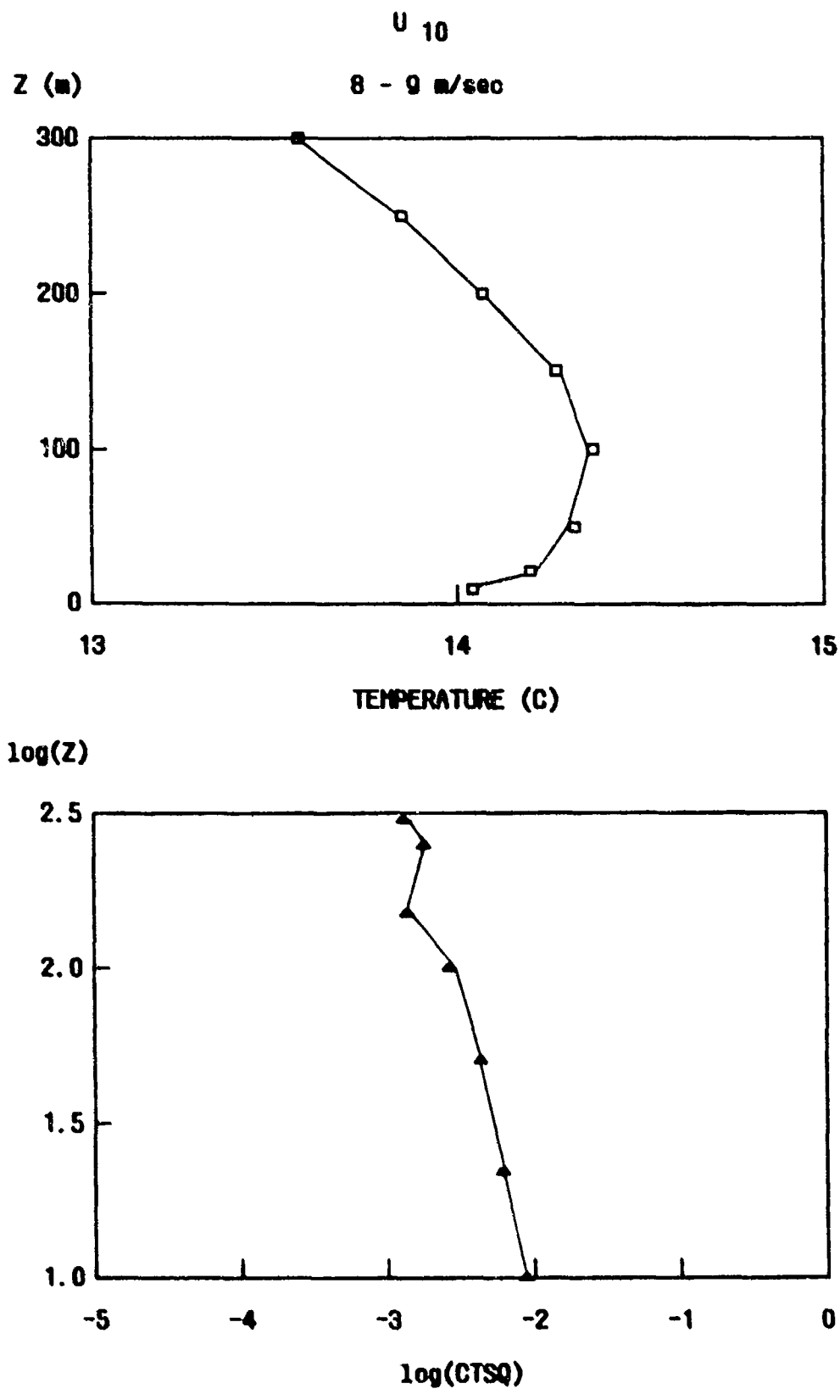

Fig. 13i Same as 13a but with u_{10} = 8-9 ms^{-1} and a sample size of 4.

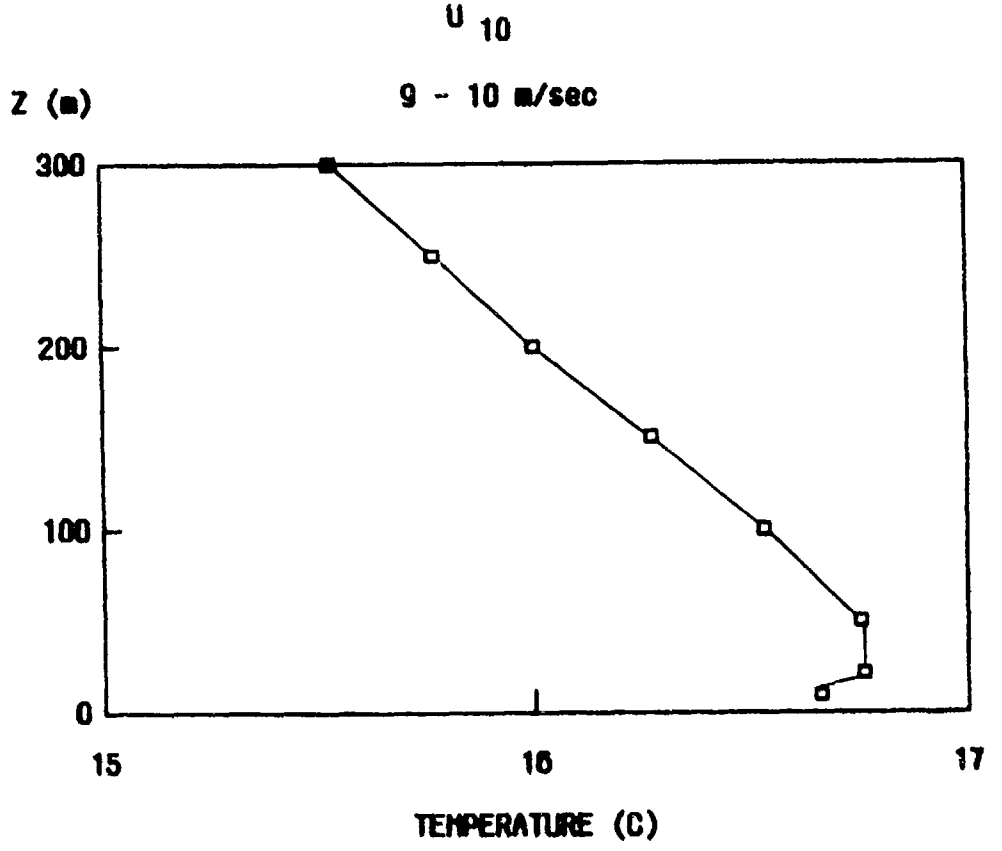

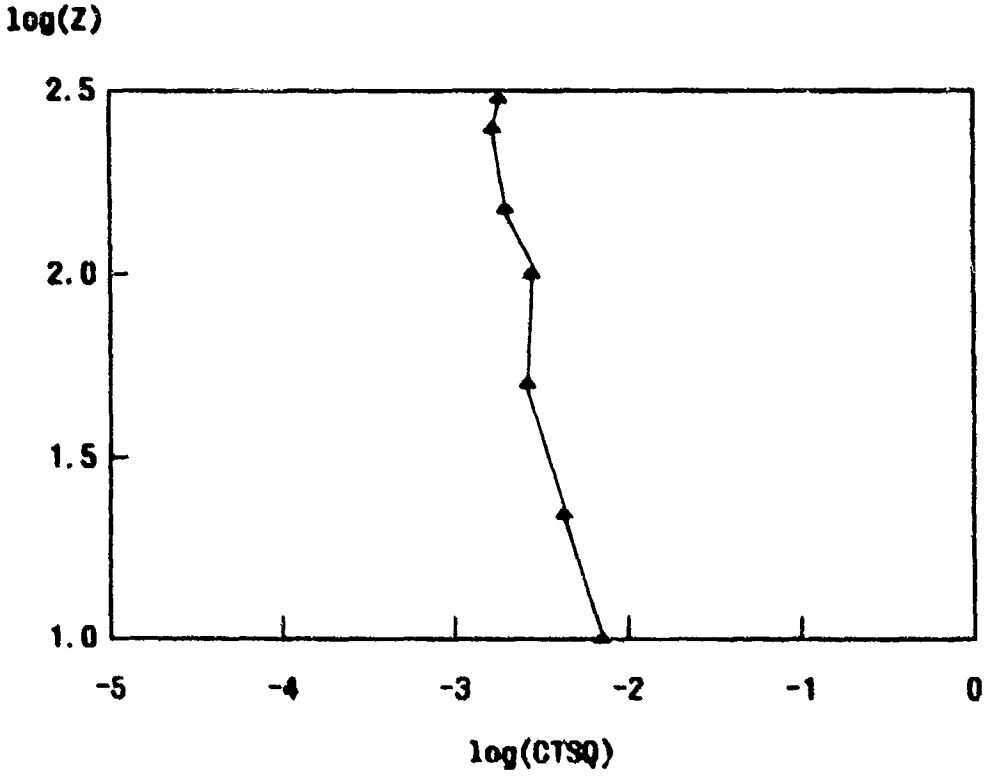

Fig. 13j Same as 13a but with u_{10} = 9-10 ms^{-1} and a sample size of 4.

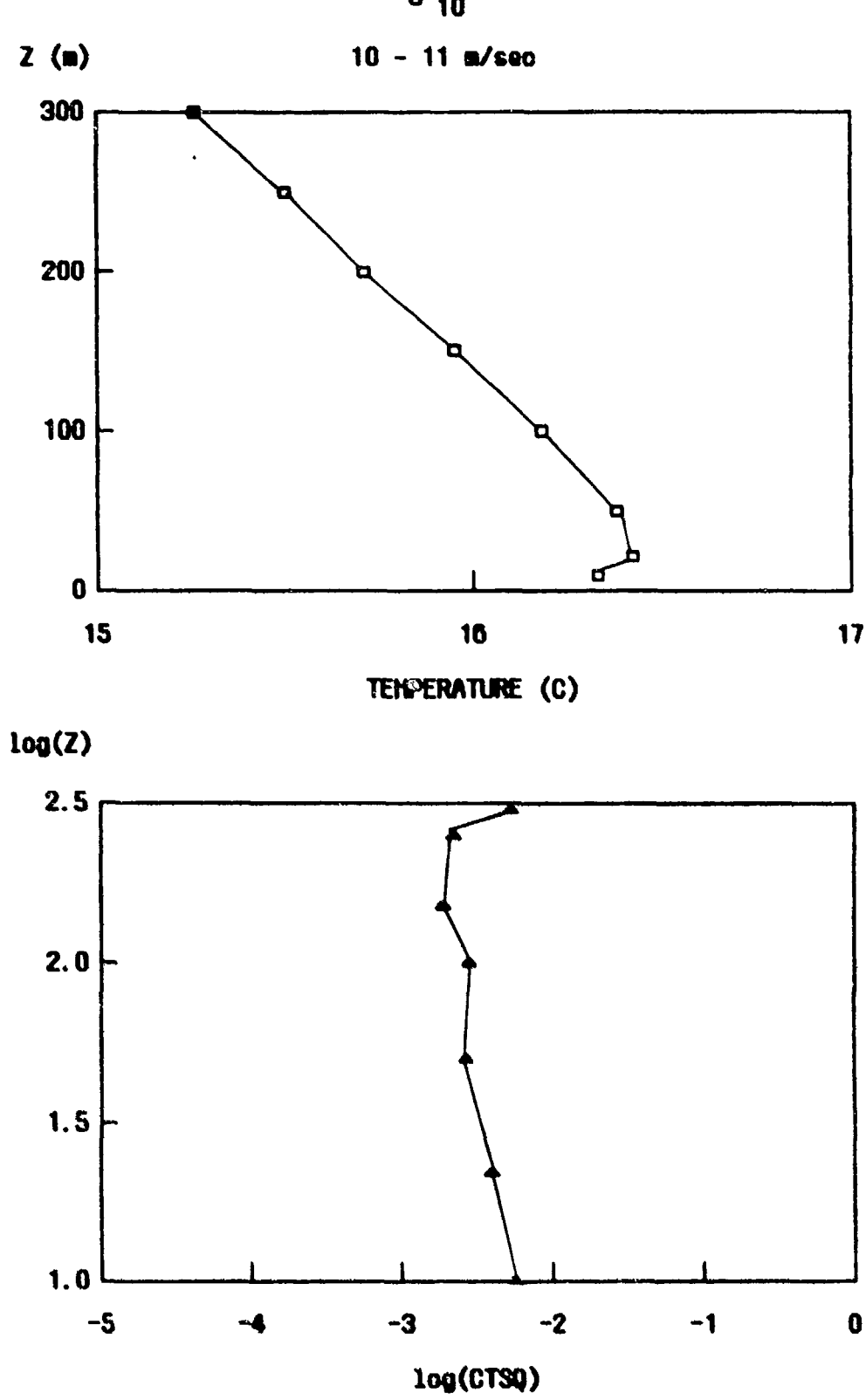

Fig. 13k Same as 13a but with u_{10} = 10-11 ms^{-1} and a sample size of 1.

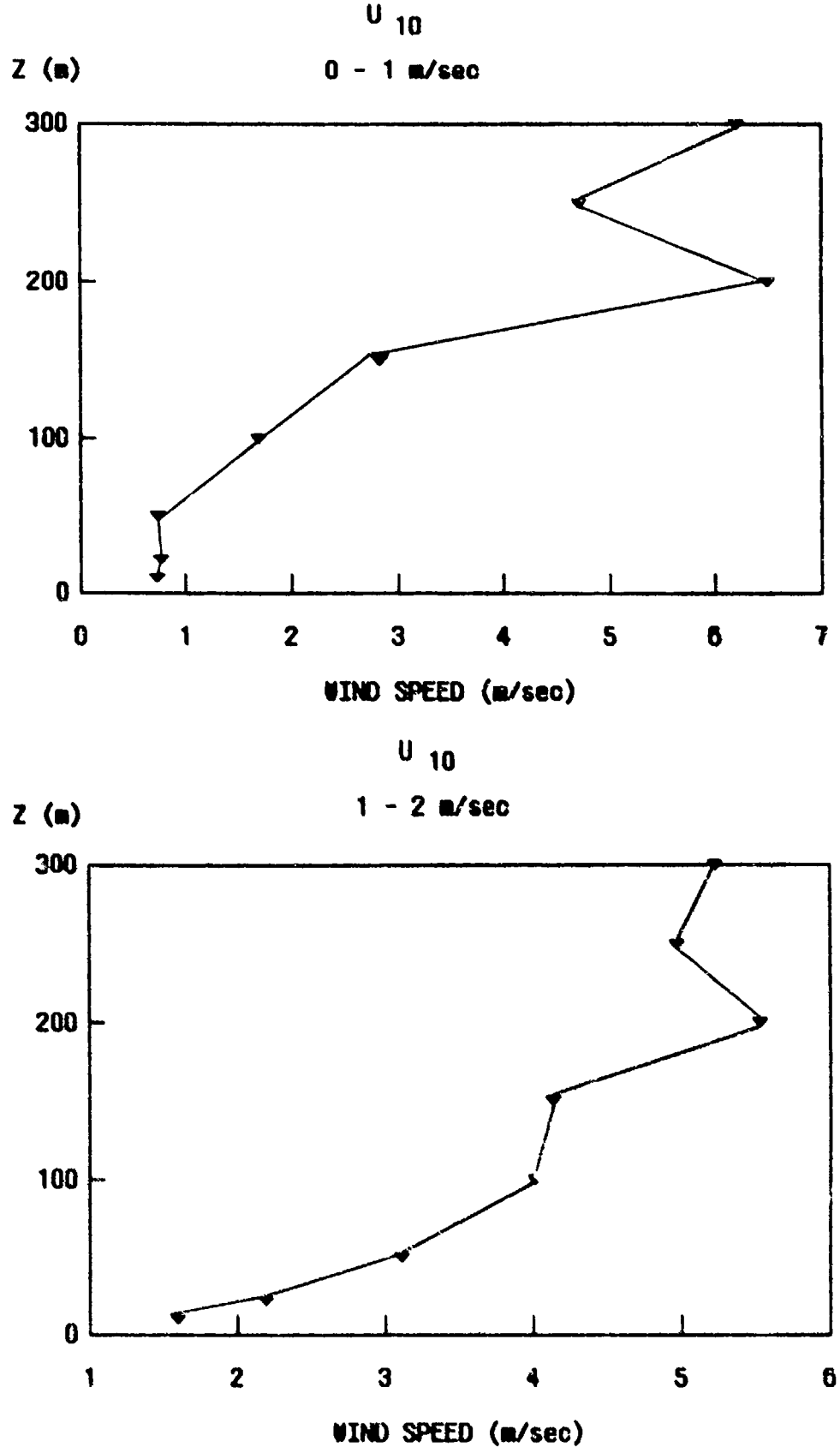

Fig. 14a Wind speed versus height at BAO for nighttime conditions with a cloudless sky or scattered clouds for wind speed categories of 0-1 ms^{-1} and 1-2 ms^{-1} corresponding to Fig. 13a and b.

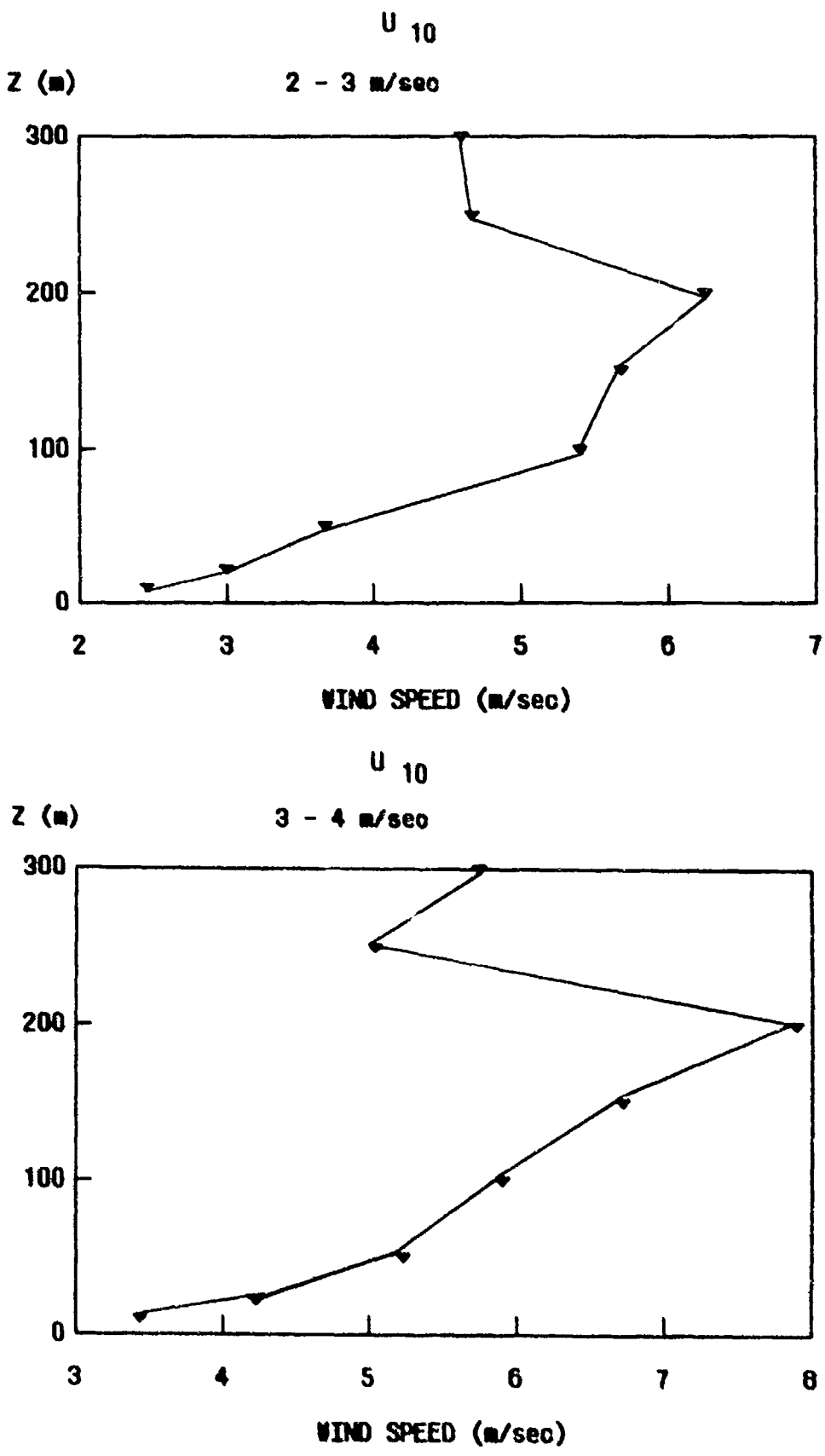

Fig. 14b Same as 14a but for wind speed categories of 2-3 ms^{-1} and 3-4 ms^{-1} corresponding to Fig. 13c and d.

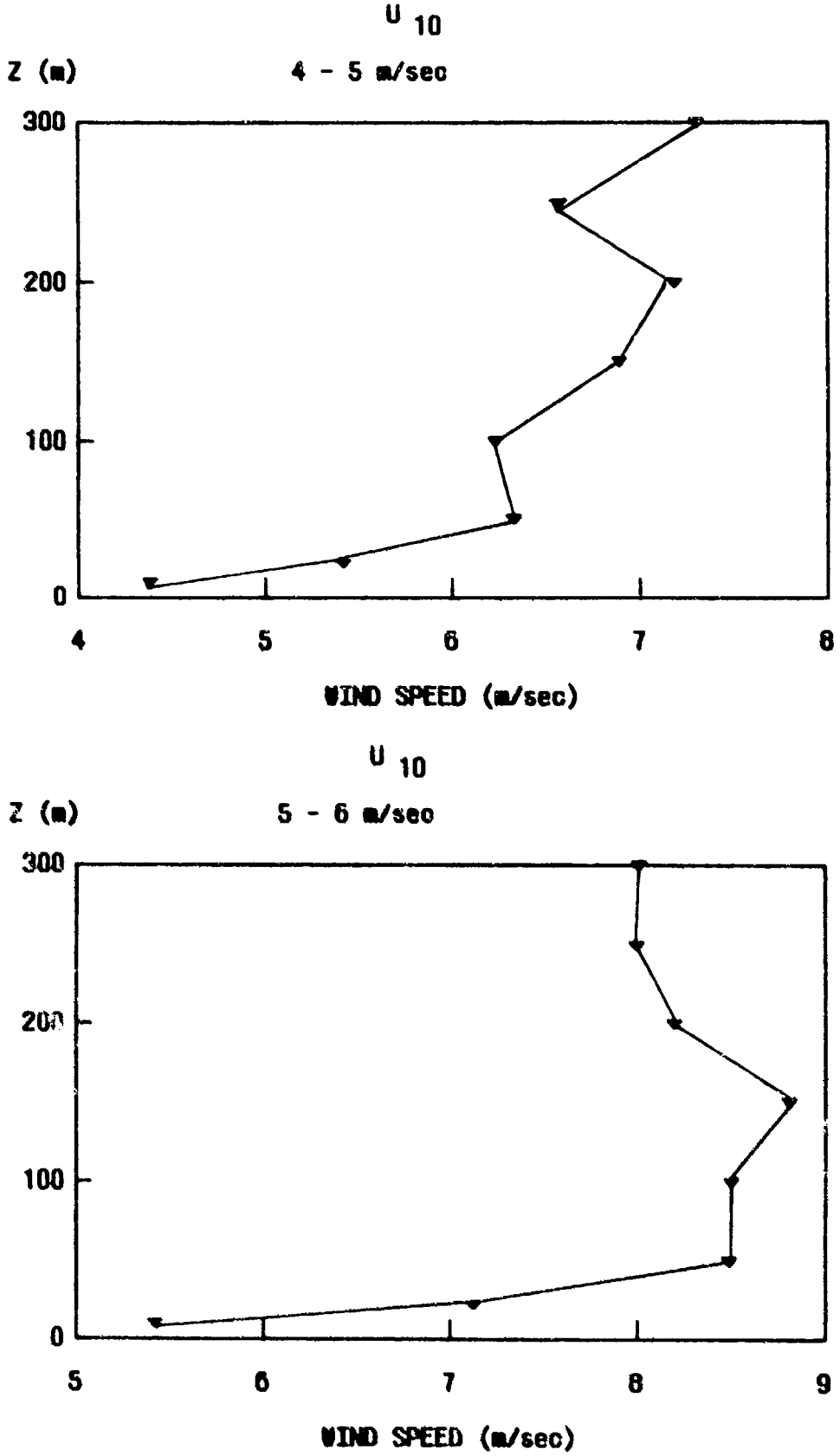

Fig. 14c Same as 14a but for wind speed categories of 4-5 ms^{-1} and 5-6 ms^{-1} corresponding to Fig. 13e and f.

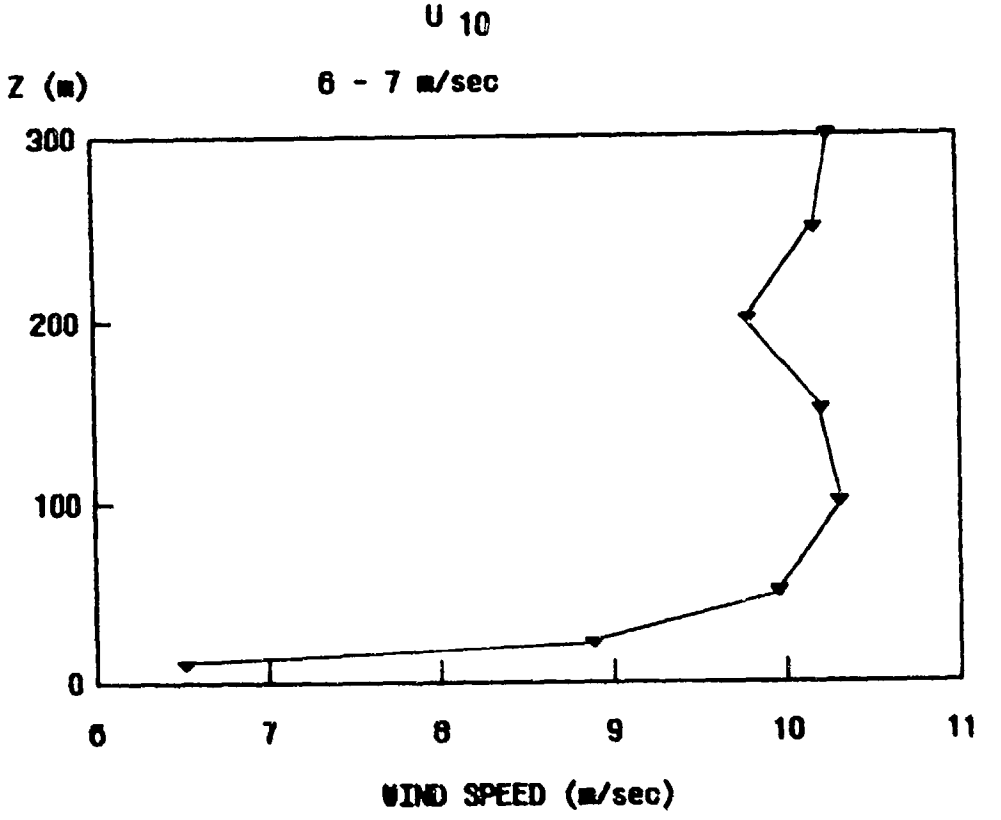

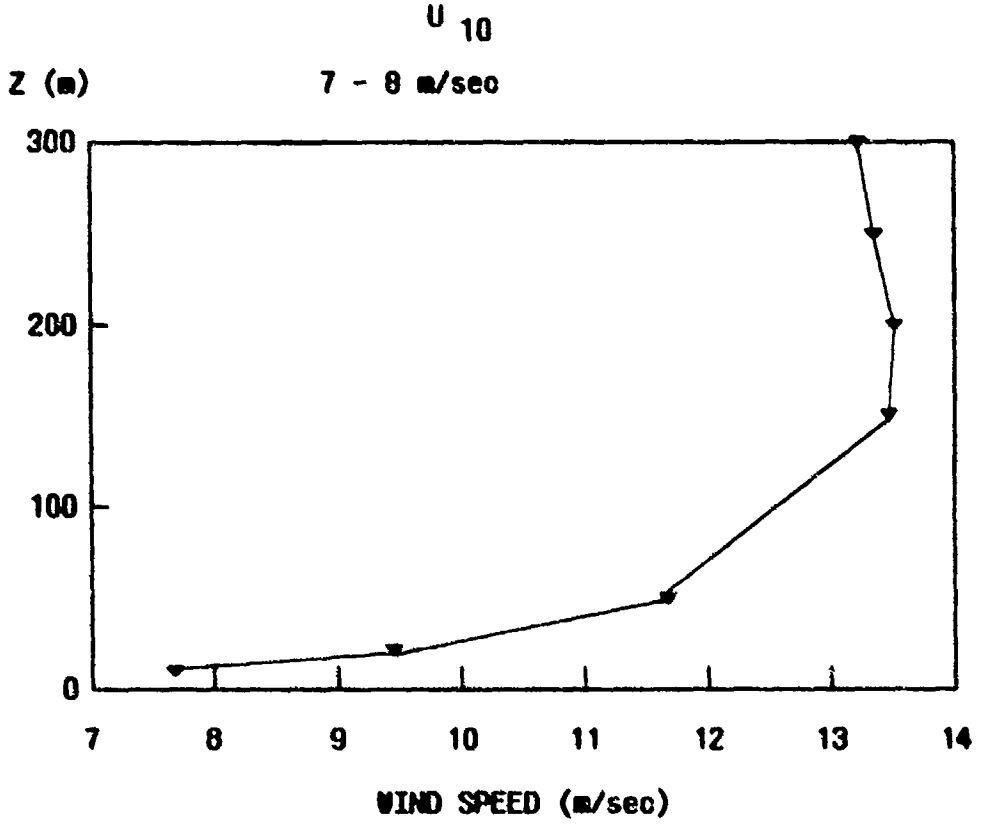

Fig. 14d Same as 14a but for wind speed categories of 6-7 ms^{-1} and 7-8 ms^{-1} corresponding to Fig. 13g and h.

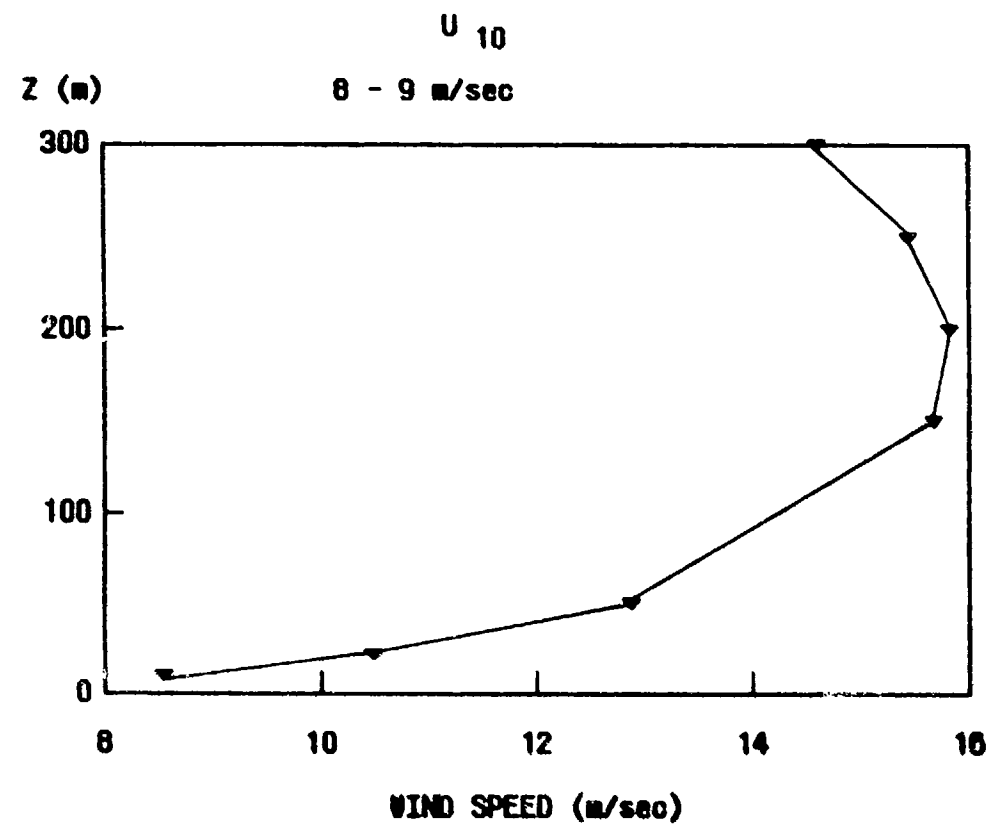

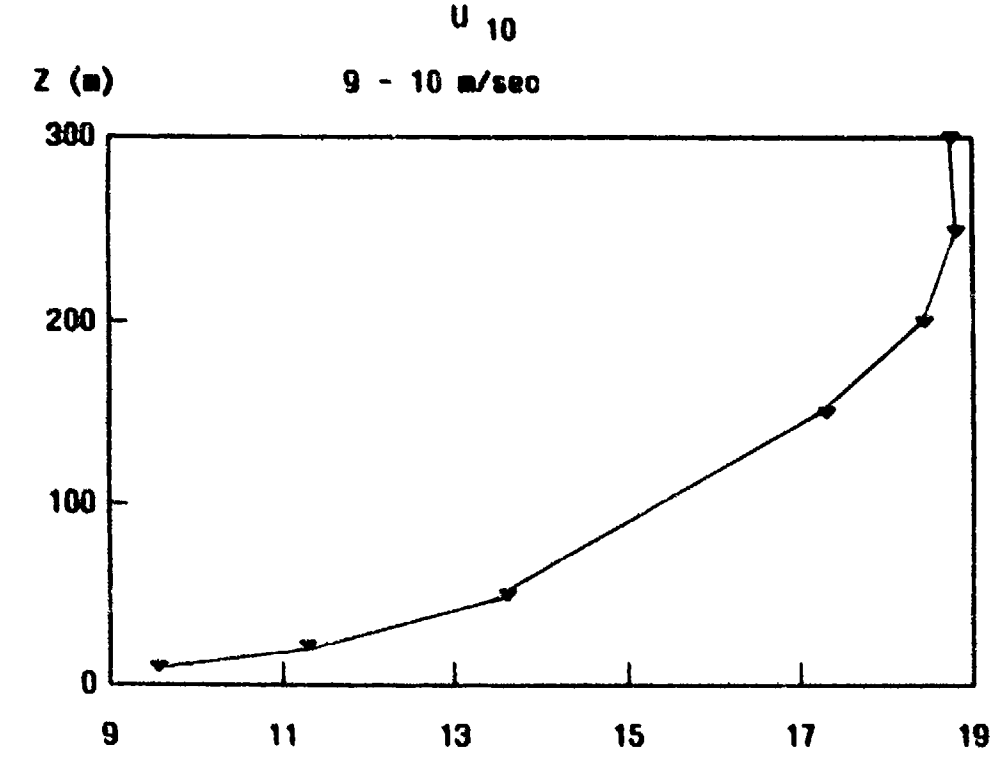

Fig. 14e Same as 14a but for wind speed categories of 8-9 ms^{-1} and 9-10 ms^{-1} corresponding to Fig. 13i and j.

Table 11 $\overline{C_T^2}$ maxima and minima at 10 m, profile slopes, and z_n for various u_{10} for the BAO profiles shown in Fig.13a through Fig. 13k.

u_{10} (ms^{-1})	Sample Size C_T^2	C_T^2 ($°C\ m^{-2/3}$) MAX	MIN	$\frac{\Delta \log C_T^2}{\Delta \log z}$	z_n (m)
0-1	2-4	0.03	0.2×10^{-4}	*	170
1-2	13-20	0.013	4.3 "	*	170
2-3	17-30	0.012	5.6 "	-0.98	120
3-4	13-28	0.017	4.1 "	-1.08	100
4-5	34-41	0.065	5.7 "	-1.67	60
5-6	19-21	0.089	5.5 "	-1.59	50
6-7	2	0.156	3.7 "	-2.16	50
7-8	2	0.010	10 " (*)	-0.50 (*)	50
8-9	4	0.009	13 " (*)	-0.55 (*)	45
9-10	4	0.007	15 " (*)	-0.45 (*)	30
10-11	1	0.006	16 " (*)	-0.36 (*)	25

* not determinable.

(*) outlying small value of C_T^2 at 200 m not considered.

near 0.1 for u_{10} near 6 ms^{-1} and decreases to less than 0.01°C $m^{-2/3}$ for $\bar{u}_{10} > 7$ ms^{-1}. These changes are similar to those for a single height discussed in Section 3.2.1 in that C_T^2 is small at low wind speeds, increases to a maximum as wind speed increases, and decreases above a certain speed. The occurrence of a maximum near $u_{10} \approx 6$ ms^{-1} seems high compared to the results in section 3.2.1, but it may be due to factors such as height differences, spectral estimates compared with scintillometer estimates, and the abrupt decrease in sample size from about 20 samples for the u_{10} = 5-6 ms^{-1} category to 2 for $u_{10} > 6$ ms^{-1}.

2) C_T^2 decreases with height for all wind speed categories, with the most marked decrease (from $\sim 10^{-2}$°C $m^{-2/3}$ to $\sim 10^{-5}$°C $m^{-2/3}$) occurring between 100 m and 300 m for u_{10} = 0-1 ms^{-1}. This height change in C_T^2 corresponds to the height interval within which the temperature profile changes from a large inversion to nearly adiabatic. These features, plus the occurrence of a wind speed maximum near 170 m as shown in Fig.14a, support the idea that for u_{10} = 0-1 ms^{-1} the region near 170 m is the top of the SBL, or z_n. With increasing wind speed, the following is indicated by the profiles regarding their slopes, shapes, and z_n:

a) The negative slope of the C_T^2 profiles, estimated for wind speeds beginning with u_{10} = 2-3 ms^{-1}, increased negatively from about -1 to near -2 for u_{10} = 6-7 ms^{-1} and decreased to -0.5 or less for $u_{10} > 7$ ms^{-1}. For speeds from 4-6 ms^{-1} it was close to -4/3. The decrease of C_T^2 between 100 m and 300 m for $u_{10} > 6$ ms^{-1} was less than half that for $u_{10} \lesssim 6$ ms^{-1}.

b) If z_n is defined by the top of the ground-based inversion, a decrease from about 170 m to 30 m occurred as u_{10} increased to $\sim$ 11 ms^{-1}, contrary to eq. 9. A similar lowering of the height of maximum wind speed in the 300-m layer was indicated.

c) A lack of sufficient samples for individual categories for $u_{10} > 6$ ms^{-1} is a shortcoming in an interpretation of these results but collectively, for $u_{10} > 6$ ms^{-1}, the results are consistent.

The BAO results are corroborated by results from the 17 and 9 CLEAR I and II soundings, respectively, that were obtained in stable and nearly cloudless conditions. Average profiles of C_n^2 and temperature from about 12 m to 600 m for the CLEAR I and II soundings are shown in Fig. 15 and Fig. 16, respectively. In each figure, the coordinates for C_n^2 are logarithmic and those for temperature are linear. For log C_n^2, the abscissa scale is the same ($\sim 10^{-16}$ to 10^{-14}). The numbers on the C_n^2 ordinate are actual heights that correspond to the logarithmic height scaling by computer. The average slope of C_T^2 is close to a -4/3 slope that is shown for reference. A dry adiabatic lapse rate ($\Gamma \sim 1°C/100$ m) is shown on the temperature graph for reference. The average height of z_n, as defined by changes in temperature and relative humidity, is near 120 m for CLEAR I and 150 m for CLEAR II.

For many profiles of C_n^2, a secondary maximum could be identified near z_n, but its magnitude and vertical extent were smaller than for a daytime CBL. An analytical description of it was not attempted for the SBL. Instead, the -4/3 slope indicated by the soundings was accepted as a reasonable approximation of $C_n^2(C_T^2)$ through the SBL up to about 2000 m.

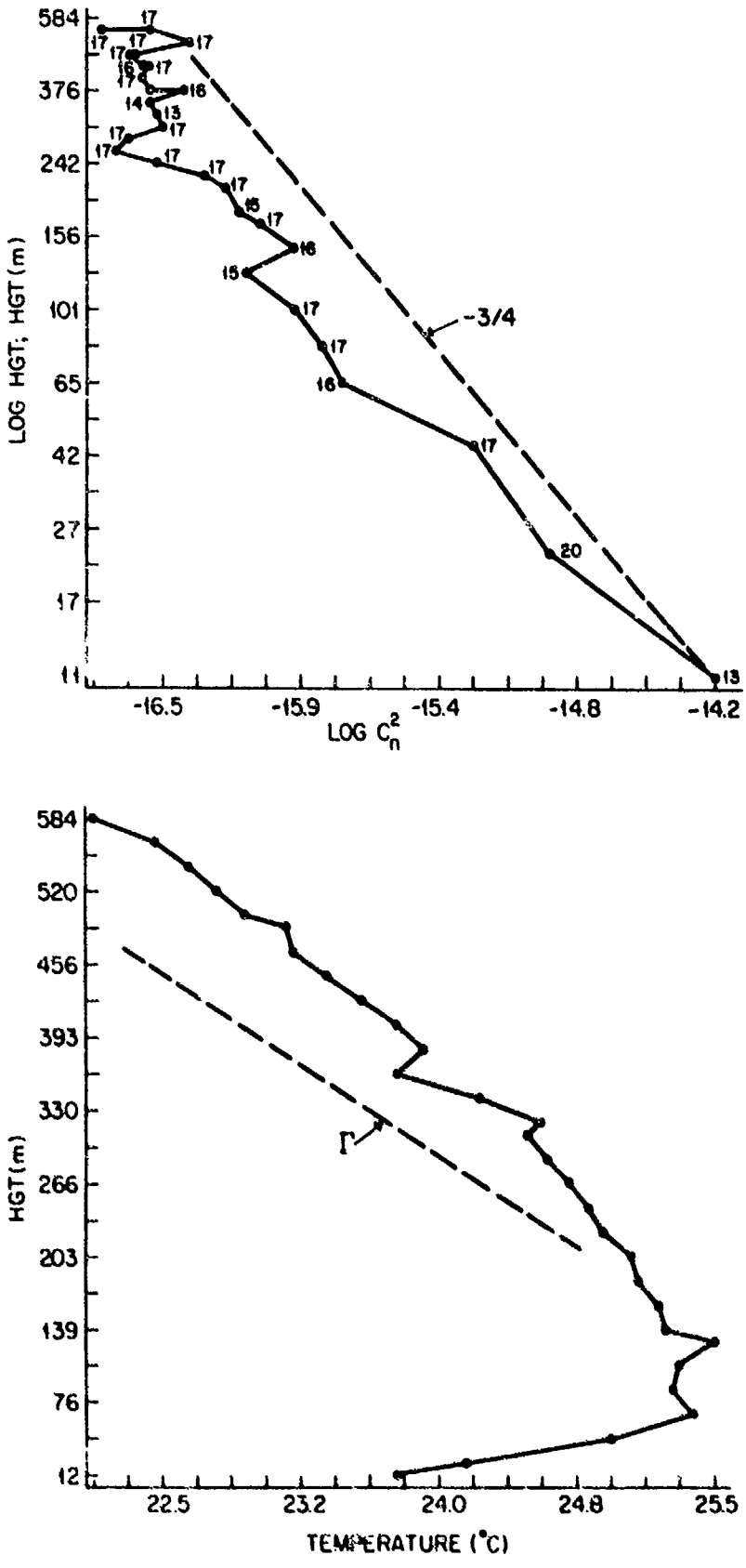

Fig. 15 Average of the profiles of C_n^2 and temperature for stable conditions for the CLEAR I data.

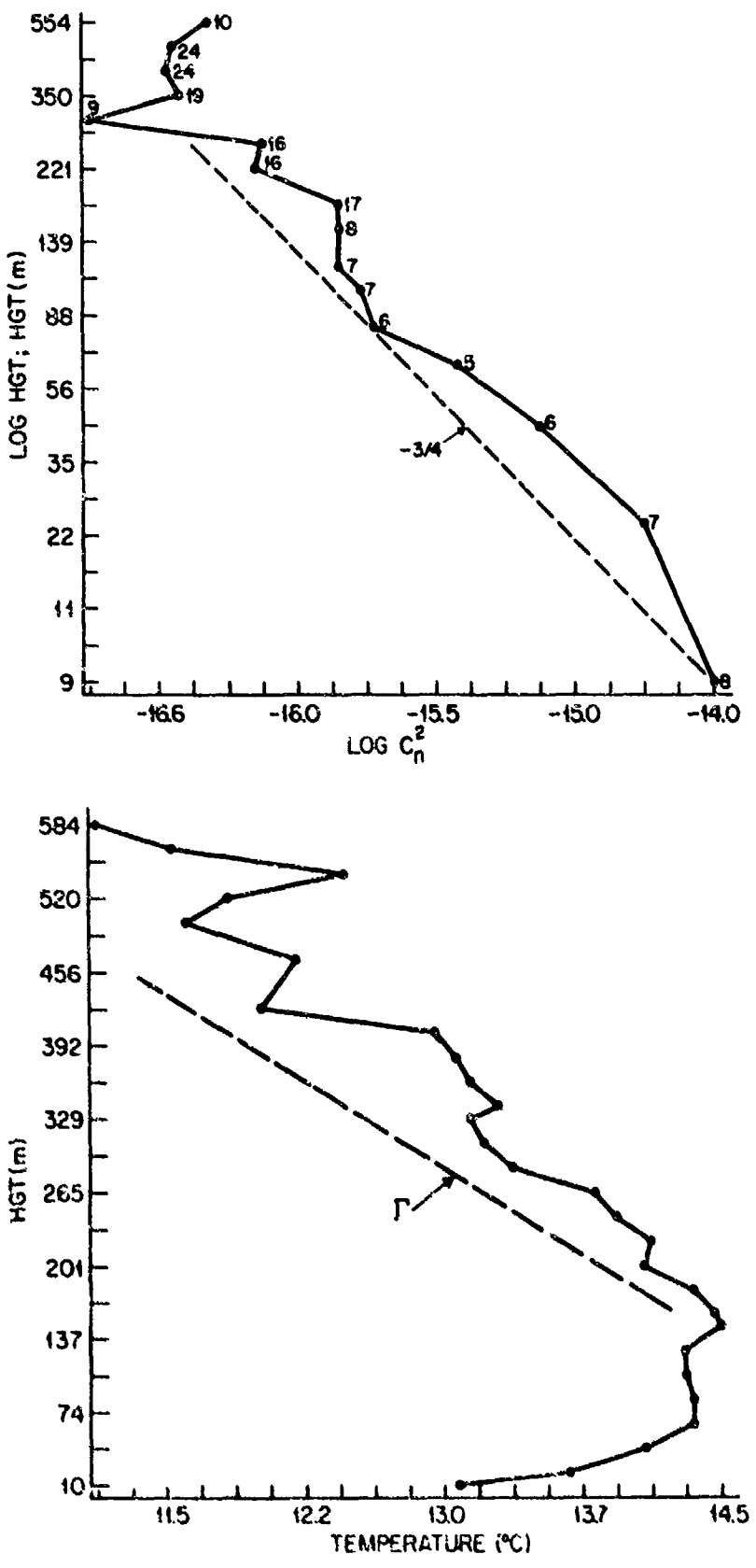

Fig. 16 Average of the profiles of C_n^2 and temperature for stable conditions for the CLEAR II data.

3.3 $C_n^2(C_T^2)$ in near-adiabatic conditions

For the CLEAR I data, the 7 profiles of C_n^2 in Table 4 that are labeled "n" are those considered to be representative of near-neutral, or adiabatic temperature profile conditions near the ground. The profiles were measured near sunrise and sunset and are near the times when the smallest values of C_n^2 were measured with the scintillometers at 4 and 14 m.

An average of the 7 profiles of C_n^2 from about 12 m to 2700 m is shown in Fig. 17 together with profiles of temperature and relative humidity. A -3/4 slope is shown for reference on the log C_n^2 profile and a dry adiabatic lapse rate (Γ) is shown on the temperature profile. Sample sizes are also given for C_n^2. The range of C_n^2 values is from 4.2×10^{-16} m $^{2/3}$ at 12 m to 4.2×10^{-18} m$^{-2/3}$ at about 1500 m. Features of the average C_n^2 profile are (1) an apparent secondary maximum near 2100 m that corresponds to a maximum in relative humidity, with some change toward stability in the temperature profile and (2) close to a -4/3 change of C_n^2 with height even though surface layer conditions were nearly adiabatic. As with the temperature profiles for unstable conditions, it can be shown that very small changes in the profile slope toward a more stable profile near z_i can produce significant changes in the distribution and exchange of heat and moisture below and through z_i.

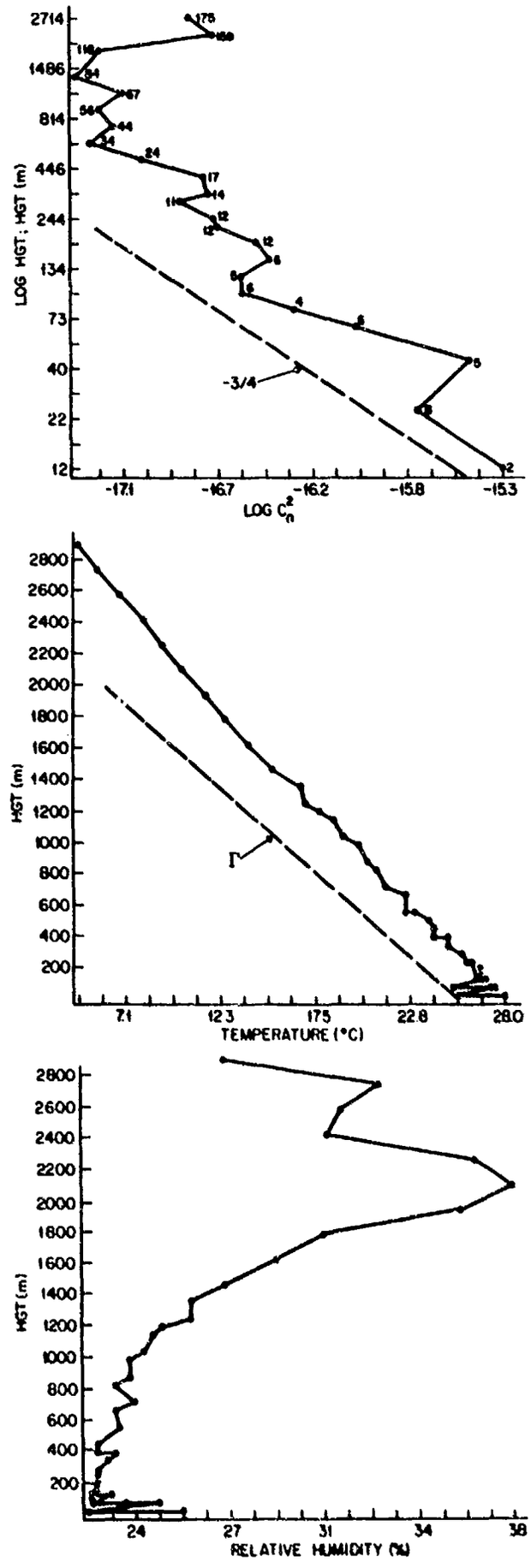

Fig. 17 Average of 7 profiles of C_n^2, temperature and relative humidity for near-adiabatic conditions for CLEAR I data.

4. Model testing and software development

Results given in prior sections have demonstrated the effectiveness of solar irradiance and wind speed in determining C_n^2 not only at a reference level near the ground but also, to some extent, C_n^2 profiles through the boundary layer. Measurements of solar irradiance, however, are not routinely available. For the C_n^2 model developed here, solar irradiance is estimated from cloud and other information; cloudiness and wind speed are the input variables. Similarly, measurements of z_i are not routinely available, but estimates can be made with cloudiness and wind speed information.

4.1 Unstable stratification

The solar irradiance (direct plus diffuse irradiance on a horizontal surface) portion of the model was developed with the following inputs:

1) Latitude & longitude,
2) Day of year,
3) Time of day,
4) Cloud amount, preferably at the height of each cloud layer,
5) Cloud heights
   a) low-middle (< 20,000 ft.)
   b) low-middle & high (mixed layers)
   c) high ($\geq$ 20,000 ft.).

Inputs 1) to 3) lead to calculations of hourly values of extraterrestrial solar irradiance on a horizontal surface and of the elevation

angle of the sun. Inputs 4), 5) and solar elevation adjust the extra-terrestrial irradiance values for determining amounts reaching the earth's surface. Steps in the program are as follows:

(1) Extraterrestrial solar irradiance is calculated with inputs 1), 2) and 3) (Paltridge and Platt, 1976).

(2) An "equivalent cloud amount" denoted by cc is determined with inputs 4) and 5) as follows:

(a) for low to middle clouds, cc = total sky cover (in tenths);

(b) for high clouds, cc = 1/2 total sky cover; and

(c) for mixed layers: cc = total sky cover - 1/2 high sky cover, or cc = .75 total sky cover if amounts at various heights are not reported.

It is assumed that low and middle clouds have similar diminution effects on solar irradiance. With an "equivalent cloud amount" and the solar elevation angle, solar irradiance is determined with the following empirical equations (Turner and Mujahid, 1984), where E is solar elevation; ETRAD is extraterrestrial irradiance; and RAD is irradiance at the surface:

$$\begin{aligned}
&\text{for } E > 60°: && RAD = ETRAD\,(.6423 + .9109(cc)^2\sin(E) - 1.2873(cc)^2 \\
&&& \qquad + 1.222\sin(E)); \\
&\text{for } E \leq 20°: && RAD = ETRAD\,(.308 - 1.165(cc)^2\sin(E) - .0586(cc)^2 \\
&&& \qquad + 1.0743\sin(E)); \qquad (17) \\
&\text{for } 20° < E \leq 40°: && RAD = ETRAD\,(.5695 - .1065(cc)^2\sin(E) - .4755(cc)^2 \\
&&& \qquad + .2809\sin(E)); \text{ and} \\
&\text{for } 40° < E \leq 60°: && RAD = ETRAD\,(.7862 - .2736(cc)^2\sin(E) + .6943(cc)^2 \\
&&& \qquad - .0467\sin(E)) .
\end{aligned}$$

Values of solar irradiance (RAD) calculated with the model were compared with measured values for 17 days in the CLEAR I data. The measured data consisted of 194 values of irradiance on the hour that were abstracted from graphs of daily variations of irradiance provided for the CLEAR I experiments. The cloud observations used in the calculations were available only for Holloman AFB, about 68 km from where the measurements were made. A ratio of calculated to measured values (R) and its inverse (Inv R) were defined:

$$\text{Ratio}(R) = \frac{\text{RAD calc}}{\text{RAD meas}}$$

$$\text{Inv } R = R \text{ if } R \geq 1 \qquad (18)$$

$$= \frac{1}{R} \text{ if } R \leq 1$$

Table 12 lists the individual days from CLEAR I, the number of samples and the average of Inv R for each day and Table 13 summarizes the test results in terms of R and Inv R. The results given in Table 12 and 13 show that the irradiance model underestimates the true irradiance more often than it overestimates it. Of the 194 calculations, 52.6% of them were within 90% of the measured values and 68.7% of them were within 75% of measured values.

The same 17 days were used to test the C_n^2 single-height model. Computations of RAD together with wind speed are the components of the model as given by Equation 13 in Section 3.1.1. The measured data consisted

Table 12 Average values of Inv R for solar irradiance for CLEAR I days

Date (1984)	Sample Size	Inv R
8/29	13	1.56
8/30	8	2.65
8/31	13	1.14
9/1	13	1.11
9/7	13	1.13
9/8	13	1.16
9/10	13	1.34
9/11	12	1.66
9/18	12	1.43
9/20	12	1.10
9/21	12	1.23
9/22	8	1.57
9/23	12	1.22
9/24	12	1.30
9/25	11	1.97
9/26	6	1.52
9/27	11	6.78

Table 13 Results of testing the solar irradiance model against measurements for CLEAR I for 194 samples. R is the ratio of calculated to measured values of solar irradiance

	Min.	Max.	Avg.	Sample Size	% of Samples
R < 1	.02	.99	.85	106	54.6%
R = 1	1.00	1.00	1.00	5	2.6%
R > 1	1.01	8.84	1.55	83	42.8%

of tower 1, HIDL values on the hour of (1) wind speed at 4 m (2) solar irradiance and (3) C_n^2 for the 4-m scintillometer. For the calculations of C_n^2, RAD was estimated as described above and a 10-m wind speed (WS_{10}) was estimated with the 4-m speed (WS_4) with the power law relationship:

$$WS_{10} \approx WS_4 \left(\frac{10}{4}\right)^{0.209} \approx 1.211\ WS_4 \ , \qquad (19)$$

where the power law exponent for unstable conditions is an interpolated value based on work by Touma (1977). This approximation for WS_{10} is considered sufficient in view of the comparatively much larger effect of RAD on C_n^2.

The ratios of calculated to measured values of C_n^2 are as defined in Eq. 18. Table 14 lists the individual days, sample sizes and the average of Inv R for C_n^2 for each day and Table 15 summarizes the results. They show that the model overestimates C_n^2 nearly as often as it underestimates it. In addition, they show that 67.9% of the estimated values are within a factor of 2 of the measured values. As would be expected, the best agreement for both RAD and C_n^2 was found for periods with no cloudiness.

The entire C_n^2 model for unstable stratification, from estimates of C_n^2 for a single height with cloudiness and wind speed information to estimates of boundary layer profiles with the K-T model and estimates of z_i was tested against 3 measured C_n^2 profiles for the CLEAR I period and 3 for the CLEAR II period. Table 16 lists the dates and times of the soundings along with relevant information defined below. The symbols are as used in the software for the model.

Table 14 Average values of Inv R for C_n^2 for CLEAR I days

Date (1984)	Sample Size	Inv R
8/29	13	3.66
8/30	7	3.53
8/31	13	1.86
9/1	13	1.82
9/7	11	1.22
9/8	11	1.49
9/10	12	2.68
9/11	10	2.19
9/18	13	2.52
9/20	13	2.20
9/21	12	1.68
9/22	7	3.09
9/23	13	3.22
9/24	13	2.56
9/25	9	10.47
9/26	13	21.55
9/27	13	8.32

Table 15 Results of testing the single-height C_n^2 model. R is the ratio of C_n^2 calculated with irradiances and wind speeds to C_n^2 measured

	Min.	Max.	Avg.	Sample Size	% of Samples
$R < 1$	.10	.98	.64	105	53.6%
$R = 1$	1.00	1.00	1.00	1	.5%
$R > 1$	1.01	98.06	7.18	90	45.9%
$R < .5$	.10	.45	.25	17	8.7%
$.5 \leq R \leq 2$	.50	1.98	.94	133	67.9%
$R > 2$	2.02	98.06	12.72	46	23.5%

Table 16 Information relevant to CLEAR I and II soundings to test the C_n^2 profile model.

DATE (1984)	TIME	CC	CH	WS	z_i (est)	z_i (mea)
840907	1417	0	0	3.9	1180	2100
840908	1343	1	5	1.8	950	2600
840910	1457	3	1	3.5	1080	2700
850227	0938	2	7	3.6	820	450/1000
850301	0950	1	1	2.0	580	1700
850305	1441	<1	7	5.1	1450	1100

Time is mountain standard time.

CC is cloud amount in tenths of opaque cloudiness,

CH is the cloud height code given in the radiance model,

WS is wind speed (ms^{-1}) at 10m for CLEAR I and at 4m for CLEAR II, and

z_i is the mixed layer height (m) estimated from the Smith (1977) nomogram (est) and from temperature and humidity profiles (mea).

The model provided estimates of C_n^2 at 4m, with values at 10, 20, 40, 60m ... etc. calculated with eq. 14. The calculations were then averaged in the same manner as the measured soundings. Results are shown in Fig. 18a through 18f. The solid line is the model prediction and the dots are measured values. Except for the profile on 9/10/84, where cloudiness estimates may have been erroneous, reasonable agreement between measured and estimated values can be noted. A major source of error is the large discrepancies between estimated and measured values of z_i shown in Table 16. Reasons for the differences were not established as part of the present work.

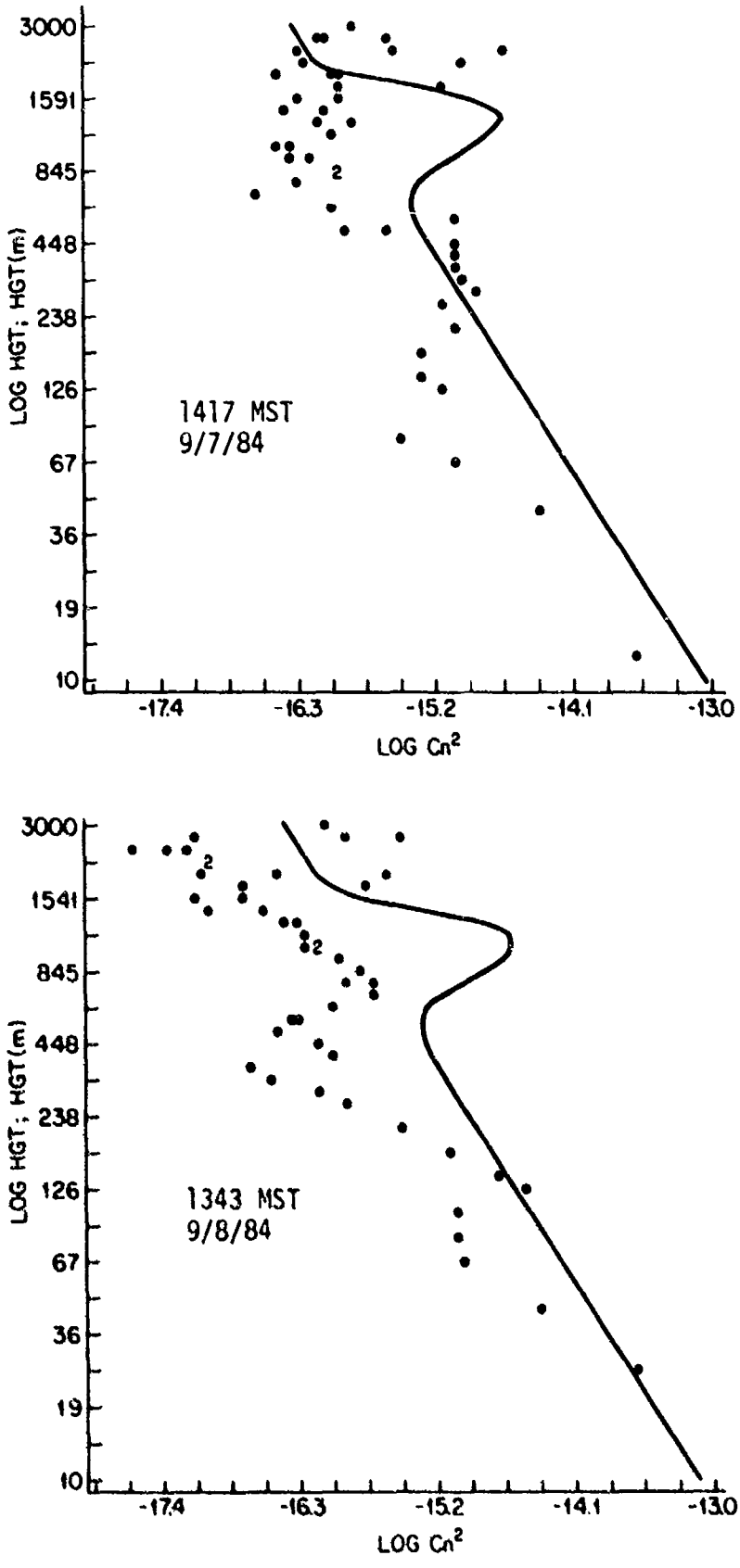

Fig. 18a Comparison of measured profiles of C_n^2 in unstable stratification (CLEAR I and II) with profiles calculated from cloudiness, wind speed, location, time and date information for 1417 MST, 9/7/84 and 1343 MST, 9/8/84.

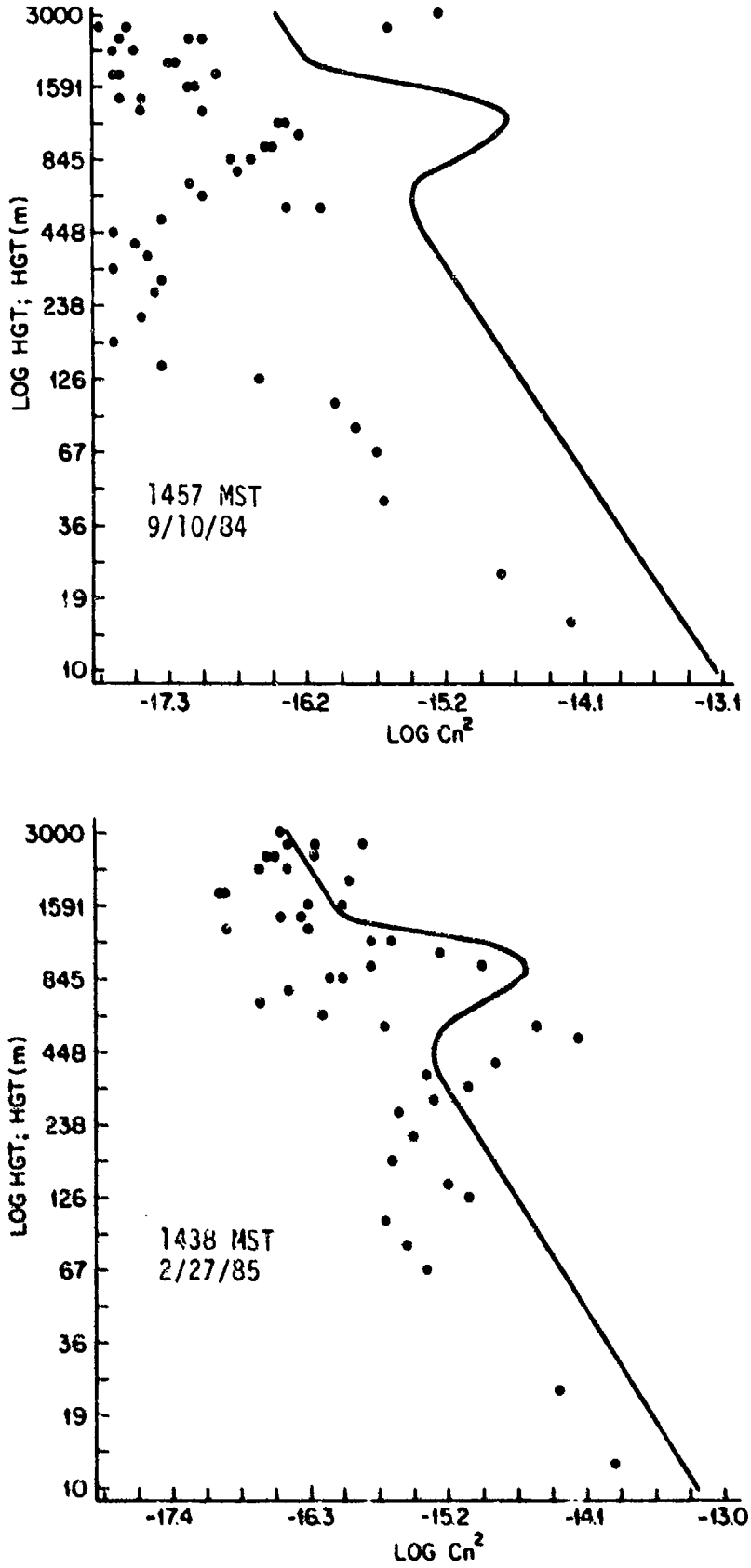

Fig. 18b Same as 18a, but for 1457 MST, 9/10/84 and 1438 MST, 2/27/85.

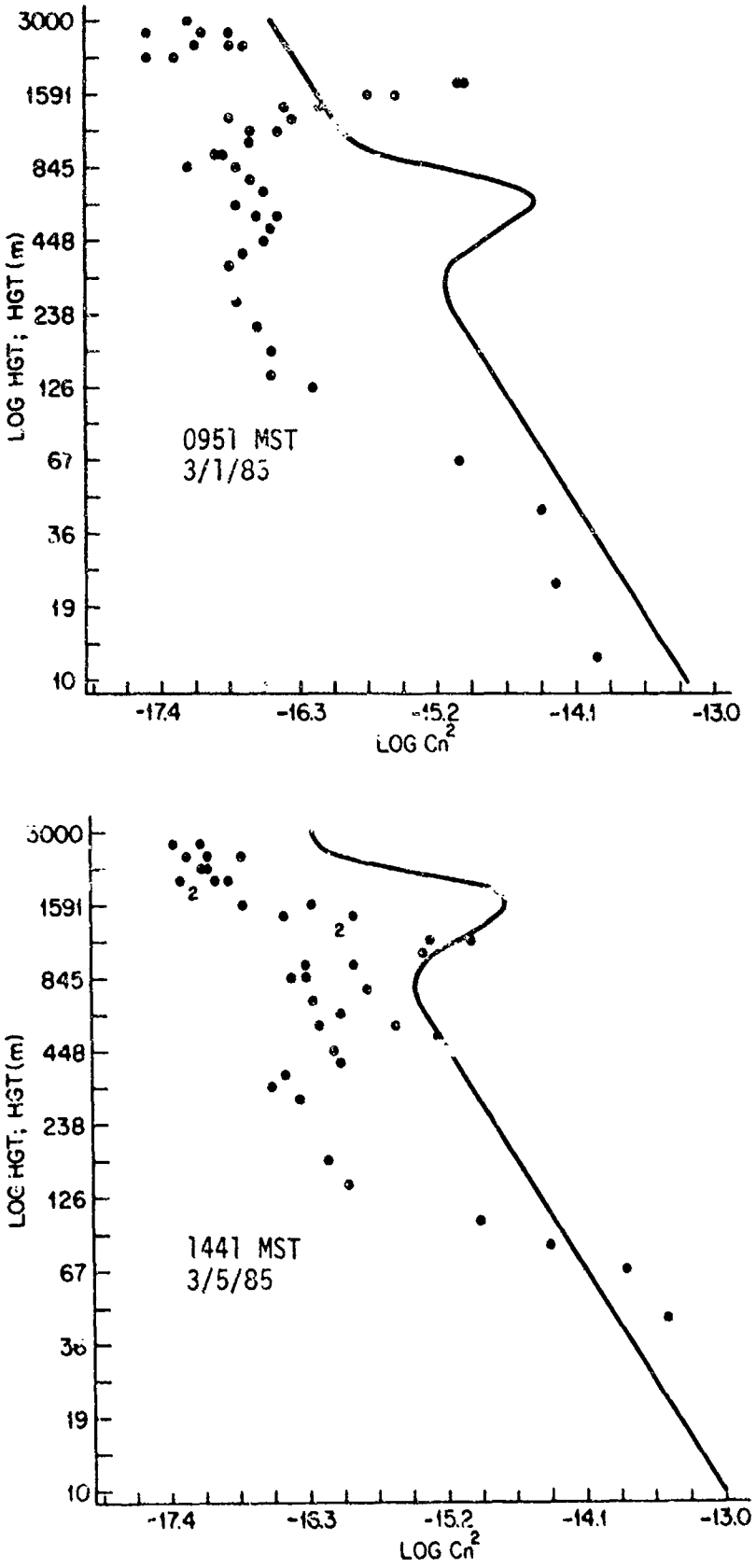

Fig. 18c Same as 18a, but for 0951 MST, 3/1/85 and 1441 MST, 3/5/85.

4.2 Stable stratification

As discussed in Section 3.2.2, the decrease in C_T^2 with height appeared to be inversely dependent on $\bar{u}_{10}$, but there were questions for $\bar{u}_{10} < 3$ ms^{-1} because of curvature in the C_T^2 profile and for $\bar{u}_{10} \gtrsim 6$ ms^{-1} because of small sample sizes. For $4 \lesssim \bar{u}_{10} \lesssim 6$ ms^{-1}, where a fully turbulent regime is likely, however, the slope was near -4/3. The average of the soundings for CLEAR I and II also indicated a slope near -4/3 above the first sounding height.

Based on these experimental results, a -4/3 slope was accepted in the present work for describing $C_n^2(C_T^2)$ in a turbulent stable boundary layer above 10m. A -2/3 dependence predicted by similarity theory may exist, but as indicated by Walters and Kunkel (1981), it is probably below the lowest measurement height which, in their case, was 8 m.

The final model for stable stratification, then, consists of the C_n^2-wind speed regression equation obtained for the BAO data for 10 m coupled with a $C_n^2 \propto z^{-4/3}$ variation above 10 m. The model was tested with 3 CLEAR I and 3 CLEAR II soundings selected arbitrarily and the results are shown in Fig. 19a through 19c for heights from 10 m to 3000 m. The solid line is the model prediction.

It can be noted that for most cases, below about 800 m, estimated values are greater than measured values, but a -4/3 slope provides a reasonable estimate of $C_n^2(z)$. There could be many reasons for the behavior and differences shown. They involve terrain effects that are especially important in stable conditions, cloudiness differences between Holloman AFB and the measurement site (for the CLEAR I data) and other effects that are less evident but possibly as important.

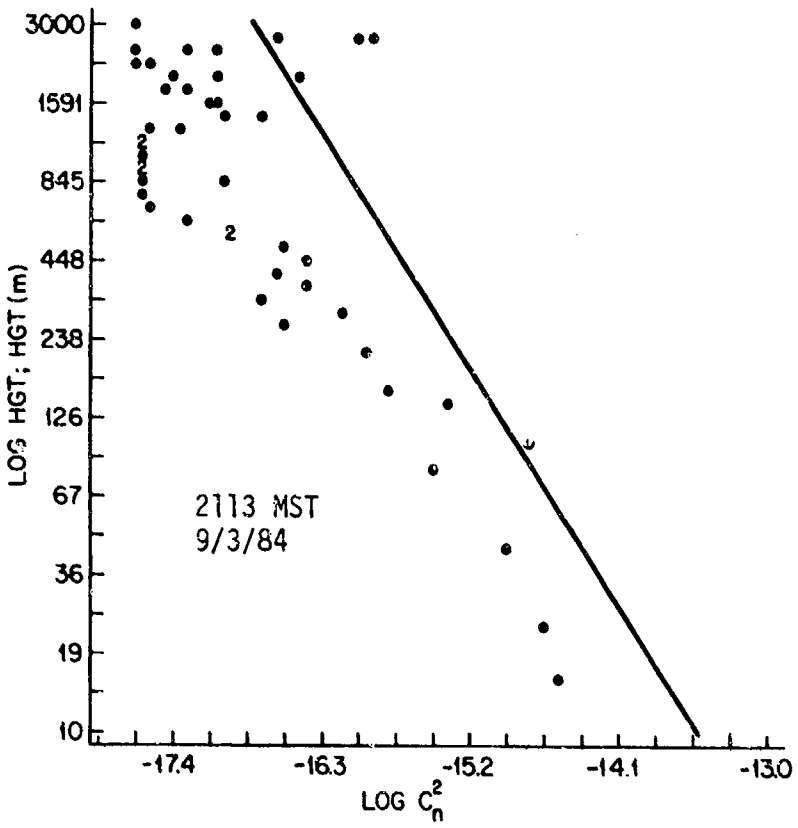

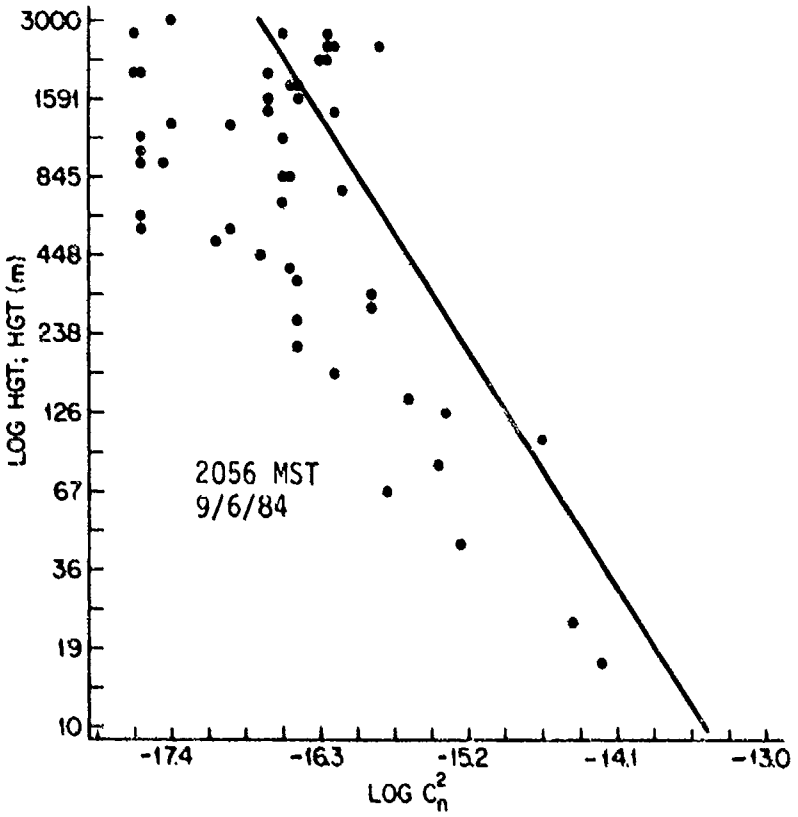

Fig. 19a Comparison of measured profiles of C_n^2 in stable stratification (CLEAR I and II) with profiles calculated from the BAO C_n^2-wind speed relationship and a -4/3 height variation; 2113 MST, 9/3/84 and 2056 MST, 9/6/84.

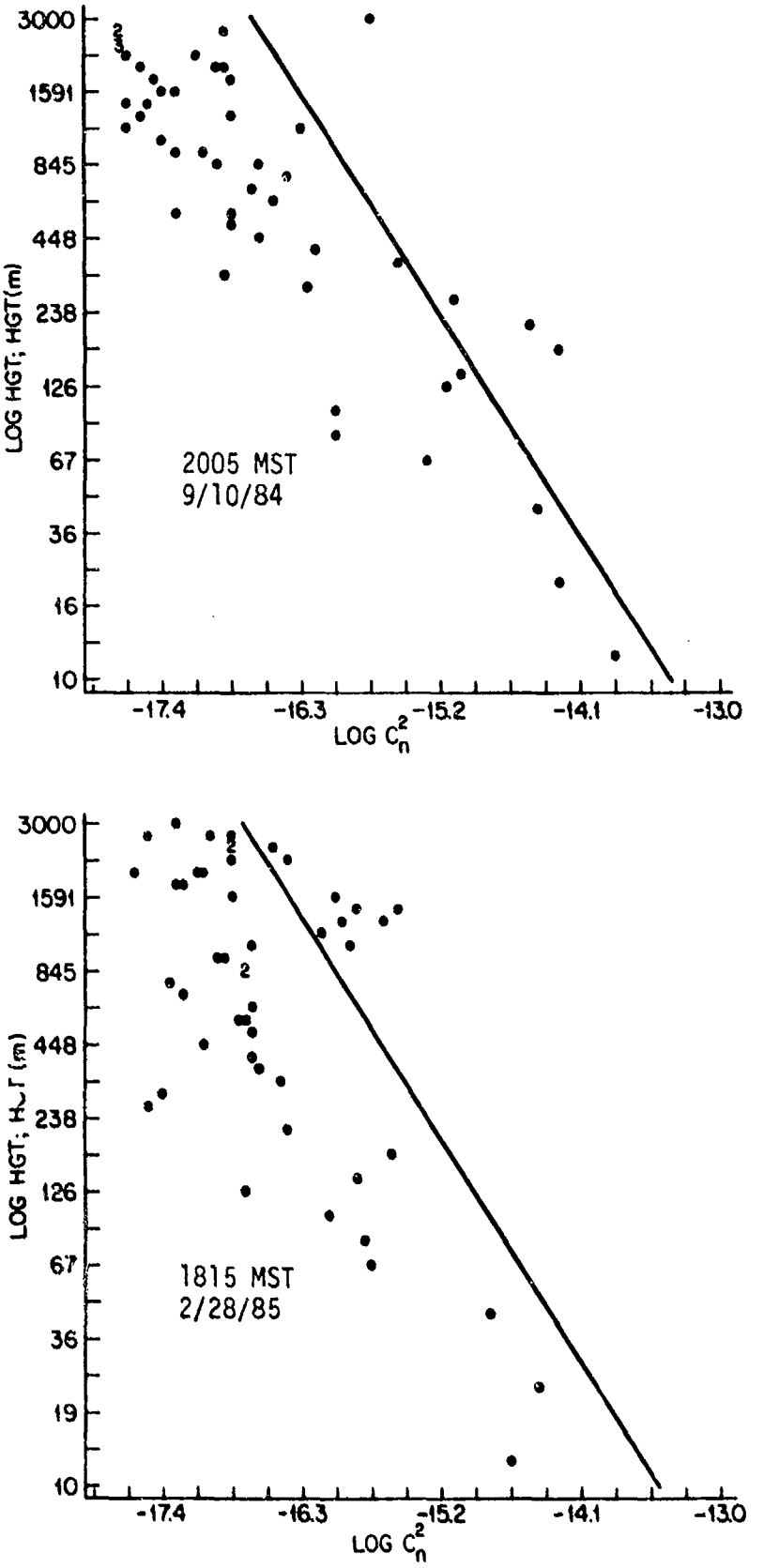

Fig. 19b Same as 19a, but for 2005 MST, 9/10/84 and 1815 MST, 2/28/85.

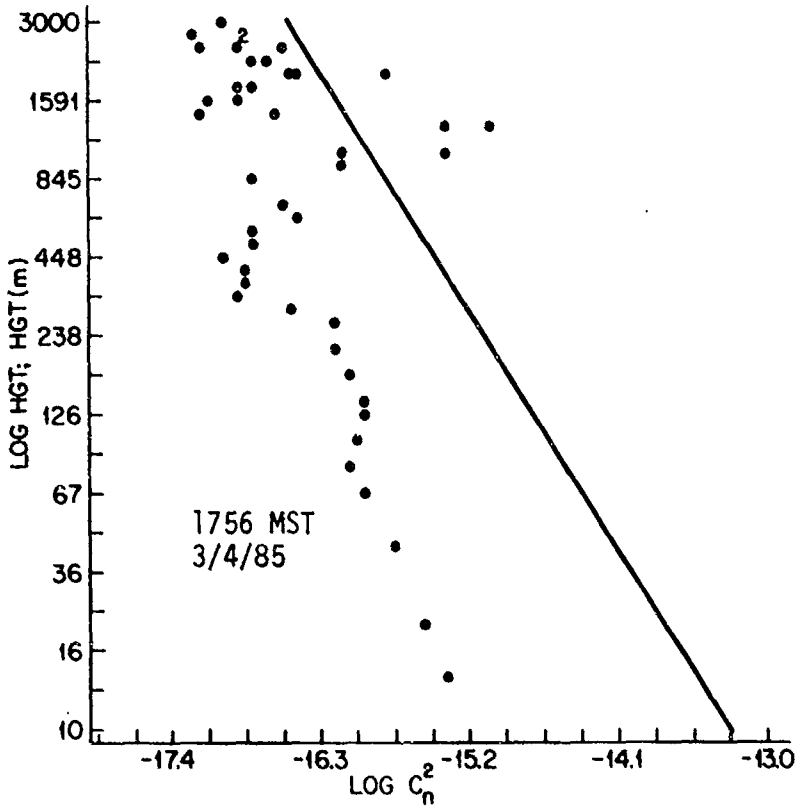

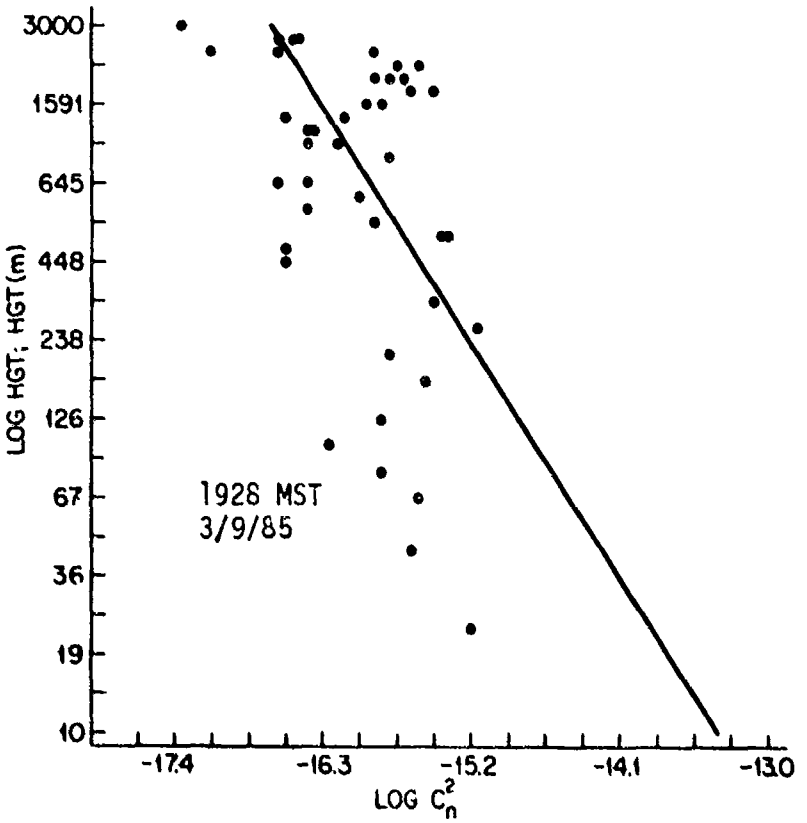

Fig. 19c Same as 19a, but for 1756 MST, 3/4/85 and 1928 MST, 3/9/85.

4.3 Fortran Program

CNSQ PROG and STABLE are FORTRAN IV programs that were developed to (1) calculate C_n^2 at one height, and with additional information, (2) calculate its height variation for the boundary layer. The programs are described, together with a discussion of input variables, operation and output variables, and adaptation for use at different sites. Examples of how they are run on the FORTRAN IV compiler on the Michigan Terminal System are also given with soundings for White Sands, NM, listed in Appendix A and B.

4.3.1 Input variables for unstable stratification

The following are the input variables for the program that are necessary for its operation:

a) Year, month, day, and time,

b) Cloud cover and cloud height code,

c) Wind speed at 10 meters and

d) Height of the mixed layer (z_i).

a) Year, month, day, and time. Because the program is presently written for White Sands, NM, time is in Mountain Standard Time. The program listed is valid for one hour after sunrise to one hour before sunset.

b) Cloud cover and cloud height code. Cloud cover is in tenths of total sky cover (preferably opaque sky cover) and the cloud height codes are described below:

0 - clear

1 - low clouds; cloud base < 10,000 ft

2 - middle clouds; 10,000 ft $\leq$ cloud base < 20,000 ft

3 - low & middle clouds

4 - low & high clouds

5 - low, middle & high clouds

6 - middle & high clouds

7 - high clouds; cloud base 20,000 ft

c) Wind speed at 10 meters. Because wind speed is routinely reported in knots as a measured variable in conventional surface weather observations, this unit was used in the program for C_n^2. If wind speed is available for a height other than 10 m, the following form of the power law for a moderately unstable boundary layer can be used (Touma, 1977):

$$WS_{10} \approx WS_z(10/z)^{0.209} ,$$

where z is the height of the measured wind speed in meters.

d) Height of the mixed layer (z_i). The time of day, cloud cover, and average wind speed at 10 m (or an estimate of it, as above) are required for z_i estimates with the Smith (1977) nomogram. The mixed layer height estimated for the example given here to illustrate the operation of the program was about 950 m.

4.3.1.1 Description and operation

The following is a brief description of the variables, statements, and functions in CNSQ.PROG:

Lines 1-8: RLAT: latitude of site in °

RLON: longitude of site in °

RZONE: 15° longitude increment for the time zone of the site (105° for MST)

SCON: The solar constant in ly/min.

EXPO: -4/3 (the slope of the variation of C_n^2 with height)

H4: 4 meters, the height for which a "surface C_n^2" value will be estimated.

Lines 9-24: enter input variables.

Line 25: IDATE is the date in I6 format (YR/MON/DAY)

Line 26-41: Calculate the zenith angle and elevation angle of the sun for the time desired, with which a value of extra-terrestrial solar irradiance is calculated.

RTIME: time in hours & tenths of an hour. For example 1344 = 13.7$\overline{333}$.

EQTM: the value from the "equation of time", which accounts for the change in solar noon as a function of time of year.

STIME: solar time.

HAS: hour angle of the sun in radians.

DECL: solar declination in radians.

COSZ: cosine of the solar zenith angle.

ETRAD: solar irradiance at the "top of the atmosphere" in ly/min.

Z: solar zenith angle in degrees.

E: solar elevation angle in degrees.

Lines 42-60: Calculate global solar irradiance at the earth's surface with cloud cover, cloud height code, and solar elevation angle as inputs.

RADC: calculated global solar irradiance at the earth's surface in ly/min.

Line 61: Converts wind speed from knots to m/sec.

Line 62-63: The regression eqn. for estimating C_n from calculated radiance and wind speed.

Line 64: sets $C_n = 10^{-8}\ m^{-1/3}$ if the regression equation produces a value below 10^{-8}.

Line 65: Calculates C_n^2 where CNSQC is calculated C_n^2 in $m^{-2/3}$ at 4 m.

Lines 66-67: Write the "surface measurement" of C_n^2, along with the input variables, into a file called "SURFACE" in the sample run.

Lines 68-77: Compute the C_n^2 profile with equation 14. Lines 72-73 calculate $\log_{10}$ of C_n^2 and height, and line 76 adjusts the height interval (20 m in this case). Line 69 determines how many values of C_n^2 will be calculated. In the example, there are 151 values from 20 m to 3000 m.

HGT: height in meters.

CNZC: calculated C_n^2 in $m^{-2/3}$.

HGTLOG: $\log_{10}$ HGT.

CNZLOG: $\log_{10} C_n^2$.

Lines 81-110: A subroutine used in line 26 which converts the year, month, and day into Julian calendar day, which is then used to compute solar declination.

IB: Julian calendar day.

4.3.1.2 Output variables and program adaptations

The output of the program is as shown for the sample run, with values of height, C_n^2, $\log_{10}$ (height), and $\log_{10} C_n^2$ printed out. The $\log_{10}$ values are retained for model output graphs of values of $\log_{10}$ (height) vs. $\log_{10} C_n^2$. Some of the statements in the program must be altered to be applicable to a site other than White Sands, NM. A list of these statements is given below.

Line 1: RLAT

Line 2: RLON

Line 3: RZONE, the 15° longitude line corresponding to the time zone of the site. For example, for the Eastern Time Zone, RZONE = 75.

In addition;

Line 69 & 76: The do-loop parameter and height interval can be adjusted as desired.

4.3.2 Input variables for stable stratification

The FORTRAN program CNSQ. STABLE was developed to calculate the profile of C_n^2 for stable conditions. It is a relatively short program and uses the "normal curve" approximation for the variation of C_n^2 with wind speed at 10 meters with eq. (16) developed for the BAO data. If wind speed is measured at a height other than 10 meters, the following equation can be used to obtain the 10-m speed for stable conditions (Touma, 1977):

$$WS_{10} = WS_z \left(\frac{10}{z}\right)^{.414} , \qquad (20)$$

where WS_{10} is the estimated wind speed at 10 m and WS_z is the speed measured at height z.

4.3.2.1 Description and operation

A brief description of the statements in CNSQ. STABLE is given below:

Line 1: the exponent (-4/3) used in the equation for the variation of C_n^2 with height.

Lines 2-5: statements that enable the user to enter the wind speed at 10 m.

Line 6: a conversion for wind speed from knots to ms^{-1}.

Line 7: calculates an estimate of C_n^2 at 4 m with equation (16) where CN SQC is $C_n^2(4m)$.

Lines 8-9: write the estimated "surface C_n^2".

Lines 10-18: involve a do-loop that calculates the C_n^2 profile. The do-loop parameter (I in Line 11) and the height interval (20 m

in Line 17) can be changed as desired. Lines 15-16 write the following variables into a file, where

HGT = height

CN2C = calculated C_n^2 at HGT

HGTLOG = $\log_{10}$(HGT)

CN2LOG = $\log_{10}(C_n^2)$.

In the example, the "surface" estimate of C_n^2 is written into the file SURFACE, and the C_n^2 profile is written into the file PROFILE. The example used corresponds to the White Sands, NM thermosounding at 21:13:31 on 9/3/84.

5. Conclusions and recommendations

1) For daytime conditions with half or less of the sky cloud-covered, C_n^2 at one height was describable in relation to solar irradiance and wind speed. C_n^2 increased with solar irradiance and wind speed until certain values were reached and was expressible in terms of a third-order polynomial involving C_n^2 and these two variables.

2) The Kukharets and Tsvang profile model for C_n^2 tested satisfactorily against thermosonde measurements of C_n^2 through a convective boundary layer up to 3000 m provided that values of mixing depth were obtainable to the nearest 100 m and that C_n^2 at a reference height was known.

3) By applying a model for calculating solar irradiance with cloud and other information, and by using the value of C_n^2 calculated with the solar irradiance-wind speed regression equation, it was possible to estimate C_n^2 at a reference height. With this information, together with estimates of mixing height and the Kukharets and Tsvang model, a goal of describing the variation of C_n^2 through the atmospheric boundary layer with conventional meteorological variables was reached for unstable stratification. A major source of error was in estimating z_i.

4) For nighttime conditions with half or less of the sky cloud-covered, C_n^2 at a reference height was describable in terms of wind speed alone. Actual values depend on the reference height, but in general, C_n^2 increased sharply as wind speed increased from nearly calm, it reached maximum values in a narrow wind speed interval, and decreased at higher speeds. These changes were expressible with appropriate coefficients in the equation for a normal curve.

5) The C_n^2-wind speed equation for calculating C_n^2 at a reference

height, together with a -4/3 height variation of C_n^2 above the reference height obtained from thermosonde data, enabled a goal of describing the variation of C_n^2 through the atmospheric boundary layer with conventional meteorological variables to be reached for stable stratification.

6) For near adiabatic conditions, C_n^2 for a reference height in the surface layer was at minimum values. Above about 10 meters, a -4/3 height variation through the boundary layer was indicated even though very small values of C_n^2 were observed.

7) Occasionally, large morning-to-afternoon differences in C_n^2 for the same value of solar irradiance were observed mainly for the RADC data but also, to a lesser extent, for other locations. They were not fully explainable because the necessary types of measurements were not available. This characteristic is probably the major source of error in the C_n^2-solar irradiance-wind speed relationship. For conditions over surfaces with high soil moisture and large evaporation, two relationships, one for morning and one for afternoon, would probably be more representative. It is recommended that this important question be answered with measurements of optical turbulence over moist (grass-covered) surfaces that are documented with measurements of temperature, humidity and wind speed profiles as well as soil moisture and radiation.

8) Significantly different values of $C_n^2(C_T^2)$ are obtainable with different methods of measurement. Not discussed here are yet other methods, such as SODAR and LIDAR that are being used for this purpose. It is recommended that an intercomparison experiment be conducted with the various methods to determine, for various turbulence conditions, not only how they compare but also which method provides the most representative values of optical turbulence as it affects the performance

of optical systems.

9) The thermosonde data used as a reference in comparing profile measurements of C_n^2 with model estimates were invaluable, but one shortcoming that limited their usefulness was a lack of a standard lowest height of measurement. It is recommended that, if possible, a thermosonde system equivalent to that being launched, together with a wind speed and direction system, be operated at one height within the first few meters before and during each thermosounding to provide a reference measurement of C_n^2 and wind velocity.

REFERENCES

Blackadar, A.K., 1957: "Boundary layer wind maxima and their significance for the growth of nocturnal inversions." Bull. Amer. Meteor. Soc., 38, 283-290.

Bonner, W.D., 1968: "Climatology of the low-level jet." Mon. Weather Rev., 96, 830-850.

Brost, R.A. and J.C. Wyngaard, 1978: "A model study of the stably stratified planetary boundary layer." J. Atmos. Sci., 35, 1427-1440.

Brown, J.H., R.E. Good, P.M. Bench, and G. Faucher, 1982: Sonde Experiments for Comparative Measurements of Optical Turbulence. AFGL-TR-82-0079, AD A118740, 46 pp.

————, and R.E. Good, 1984: Thermosonde and UHF Radar Measurements of C_n^2 at Westford, Massachusetts - July, 1981. AFGL-TR-84-0109 (ADA145398), 57 pp.

Burk, S.D., 1980: "Refractive index structure parameters: time-dependent calculations using a numerical boundary-layer model." J. Appl. Meteor., 19, 562-76.

Carson, D.J. and F.B. Smith, 1974: "Thermodynamic model for the development of a convectively unstable boundary layer." Advances in Geophysics, 18A, Academic Press, Inc., NY, 111-124.

Caughey, S.J. and S.G. Palmer, 1979: "Some aspects of turbulence structure through the depth of the convective boundary layer." Quart. J. R. Meteor. Soc., 105, 811-827.

————, J.C. Wyngaard and J.C. Kaimal, 1979: "Turbulence in the evolving stable boundary layer." J. Atmos. Sci., 36, 1041-52.

————, 1982: "Observed characteristics of the atmospheric boundary layer." In: Atmospheric Turbulence and Air Pollution Modeling, Nieuwstadt FTM and H van Dop (eds.), Dordrecht, Boston, London, 107-158.

Davidson, K.L., G.E. Schacher, C.W. Fairall and A.K. Goroch, 1981: "Verification of the bulk method for calculating overwater optical turbulence." Appl. Opt., 20, 2919-24.

Deardorff, J.W., G.E. Willis and D.K. Lilly, 1969: "Laboratory investigation of nonsteady penetrative convection." J. Fluid Mech., 7, 7-31.

————, 1972: "Numerical investigation of neutral and unstable planetary boundary layers." J. Atmos. Sci., 29, 91-115.

————, 1974: "Three-dimensional numerical study of turbulence in an entraining mixed layer." Boundary-Layer Meteor., 7, 199-226.

Dewan, E.M., 1980: Optical Turbulence Forecasting: A Tutorial. AFGL-TR-80-0030 (ADA086863), 70 pp.

————, 1982: On the Difference Between Waves and Turbulence in a Stratified Fluid. AFGL-TR-82-0352 (ADA126321), 39 pp.

Fairall, C.W., K.L. Davidson, and G.E. Schacher, 1982: "Meteorological models for optical properties in the marine atmospheric boundary layer." Opt. Eng., 21, 847-57.

Fragapane, S.E., J.J. Eric, and J.S. Foster, 1983: (Private communication).

Gamo, M., O. Yokoyama, S. Yamamoto and M. Mitsuta, 1976: "Structure of the atmospheric boundary layer derived from airborne measurements of the energy dissipation rate ε." J. Meteor. Soc. Japan, 54.

Garrat, J.R., 1982: "Observations in the nocturnal boundary layer." Boundary-Layer Meteor., 22, 21-48.

Gurvich, A.S., A.I. Kon, B.L. Mironov and S.S. Khmelevstov, 1976: Lazernoe Izluchenie v Turbulentnoi Atmosfere (Laser Radiation in a Turbulent Atmosphere) AN SSSR Institute of the Physics of the Atmosphere, Moscow. 277 pp.

Haugen, D.A., J.C. Kaimal and E.F. Bradley, 1971: "An experimental study of Reynolds stress and heat flux in the atmospheric surface layer." Quart. J. Roy. Meteor. Soc., 97, 168-80.

Hill, R.J., S.F. Clifford and R.S. Laurence, 1980: "Refractive-index and absorption fluctuations in the infrared caused by temperature, humidity and pressure fluctuations." J. Opt. Soc. Amer., 70, 1192-1205.

Hooke, W.H., 1979: Project Phoenix. NOAA/ERL Wave Propagation Laboratory, 281 pp.

Kaimal, J.C., 1973: "Turbulence spectra, length scales, and structure parameters in the stable surface layer". Boundary-Layer Meteor., 4, 289-309.

————, J.C. Wyngaard, D.A. Haugen, O.R. Cote, Y. Izumi, S.J. Caughey, and C.J. Readings, 1976: "Turbulence structure in the convective boundary layer". J. Atmos. Sci., 33, 2152-69.

————, and J.E. Gaynor, 1983: "The Boulder Atmospheric Observatory." J. App. Meteor., 22, 863-880.

————, N.L. Abshire, R.B. Chadwick, M.T. Decker, W.H. Hooke, R.A. Kropfli, W.D. Neff and F. Pasqualucci, 1980: "Convective boundary layer thickness estimated by in-situ and remote probes". Proc. Nineteenth Conf. on Radar Meteor., Apr. 15-18, 1980, Am. Meteor. Soc. 633-636.

————, N.L. Abshire, R.B. Chadwick, M.T. Decker, W.H. Hooke, R.A. Kropfli, W.D. Neff and F. Pasqualucci, 1982: "Estimating the depth of the daytime convective boundary layer". J. Appl. Meteor., 21, 1123-1129.

Kasten, F. and G. Czeplak, 1980: "Solar and terrestrial radiation dependence on the amount and type of cloud." Solar Energy, 24, 177-189.

Kjelaas, A.G. and G.R. Ochs, 1974: "Study of divergence in the boundary layer using optical propagation techniques." J. Appl. Meteor., 13, 242-248.

Kohsiek, W., 1985: "A comparison of line-averaged observation of C_n^2 from scintillation of a CO_2 laser beam and time averaged in situ observations." J. Appl. Meteor., 24, 1099-1103.

Kukharets, V.P. and L.R. Tsvang, 1977: "Turbulent energy dissipation rate in the unstably stratified boundary layer." Izv. AN SSSR atmos. and Oceanic Physics, 13, 620-628.

———————————, 1980: "Structure parameter of the refractive index in the atmospheric boundary layer." Izv. AN SSSR Atmos. and Oceanic Physics, 16, 73-77.

Kunkel, K.E., D.L. Walters, and G.A. Ely, 1981: "Behavior of the temperature structure parameter in a desert basin". J. Appl. Meteor., 20, 130-36.

———, 1982: "2-dimensional field of thermal turbulence at the edge of an escarpment". Boundary-Layer Meteor., 23, 473-87.

———, and D.L. Walters, 1982: "Intermittent turbulence in measurements of the temperature structure parameter under very stable conditions". Boundary-Layer Meteor., 22, 49-60.

———, and D.L. Walters, 1983: "Modeling the diurnal dependence of the optical refractive index structure parameter". J. Geophys. Res., 88, 10.999-11.004.

Monin, A.S. and A.M. Obukhov, 1954: "Basic laws of turbulent mixing in the ground layer of the atmosphere." AN SSSR, Trudy, Leningrad Geophys. Inst., 151, 163-187.

Murphy, E.A., E.M. Dewan and S.M. Sheldon, 1985: "Daytime comparisons of C_n^2 models to measurements in a desert location." Paper presented at meeting of Society of Photo-Optical Instrumentation Engineers (SPIE), April 1985.

Nieuwstadt, F.T.M. and A.G.M. Driedoncks, 1979: "The nocturnal boundary layer: a case study compared with model calculations." J. Appl. Meteor., 18, 1397-1405.

————————, 1984: "Some aspects of the turbulent stable boundary layer." Boundary-Layer Meteor., 30, 32-55.

Obukhov, A.M., 1960: "The structure of temperature and velocity fields in free convection." Izv. Akad. Nauk USSR, Geophys. Series, No. 9, 1392-96.

Ochs, G.R., R.F. Quintana and G.F. Miller, 1977: An Optical Device for Measuring Refractive - Index Fluctuation in the Atmosphere, NOAA Tech. Memo. ERL WPL-30, (AD 51 435/6GI), 10 pp.

Paltridge, G.W. and C.M.R. Platt, 1976: Radiative Processes in Meteorology and Climatology. Elsevier, 318 pp.

Portman, D.J., F.C. Elder, E. Ryznar, and V.E. Noble, 1962: "Some Optical properties of turbulence in stratified flow near the ground." J. Geophys. Res., 67, 3223-3235.

————, E. Ryznar and A.A. Waqif, 1968: Laser Scintillation Caused by Turbulence Near the Ground. Res. Report 225, US Army Cold Regions Research and Engineering Laboratory, Hanover, NH, (AD 666 798), 77 pp.

Ryznar, E., 1963: "Visual resolution and optical scintillation in stable stratification over snow." J. Appl. Meteor., 2, 526-530.

————, 1971: Wind and Temperature Structure in the Surface Layer of the Atmosphere. Univ. Mich. Final Report, US Army Contract DAGCO 4-67-C-0027, (AD 735 393), 81 pp.

Smith, F.B., 1977: "Application of data from field programs to estimation of K profiles and vertical dispersion." TDN No. 86, Meteorol. Office, Boundary Layer Res. Branch, Bracknell, Berkshire, U.K.

Smith, G.R., 1984: Surface Soil Moisture Measurements of the White Sands, New Mexico. NOAA Tech. Memo. NESDIS 7, (PB-135754/XAB), 12 pp.

Tatarski, V.I., 1961: Wave Propagation in a Turbulent Medium, McGraw-Hill, New York, 285 pp.

Thorpe, A.J. and T.H. Guymer, 1977: "The nocturnal jet." Quart. J. R. Meteor. Soc., 103, 633-653.

Touma, J.S., 1977: "Dependence of the wind profile power law on stability for various locations." J. Air Poll. Assoc., 27, 863-866.

Turner, W.D. and A. Mujahid, 1984: "The estimation of hourly global solar radiation using a cloud cover model developed at Blytheville, Arkansas. J. Appl. Meteor., 23, 781-786.

Voyt, F. Ya., Ye. Ye. Korniyenko, V.P. Kukharets, S.B. Khusid and L.R. Tsvang, 1973: "Structural characteristics of the temperature field in the surface layer of the atmosphere." Izv. Atmos. and Ocean. Physics, Akad Nauk. USSR, 9, 451-459.

Walters, D.L., and K.E. Kunkel, 1981: "Atmospheric modulation transfer function for desert and mountain locations: the atmospheric effects on r_0." J. Opt. Soc. Am., 71, 397-405.

Webb, E.K., 1984: "Temperature and humidity structure in the lower atmosphere." Geodetic Refraction-Effects of Electromagnetic Wave Propagation through the Atmosphere (ed. F.K. Brunner). Springer: Berlin, Heidelberg, New York, Tokyo, 85-141.

Wesely, M.L., 1976: "The combined effect of temperature and humidity fluctuations on refractive index." J. Appl. Meteor., 15, 43-49.

———— and E.C. Alcaraz, 1973: "Diurnal cycles of the refractive index structure function coefficient." J. Geophys. Res., 78, 6224-6232.

Wyngaard, J.C., Y. Izumi, and S.A. Collins, 1971: "Behavior of the refractive index structure parameter near the ground". J. Opt. Soc. Am., 61, 1646-50.

Wyngaard, J.C. and M.A. LeMone, 1980: "Behavior of the refractive index structure parameter in the entraining convective boundary Layer". J. Atmos. Sci., 37, 1573-1585.

Zhou, M.Y., D.H. Lenschow, B.B. Stankov, J.C. Kaimal and J.E. Gaynor, 1985: "Wave and turbulence structure in a shallow baroclinic boundary layer and overlying inversion." J. Atmos. Sci., 42, 47-57.

Appendix A. Fortran IV program for C_n^2 model for unstable stratification, with example for 1344 MST, 8 Sept. 1984 for White Sands, NM.

CNSQ.PROG

```
      RLAT=32.4
      RLON=106.37
      RZONE=105.
      PI=3.141592654
      DTR=PI/180.
      SCON=1370./697.8
      EXPO=-4./3.
      H4=4.
      WRITE(6,101)
  101 FORMAT('$Enter year, month, day, and time (MST)  (3I2,I5): ')
      READ(5,102) IYR,IMON,IDAY,ITIME
  102 FORMAT(3I2,I5)
      WRITE(6,201)
  201 FORMAT('$Enter cloud cover (in tenths) and cloud height code (2I2):')
      READ(5,202) ICC,ICH
  202 FORMAT(2I2)
      WRITE(6,301)
  301 FORMAT('$Enter wind speed at 10 metres (in knots)  (F4.1): ')
      READ(5,302) WS
  302 FORMAT(F4.1)
      WRITE(6,401)
  401 FORMAT('$Enter estimated height of mixed layer (in metres)  (F5.0):')
      READ(5,402) ZI
  402 FORMAT(F5.0)
      IDATE=IYR*10000+IMON*100+IDAY
      CALL IYRC(IB,IYR,IMON,IDAY)
      RMIN=ITIME-ITIME/100*100
      RTIME=ITIME/100+RMIN/60.
      EQTM=-2.721175+IB*(-.5070817+IB*(.5082854E-02+IB*(-.2113816E-04
     1      +IB*(.1543856E-05+IB*(-.2542001E-07+IB*(.1692641E-09+IB*(-
     2      .5555747E-12+IB*(.8987469E-15+IB*(-.5744318E-18)))))))))
      STIME=RTIME-((RLON-RZONE)/15.-EQTM/60.)
      HAS=(STIME-12.)*15.*DTR
      DS=(IB-1)*2.*PI/365.
      DECL=.006918-.399912*COS(DS)+.070257*SIN(DS)-.006758*COS(2.*DS)
     1      +.000907*SIN(2.*DS)-.002697*COS(3.*DS)+.00148*SIN(3.*DS)
      RLAT=RLAT*DTR
      COSZ=SIN(RLAT)*SIN(DECL)+COS(RLAT)*COS(DECL)*COS(HAS)
      ETRAD=SCON*COSZ
      Z=ARCOS(COSZ)/DTR
      E=90.-Z
      IF(ICH .GE. 4  .AND.  ICH .LE. 6) GO TO 24
      IF(ICH .EQ. 7) GO TO 25
      CC=1.*ICC
      GO TO 26
   24 CC=.75*ICC
      GO TO 26
   25 CC=.5*ICC
```

```
      26  CC=.1*CC
          IF(E .LE. 20.) GO TO 27
          IF(E .LE. 40.) GO TO 28
          IF(E .LE. 60.) GO TO 29
          RADC=ETRAD*(.6423+.9109*CC**2*SIN(E*DTR)-1.2873*CC**2+.1222*SIN(E*DTR)
          GO TO 31
      27  RADC=ETRAD*(.308-1.165*CC**2*SIN(E*DTR)-.0586*CC**2+1.0743*SIN(E*DTR)
          GO TO 31
      28  RADC=ETRAD*(.5695-.1065*CC**2*SIN(E*DTR)-.4755*CC**2+.2809*SIN(E*DTR)
          GO TO 31
      29  RADC=ETRAD*(.7862-.2736*CC**2*SIN(E*DTR)+.6943*CC**2-.0467*SIN(E*DTR)
      31  IF(RADC .LT. 0.) RADC=0.

          WS=WS*.51479
          CNC=.12724E-06+.17314E-06*RADC-.33899E-07*WS+.62238E-06*RADC**2
         1     +.10264E-07*WS**2-.39727E-06*RADC**3-.53824E-09*WS**3
          IF(CNC .LT. 1.E-08) CNC=1.E-08
          CNSQC=CNC**2
          WRITE(7,100) IDATE,ITIME,ICC,ICH,WS,RADC,CNSQC
     100  FORMAT(I6,I5,2I4,F7.1,F9.2,E14.5)
          HGT=10.
          DO 10 I=1,151
          CN2C=CNSQC*(.046*(HGT/ZI)**EXPO+.6*EXP(-12*(HGT/ZI-1.1)**2))
         1      /(.046*(H4/ZI)**EXPO)
          HGTLOG=ALOG10(HGT)
          CN2LOG=ALOG10(CN2C)
          WRITE(8,200) HGT,CN2C,HGTLOG,CN2LOG
     200  FORMAT(F5.0,E15.6,3X,2F12.5)
          HGT=I*20.
      10  CONTINUE
          STOP
          END
C
          SUBROUTINE IYRC(IB,IYR,IMON,IDAY)
          GO TO(1,2,3,4,5,6,7,8,9,10,11,12),IMON
        1 IB=0
          GO TO 14
        2 IB=31
          GO TO 14
        3 IB=59
          GO TO 13
        4 IB=90
          GO TO 13
        5 IB=120
          GO TO 13
        6 IB=131
          GO TO 13
        7 IB=181
          GO TO 13
        8 IB=212
          GO TO 13
        9 IB=243
          GO TO 13
       10 IB=273
          GO TO 13
       11 IB=304
          GO TO 13
       12 IB=334
       13 IF(MOD(IYR,4).EQ.0) IB=IB+1
       14 IB=IB+IDAY
          IF(IDAY.EQ.0) IB=IB+15
          RETURN
          END
```

EXAMPLE

```
#RUN *FTN SCARDS=CNSQ.PROG
#Execution begins   14:36:05
 No errors in MAIN
 No errors in IYRC
#Execution terminated   14:36:07  T=0.148  $0.09
#RUN -LOAD 7=SURFACE 8=PROFILE
#Execution begins   14:36:24
 Enter year, month, day, and time (MST)  (3I2,I5):  840908 1344
 Enter cloud cover (in tenths) and cloud height code (2I2):   1 5
 Enter wind speed at 10 metres (in knots)  (F4.1):   1.8
 Enter estimated height of mixed layer (in metres)  (F5.0):   947.
#Execution terminated   14:36:44  T=0.054  $0.04
#
```

```
#LIST SURFACE

      1     840908 1344   1   5    0.9     1.20    0.27228E-12
#
```

#LIST PROFILE

	z(m)	$C_n^2(m^{-2/3})$	$\log_{10}(z)$	$\log_{10} C_n^2$
1	10.	0.802465E-13	1.00000	-13.09557
2	20.	0.318458E-13	1.30103	-13.49695
3	40.	0.126380E-13	1.60206	-13.89832
4	60.	0.736023E-14	1.77815	-14.13311
5	80.	0.501541E-14	1.90309	-14.29969
6	100.	0.372473E-14	2.00000	-14.42890
7	120.	0.292094E-14	2.07918	-14.53448
8	140.	0.237828E-14	2.14613	-14.62374
9	160.	0.199044E-14	2.20412	-14.70105
10	180.	0.170122E-14	2.25527	-14.76924
11	200.	0.147834E-14	2.30103	-14.83023
12	220.	0.130204E-14	2.34242	-14.88538
13	240.	0.115961E-14	2.38021	-14.93569
14	260.	0.104251E-14	2.41497	-14.98192
15	280.	0.944834E-15	2.44716	-15.02464
16	300.	0.862398E-15	2.47712	-15.06429
17	320.	0.792157E-15	2.50515	-15.10119
18	340.	0.731878E-15	2.53148	-15.13556
19	360.	0.679914E-15	2.55630	-15.16755
20	380.	0.635051E-15	2.57978	-15.19719
21	400.	0.596418E-15	2.60206	-15.22445
22	420.	0.563419E-15	2.62325	-15.24917
23	440.	0.535691E-15	2.64345	-15.27108
24	460.	0.513075E-15	2.66276	-15.28982
25	480.	0.495595E-15	2.68124	-15.30487
26	500.	0.483449E-15	2.69897	-15.31565
27	520.	0.476989E-15	2.71600	-15.32149

28	540.	0.476718E-15	2.73239	-15.32174
29	560.	0.483264E-15	2.74819	-15.31581
30	580.	0.497366E-15	2.76343	-15.30332
31	600.	0.519841E-15	2.77815	-15.28413
32	620.	0.551550E-15	2.79239	-15.25841
33	640.	0.593347E-15	2.80618	-15.22669
34	660.	0.646028E-15	2.81954	-15.18974
35	680.	0.710264E-15	2.83251	-15.14858
36	700.	0.786531E-15	2.84510	-15.10429
37	720.	0.875037E-15	2.85733	-15.05797
38	740.	0.975655E-15	2.86923	-15.01070
39	760.	0.108785E-14	2.88081	-14.96343
40	780.	0.121062E-14	2.89209	-14.91699
41	800.	0.134249E-14	2.90309	-14.87209
42	820.	0.148147E-14	2.91381	-14.82931
43	840.	0.162506E-14	2.92428	-14.78913
44	860.	0.177034E-14	2.93450	-14.75194
45	880.	0.191402E-14	2.94448	-14.71805
46	900.	0.205251E-14	2.95424	-14.68771
47	920.	0.218214E-14	2.96379	-14.66112
48	940.	0.229921E-14	2.97313	-14.63842
49	960.	0.240023E-14	2.98227	-14.61975
50	980.	0.248204E-14	2.99123	-14.60519
51	1000.	0.254198E-14	3.00000	-14.59483
52	1020.	0.257801E-14	3.00860	-14.58871
53	1040.	0.258884E-14	3.01703	-14.58689
54	1060.	0.257398E-14	3.02531	-14.58940
55	1080.	0.253375E-14	3.03342	-14.59623
56	1100.	0.246930E-14	3.04139	-14.60743
57	1120.	0.238251E-14	3.04922	-14.62296
58	1140.	0.227593E-14	3.05690	-14.64284
59	1160.	0.215260E-14	3.06446	-14.66704
60	1180.	0.201596E-14	3.07188	-14.69552
61	1200.	0.186964E-14	3.07918	-14.72824
62	1220.	0.171731E-14	3.08636	-14.76515
63	1240.	0.156254E-14	3.09342	-14.80617
64	1260.	0.140864E-14	3.10037	-14.85119
65	1280.	0.125859E-14	3.10721	-14.90011
66	1300.	0.111490E-14	3.11394	-14.95276
67	1320.	0.979605E-15	3.12057	-15.00895
68	1340.	0.854234E-15	3.12710	-15.06842
69	1360.	0.739805E-15	3.13354	-15.13088
70	1380.	0.636869E-15	3.13988	-15.19595
71	1400.	0.545549E-15	3.14613	-15.26316
72	1420.	0.465626E-15	3.15229	-15.33196
73	1440.	0.396575E-15	3.15836	-15.40168
74	1460.	0.337660E-15	3.16435	-15.47152
75	1480.	0.287992E-15	3.17026	-15.54062
76	1500.	0.246604E-15	3.17609	-15.60800
77	1520.	0.212491E-15	3.18184	-15.67266
78	1540.	0.184663E-15	3.18752	-15.73362
79	1560.	0.162176E-15	3.19312	-15.79001

80	1580.	0.144157E-15	3.19866	-15.84116
81	1600.	0.129825E-15	3.20412	-15.88664
82	1620.	0.118488E-15	3.20951	-15.92632
83	1640.	0.109553E-15	3.21484	-15.96038
84	1660.	0.102517E-15	3.22011	-15.98920
85	1680.	0.969663E-16	3.22531	-16.01337
86	1700.	0.925619E-16	3.23045	-16.03357
87	1720.	0.890328E-16	3.23553	-16.05045
88	1740.	0.861656E-16	3.24055	-16.06465
89	1760.	0.837940E-16	3.24551	-16.07678
90	1780.	0.817916E-16	3.25042	-16.08728
91	1800.	0.800625E-16	3.25527	-16.09656
92	1820.	0.785354E-16	3.26007	-16.10492
93	1840.	0.771579E-16	3.26482	-16.11261
94	1860.	0.758919E-16	3.26951	-16.11980
95	1880.	0.747102E-16	3.27416	-16.12660
96	1900.	0.735933E-16	3.27875	-16.13316
97	1920.	0.725276E-16	3.28330	-16.13950
98	1940.	0.715033E-16	3.28780	-16.14566
99	1960.	0.705136E-16	3.29226	-16.15172
100	1980.	0.695540E-16	3.29667	-16.15767
101	2000.	0.686211E-16	3.30103	-16.16353
102	2020.	0.677123E-16	3.30535	-16.16933
103	2040.	0.668260E-16	3.30963	-16.17505
104	2060.	0.659607E-16	3.31387	-16.18071
105	2080.	0.651155E-16	3.31806	-16.18631
106	2100.	0.642894E-16	3.32222	-16.19185
107	2120.	0.634817E-16	3.32634	-16.19734
108	2140.	0.626917E-16	3.33041	-16.20279
109	2160.	0.619188E-16	3.33445	-16.20818
110	2180.	0.611625E-16	3.33846	-16.21350
111	2200.	0.604223E-16	3.34242	-16.21880
112	2220.	0.596975E-16	3.34635	-16.22403
113	2240.	0.589879E-16	3.35025	-16.22923
114	2260.	0.582929E-16	3.35411	-16.23438
115	2280.	0.576121E-16	3.35793	-16.23947
116	2300.	0.569451E-16	3.36173	-16.24454
117	2320.	0.562915E-16	3.36549	-16.24954
118	2340.	0.556509E-16	3.36922	-16.25452
119	2360.	0.550230E-16	3.37291	-16.25945
120	2380.	0.544074E-16	3.37658	-16.26433
121	2400.	0.538037E-16	3.38021	-16.26918
122	2420.	0.532116E-16	3.38381	-16.27399
123	2440.	0.526309E-16	3.38739	-16.27875
124	2460.	0.520611E-16	3.39093	-16.28348
125	2480.	0.515021E-16	3.39445	-16.28816
126	2500.	0.509534E-16	3.39794	-16.29282
127	2520.	0.504150E-16	3.40140	-16.29744
128	2540.	0.498864E-16	3.40483	-16.30200
129	2560.	0.493674E-16	3.40824	-16.30655
130	2580.	0.488579E-16	3.41162	-16.31107
131	2600.	0.483574E-16	3.41497	-16.31552
132	2620.	0.478659E-16	3.41830	-16.31996
133	2640.	0.473830E-16	3.42160	-16.32437

134	2660.	0.469085E-16	3.42488	-16.32874
135	2680.	0.464423E-16	3.42813	-16.33308
136	2700.	0.459842E-16	3.43136	-16.33739
137	2720.	0.455340E-16	3.43457	-16.34166
138	2740.	0.450914E-16	3.43775	-16.34590
139	2760.	0.446562E-16	3.44091	-16.35011
140	2780.	0.442284E-16	3.44405	-16.35429
141	2800.	0.438076E-16	3.44716	-16.35844
142	2820.	0.433939E-16	3.45025	-16.36256
143	2840.	0.429869E-16	3.45332	-16.36665
144	2860.	0.425866E-16	3.45637	-16.37073
145	2880.	0.421927E-16	3.45939	-16.37476
146	2900.	0.418052E-16	3.46240	-16.37875
147	2920.	0.414238E-16	3.46538	-16.38274
148	2940.	0.410485E-16	3.46835	-16.38669
149	2960.	0.406791E-16	3.47129	-16.39063
150	2980.	0.403155E-16	3.47422	-16.39452
151	3000.	0.399576E-16	3.47712	-16.39839

Appendix B. Fortran IV program for C_n^2 model for stable stratification with example for 2113 MST, 3 Sept. 1984 for White Sands, NM.

```
LIST CNSQ.STABLE

     1              EXPO=-4./3.
     2              WRITE(6,101)
     3        101   FORMAT('$Enter wind speed at 10 metres (in knots)  (F4.1): ')
     4              READ(5,102) WS
     5        102   FORMAT(F4.1)
     6              WS=WS*.51479
     7              CNSQC=1.28E-13*EXP((-(WS-4.)**2)/(2.*2.3**2))
     8              WRITE(7,100) CNSQC
     9        100   FORMAT(E14.5)
    10              HGT=10.
    11              DO 10 I=1,31
    12              CN2C=CNSQC*(HGT/4.)**EXPO
    13              HGTLOG=ALOG10(HGT)
    14              CN2LOG=ALOG10(CN2C)
    15              WRITE(8,200) HGT,CN2C,HGTLOG,CN2LOG
    16        200   FORMAT(F5.0,E15.6,2X,2F12.5)
    17              HGT=I*20.
    18         10   CONTINUE
    19              STOP
    20              END
```

EXAMPLE

```
#RUN *FTN SCARDS=CNSQ.STABLE
#Execution begins   15:55:13
 No errors in MAIN
#Execution terminated   15:55:14  T=0.066  $0.04
#RUN -LOAD 7=SURFACE 8=PROFILE
#Execution begins   15:55:25
 Enter wind speed at 10 metres (in knots)  (F4.1):   9.9
#Execution terminated   15:55:30  T=0.022  $0.02
#
```

2113 MST, 9/3/84

```
#LIST SURFACE

      1         0.11425E-12
#
```

#LIST PROFILE

	z(m)	$C_n^2(m^{-2/3})$	$\log_{10}(z)$	$\log_{10} C_n^2$
1	10.	0.336726E-13	1.00000	-13.47272
2	20.	0.133630E-13	1.30103	-13.87409
3	40.	0.530312E-14	1.60206	-14.27547
4	60.	0.308847E-14	1.77815	-14.51026
5	80.	0.210454E-14	1.90309	-14.67684
6	100.	0.156295E-14	2.00000	-14.80605
7	120.	0.122566E-14	2.07918	-14.91163
8	140.	0.997945E-15	2.14613	-15.00089
9	160.	0.835189E-15	2.20412	-15.07822
10	180.	0.713808E-15	2.25527	-15.14642
11	200.	0.620256E-15	2.30103	-15.20743
12	220.	0.546237E-15	2.34242	-15.26262
13	240.	0.486403E-15	2.38021	-15.31300
14	260.	0.437166E-15	2.41497	-15.35935
15	280.	0.396035E-15	2.44716	-15.40227
16	300.	0.361229E-15	2.47712	-15.44221
17	320.	0.331445E-15	2.50515	-15.47959
18	340.	0.305708E-15	2.53148	-15.51469
19	360.	0.283275E-15	2.55630	-15.54779
20	380.	0.263572E-15	2.57978	-15.57910
21	400.	0.246149E-15	2.60206	-15.60880
22	420.	0.230646E-15	2.62325	-15.63705
23	440.	0.216774E-15	2.64345	-15.66399
24	460.	0.204300E-15	2.66276	-15.68973
25	480.	0.193029E-15	2.68124	-15.71438
26	500.	0.182803E-15	2.69897	-15.73801
27	520.	0.173490E-15	2.71600	-15.76072
28	540.	0.164976E-15	2.73239	-15.78258
29	560.	0.157167E-15	2.74819	-15.80364
30	580.	0.149982E-15	2.76343	-15.82396
31	600.	0.143354E-15	2.77815	-15.84359

#